Lawrence Berkeley National Laboratory

Lawrence Berkeley National Laboratory

Title

In-situ Studies of the Reactions of Bifunctional and Heterocyclic Molecules over Noble Metal Single Crystal and Nanoparticle Catalysts Studied with Kinetics and Sum-Frequency Generation Vibrational Spectroscopy

Permalink

https://escholarship.org/uc/item/1s53134n

Author

Kliewer, Christopher J.

Publication Date

2009-09-01

Peer reviewed

eScholarship.org Powered by the California Digital Library
University of California

In-situ Studies of the Reactions of Bifunctional and Heterocyclic Molecules over Noble Metal Single Crystal and Nanoparticle Catalysts Studied with Kinetics and Sum-Frequency Generation Vibrational Spectroscopy

by

Christopher J. Kliewer

B.S. (George Fox University) 2005

A dissertation submitted in partial fulfillment of

the requirements for the degree of

Doctor of Philosophy

in

Chemistry

in the

Graduate Division

of the

University of California, Berkeley

Committee in charge:

Professor Gabor A. Somorjai, Chair

Professor Peidong Yang

Professor Elton J. Cairns

Fall 2009

Abstract

In-situ Studies of the Reactions of Bifunctional and Heterocyclic Molecules over Noble Metal Single Crystal and Nanoparticle Catalysts Studied with Kinetics and Sum-Frequency Generation Vibrational Spectroscopy

by

Christopher J. Kliewer

Doctor of Philosophy in Chemistry

University of California, Berkeley

Professor Gabor A. Somorjai, Chair

Sum frequency generation surface vibrational spectroscopy (SFG-VS) in combination with gas chromatography (GC) was used *in-situ* to monitor surface bound reaction intermediates and reaction selectivities for the hydrogenation reactions of pyrrole, furan, pyridine, acrolein, crotonaldehyde, and prenal over Pt(111), Pt(100), Rh(111), and platinum nanoparticles under Torr reactant pressures and temperatures of 300K to 450K. The focus of this work is the correlation between the SFG-VS observed surface bound reaction intermediates and adsorption modes with the reaction selectivity, and how this is affected by catalyst structure and temperature.

Pyrrole hydrogenation was investigated over Pt(111) and Rh(111) single crystals at Torr pressures. It was found that pyrrole adsorbs to Pt(111) perpendicularly by cleaving the N-H bond and binding through the nitrogen. However, over Rh(111) pyrrole adsorbs in a tilted geometry binding through the π-aromatic orbitals. A surface-bound

pyrroline reaction intermediate was detected over both surfaces with SFG-VS. It was found that the ring-cracking product butylamine is a reaction poison over both surfaces studied.

Furan hydrogenation was studied over Pt(111), Pt(100), 10 nm cubic platinum nanoparticles and 1 nm platinum nanoparticles. The product distribution was observed to be highly structure sensitive and the acquired SFG-VS spectra reflected this sensitivity. Pt(100) exhibited more ring-cracking to form butanol than Pt(111), while the nanoparticles yielded higher selectivities for the partially saturated ring dihydrofuran.

Pyridine hydrogenation was investigated over Pt(111) and Pt(100). The α-pyridyl surface adsorption mode was observed with SFG-VS over both surfaces. 1,4-dihydropyridine was seen as a surface intermediate over Pt(100) but not Pt(111). Upon heating the surfaces to 350K, the adsorbed pyridine changes to a flat-lying adsorption mode. No evidence was found for the pyridinium cation.

The hydrogenation of the α,β-unsaturated aldehydes acrolein, crotonaldehyde, and prenal were investigated over Pt(111) and Pt(100). The selectivity for the hydrogenation of the C=C bond was found to depend on the number of methyl groups added to the bond. The adsorption modes of the three aldehydes were determined. The hydrogenation of crotonaldehyde was found to be nearly structure insensitive as the TOF and selectivity were very close to the same over Pt(111) and Pt(100). SFG-VS indicated identical surface intermediates over the two crystal faces during crotonaldehyde hydrogenation.

Professor Gabor A. Somorjai
Dissertation Committee Chair

Table of Contents

List of Figures

ACKNOWLEDGEMENTS

I would first like to thank Professor Gabor Somorjai as my research advisor for the opportunity to work and learn in his group. His enthusiasm for surface science and its many diverse applications certainly served as an inspiration, and his thoughtful advice throughout my career at Berkeley has led to the success of my research as well as my growth individually.

I am exceedingly grateful to my wife, Shannon Kliewer, for her constant support during my time in graduate school. Her optimism always served to lift my spirits. I don't think I ever would have left the lab if it wasn't for her helping me to maintain a good life balance. I love you and could not have done this without you. I thank my first-born child Chloe May Kliewer for the many laughs, cries, and hugs that reminded me of what is important in life. I am thankful to God for blessing me with this opportunity.

I want to thank my parents for their never-ending love and support and the work ethic they instilled in me throughout my childhood. You have always given so much so that I could succeed in life.

I must thank all of the people here at Berkeley that have given me both guidance and friendship. I thank Dr. Sasha Kweskin for teaching me everything I needed to know about maintaining our laser systems. I thank Dr. Kaitlin Bratlie for teaching me about ultra-high vacuum and surface science techniques. Derek Butcher, Russ Renzas, and George Holinga all entered Berkeley with me, and we have jumped all of the hurdles of graduate school togother, thank you for the many conversations and fun times, some of which were related to science. I thank the Department of Energy for funding under contract No. DE-AC02-05CH11231.

Chapter 1

Introduction

As we continue into the twenty-first century, heterogeneous catalysis has never held a more pivotal role. Not only do a great many industrial processes rely on heterogeneous catalysts today, but as the global concerns of energy production and conversion, alternative energy sources, and climate change garner attention, the importance of heterogeneous catalysis is again paramount. Although many reactions can be promoted with either homogeneous or heterogeneous catalysis, the latter generally allows for less waste, fewer toxic reagents, and easier retrieval and recycling of the catalyst[1]. This allows for a more "green" chemistry. In this same regard, the ultimate goal in heterogeneous catalysis must be for 100% selectivity for the desired product in a multi-pathway reaction, eliminating unwanted byproducts.

The only way to gain a full understanding of selectivity in heterogeneous catalysis is to probe the catalytic reactions at a molecular level while varying parameters such as temperature, pressure, catalyst composition, and catalyst structure. The development of ultrahigh vacuum (UHV) surface science techniques greatly enhanced our knowledge of such molecular level processes on catalyst surfaces. For instance, high resolution electron energy loss spectroscopy (HREELS) can be used to obtain a vibrational spectrum of molecules and reaction intermediates bound to a catalyst surface. Low energy electron diffraction (LEED) provides information about how adsorbate molecules order across a catalyst surface. Auger electron spectroscopy (AES) gives an elemental analysis of a surface with sensitivity down to 1% of a monolayer.[2] Many

other techniques were developed which take advantage of electron or ion scattering from a surface to garner intricate molecular level details about the interaction of molecules and a catalyst surface.

The limitation of the electron and ion scattering techniques, however, is that they are bound to the low pressure regime due to the large collisional cross-section of these probes with gas or liquid phase molecules. This creates a "gap" in pressure between the fundamental research done in surface science laboratories using these techniques and the pressures at which catalytic reactions are carried out industrially. Being limited to the low-pressure regime makes it difficult to study such reactions as hydrocarbon reforming which have very low reaction probabilities[3] necessitating high pressure conditions. Further, short lived surface reaction intermediates can only be observed under conditions of low temperature or high pressure, but low temperature conditions can yield reduced adsorbate mobility, reducing the ability of the adsorbates to follow the reaction mechanism. In addition to the mobility of the adsorbate, the mobility of the substrate metal atoms is also of concern.

Photon based surface interrogation techniques are applicable at higher pressure regimes than the electron based techniques listed above. Both infrared and Raman spectroscopies have been applied to study adsorbates on catalyst surfaces. These techniques suffer from the fact that the gas phase molecules and bulk metal crystal can contribute to the acquired spectrum. Thus, the spectrum for the gas phase and bulk crystal must be subtracted from the acquired spectrum to yield the surface adsorbate spectrum. As the reactant pressures get higher, this will lead to an increasingly worse

signal-to-noise ratio, and one can not be completely sure the acquired spectrum is that of the surface adsorbates.

Recently, through the application of nonlinear optics, sum frequency generation vibrational spectroscopy (SFG-VS) has been shown to be an inherently surface specific vibrational spectroscopy.[4-7] This is a technique in which two high energy laser beams, one in the visible and one in the infrared, are overlapped spatially and temporally on an interface of interest, and a beam is created at the interface which is at the sum of the two incoming frequencies. Due to the properties of the nonlinear susceptibility tensor, this process is forbidden in any medium with inversion symmetry, such as the isotropic gases in a reaction cell or the bulk metal atoms of a catalyst. Signal can be generated only at an interface. Further, if the incoming infrared beam is scanned in frequency, when it comes into resonance with a vibrational mode of a molecule at the interface being probed the overall process is resonantly enhanced and an increase in SFG signal is obtained. In this manner, a vibrational spectrum of surface-bound adsorbates can be acquired.

The work presented in this dissertation focuses on the relationship between adsorption modes, reaction intermediates, and reaction selectivity as the parameters of temperature, catalyst composition, and catalyst structure are varied. To accomplish this task, SFG-VS was applied *in-situ* during the course of several different catalyzed reactions to identify the surface bound species while at the same time collecting kinetic data on the reaction via gas chromatography. Simultaneous monitoring of the gas phase kinetics with GC and surface bound species with SFG-VS allows for a unique perspective on the factors controlling catalytic selectivity and activity.

Two major classes of reactions were studied in this work. First, the hydrogenation of heterocyclic aromatics was studied including the reactions of pyrrole, furan, and pyridine. Second, the reactions of bifunctional molecules were studied, including the hydrogenation of acrolein, crotonaldehyde, and prenal. These reactions were carried out over well-defined model single crystal catalysts of a particular crystal face, including Pt(111), Pt(100), and Rh(111), as well as size-controlled 1 nm and 10 nm platinum nanoparticles to help elucidate the effect that catalyst structure and size plays in a reaction.

Pyrrole hydrogenation was studied over Pt(111) and Rh(111) single crystals at Torr pressures. The reaction mechanisms were clarified with SFG-VS and correlated with the observed reaction selectivities. The effect of coadsorption was explored as it was found that pre-adsorbing a surface layer of 1-methylpyrrole on the surfaces prior to reaction coincided with a 17 fold increase in reaction rate. The mechanism of rate-enhancement was clarified with SFG-VS. It was found that the ring-cracking product butylamine was a reaction poison over both surfaces studied.

Furan hydrogenation was studied over Pt(111) and Pt(100) single crystals as well as 1 nm and 10 nm platinum nanoparticles. This reaction was found to be quite structure sensitive as the product distributions were quite different over the various catalysts. The selectivities were then correlated with the observed surface intermediates seen with SFG.

Pyridine hydrogenation was studied over Pt(111) and Pt(100). Several possible reaction intermediates for this reaction have been proposed in the literature, including a pyridinium cation, α-pyridyl, and 1,4-dihydropyridine. The surface species present as a function of catalyst geometry and temperature were investigated.

Chapter 7 deals with the reactions of bifunctional molecules. Acrolein, crotonaldehyde, and prenal hydrogenation were explored. These belong to a class of compounds known as α,β-unsaturated aldehydes as they contain both a carbonyl and a vinylic group in conjugation. Either one of those two functional groups may be hydrogenated, and the factors which govern this selectivity are explored. The three compounds differ only in the number of methyl groups attached to the C=C. This investigation correlates observed reaction selectivity with reactant adsorption mode.

References

(1) Zaera, F. "Mechanisms of hydrocarbon conversion reactions on heterogeneous catalysts: analogies with organometallic chemistry", 2005.

(2) Somorjai, G. *Introduction to Surface Science and Catalysis*; Wiley: New York, 1994.

(3) Wilson, J.; Guo, H.; Morales, R.; Podgornov, E.; Lee, I.; Zaera, F. *Physical Chemistry Chemical Physics* **2007**, *9*, 3830.

(4) Du, Q.; Superfine, R.; Freysz, E.; Shen, Y. R. *Physical Review Letters* **1993**, *70*, 2313.

(5) Johal, M. S.; Ward, R. N.; Davies, P. B. *Journal of Physical Chemistry* **1996**, *100*, 274.

(6) Shen, Y. R. *Nature* **1989**, *337*, 519.

(7) Shen, Y. R. *Surface Science* **1994**, *299*, 551.

Chapter 2

Experimental Considerations

The work reported in this dissertation primarily focuses on the use of platinum and rhodium single crystals of clearly defined crystal face to carry out chemical reactions at Torr pressures. The techniques of sum frequency generation vibrational spectroscopy, a surface-specific vibrational spectroscopy, and gas chromatography were used together *in-situ* during the catalytic reactions to help elucidate surface species while monitoring product distributions. An ultra high vacuum surface science chamber was used to prepare and characterize clean single crystal surfaces which were then transferred into a newly constructed high pressure cell for high pressure reaction studies while acquiring SFG-VS spectra during the course of the reaction. The results of these single crystal studies can then be compared to nanoparticle catalysts which more closely resemble traditional industrial catalysts.

2.1 Ultra High Vacuum System / High Pressure Cell

A schematic of the UHV/ HPC system used in this work is presented in figure 2.1. The system is equipped with an ion bombardment gun for argon sputtering of single crystal surfaces, a quadrupole mass spectrometer for analyzing the gas phase constituents present in the UHV chamber, a combined Auger electron spectrometer and rear-view LEED (Omikron) for surface analysis, leak valves connected to a gas manifold for gas dosing, and annealing capabilities. The UHV chamber is pumped with a 60 L/sec Pheiffer turbomolecular pump, ion pump, and titanium sublimation pump. During typical

operation the system holds a baseline pressure of 2 X 10^{-10} Torr residual gases.

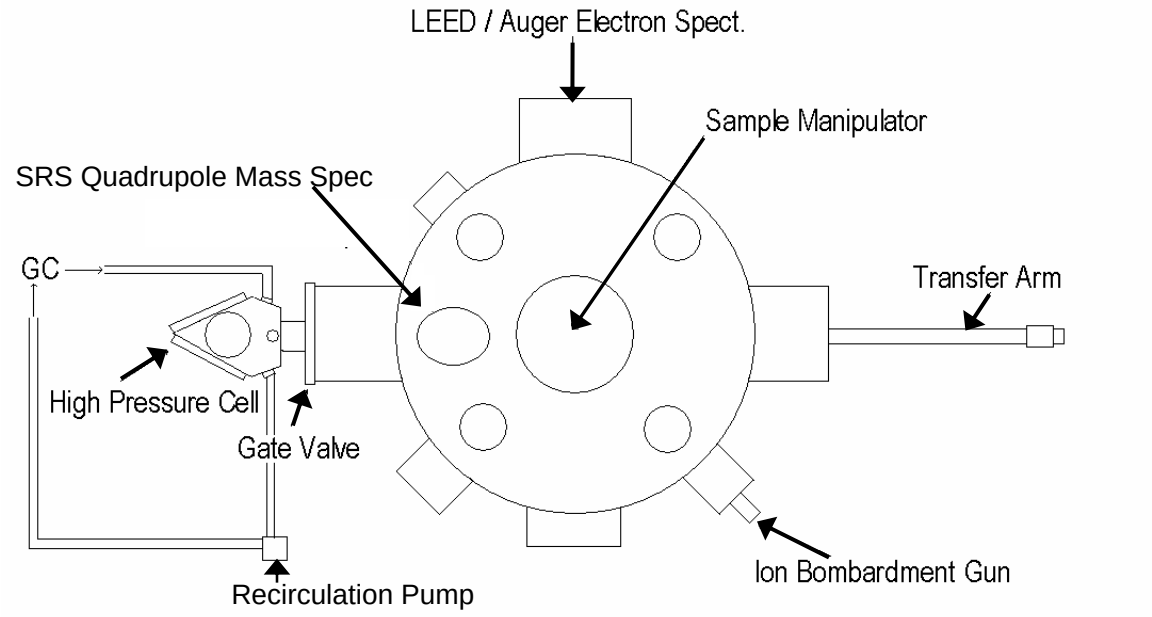

Figure 2.1. Birds-eye schematic of the ultra high vacuum chamber and high pressure cell.

A new high pressure cell was constructed for *in-situ* catalytic studies at high (up to 760 Torr) pressures. The high pressure cell is separately pumped with a turbomolecular pump (Pheiffer, 56 L/sec) and separated from the UHV chamber via a 2.75" gate valve. A photograph is shown in figure 2.2. This high pressure cell was machined from stainless steel and electroplated with gold to reduce any background catalytic activity from the cell walls. It was specifically designed to have a small volume (~400 mL) so that pump down following catalytic reaction would proceed as quickly as possible. The two windows for the transmission of laser light, as seen in figure 2.2, are made of CaF_2, which has near 100% transmission in the infrared frequency range for

which we collect SFG spectra. The exit window was also made of CaF_2 so that a proper normalization of the SFG-VS signal could be done. The small size of the high pressure cell allowed for a short path length, ~4 cm, from the window to the sample so as to minimize the attenuation of the incoming infrared beam from gas phase absorption.

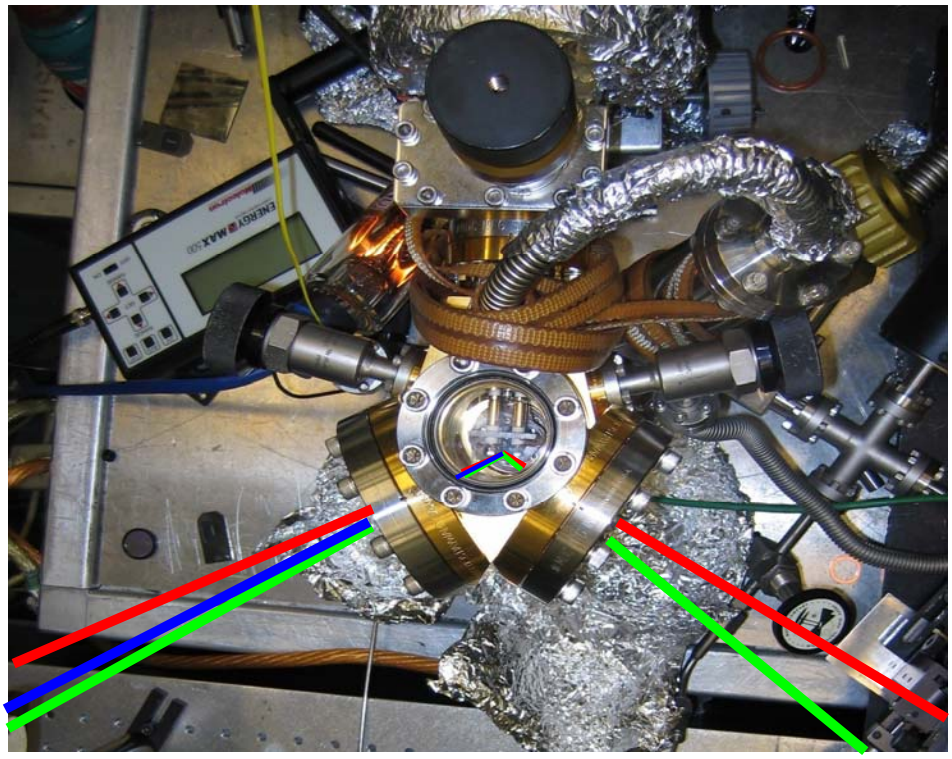

Figure 2.2. Photograph of the newly constructed high pressure cell for *in-situ* catalytic studies.

The high pressure cell was equipped with a recirculation loop which included a recirculation pump (diaphragm). The loop ran through a six-way valve on a gas chromatograph (Hewlett Packard 5890) for periodic sampling of the reaction mixture. The gas chromatograph used a 5% Carbowax 20M 15' stainless steel column as the stationary phase. GC detection was made with a flame ionization detector (FID). The FID response to the various products was always calibrated by adding a specific amount

of the species in question, 10 Torr for example, to the high pressure cell and fill to atmospheric pressure with argon. Dividing the FID observed peak area by the amount added yielded a sensitivity factor for each possible reactant and product.

2.2 Single Crystal Sample Preparation

The single crystals used for this dissertation were all obtained from Matek Corporation and cut to within 0.3° from the intended crystal plane. Pt(111), Pt(100), and Rh(111) were used in this work. If the crystal face was scratched or otherwise damaged the following procedure was used for polishing the crystal face. The crystal was mounted in Koldmount commercial epoxy by pouring it over the top of the crystal in a Teflon mold. Metadi diamond paste was applied to a Buehler Microcloth polishing pad. 15 μm diamond grit was initially used to polish out any scratches; this process usually required one hour or so of figure 8 motion over the polishing pad. Then the 6, 1, and 0.25 μm grit sizes were used successively until the crystal face was highly polished. The Koldmount was removed by sonication in acetone overnight. The crystal was then removed and chemically etched in aqua regia acid mixture for 10 minutes to remove the surface defects caused by the polishing process. The crystal was then sonicated in deionized water for 30 minutes.

The single crystals were placed on a sample mount by spot welding to a strip of 2 mm thick tantalum. The tantalum was cut thin enough such that a thermocouple could also be spot welded to the back of the crystal for temperature measurement.

The Pt and Rh single crystals were cleaned in the UHV chamber by Ar ion bombardment and annealing cycles. Roughly 5 X 10^{-5} Torr argon was leaked into the

chamber and the argon ions from the ion bombardment gun were accelerated to 1000 eV at the surface for 20 minutes. After the bombardment procedure the crystal face is left with topmost layers unevenly stripped away. To heal any surface imperfections the crystals are annealed to 850°C in the presence of 5 X 10^{-7} Torr oxygen for 2 minutes, and then annealed at that temperature an additional 2 minutes in ultra high vacuum. The oxygen serves to combust away any residual hydrocarbons on the catalyst surface. The surface is then verified to be clean using Auger electron spectroscopy.

2.3 Auger Electron Spectroscopy (AES)

Auger electron spectroscopy (AES) is a powerful surface analytical technique for surface elemental analysis and sensitivity down to 1% of a monolayer.[1] The technique is sensitive to just the top few atomic layers with decreasing signal from each successively deeper layer. This is due to the low mean free path of ballistic electrons in a metal. The generation of Auger electrons, first reported by Pierre Auger in 1925, occurs via a four-step process.

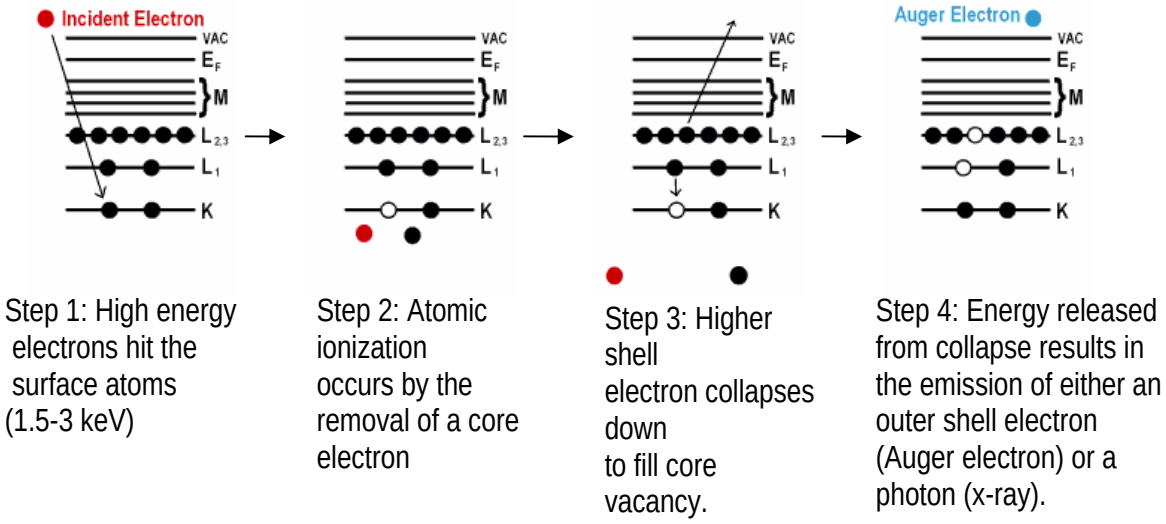

Figure 2.3. Schematic of the Auger electron emission process.

In the example given in figure 2.3, the kinetic energy of the Auger electron departing from the surface will be given by equation 2.1:

$$E_{kin} = (E_K - E_{L1}) - E_{L23} \qquad 2.1$$

Due to the fact that every element has its own unique electronic orbital structure, the kinetic energies of the Auger electrons emitted can be used to identify the atoms from which they are being emitted, with the exception of helium and hydrogen.

The Auger electron must be able to escape the surface in order to be emitted. Due to the very low mean free path of an Auger electron in a metal/solid material in the typical range of Auger energies (50-1500 eV), the useful signal is generated solely from the first few atomic layers of the sample. This is the primary benefit of the technique; it is a surface specific signal.

While AES can be made very quantitative, for example by the method of Biberian and Somorjai[2], a simple calculation can yield surface coverages according to equation 2.2.

$$C_i = \frac{I_i / S_i}{\sum I_j / S_j} \qquad 2.2$$

where C_i is the surface concentration of element i, I_i is the intensity of the Auger peak for element i, S_i is the relative sensitivity factor for element i. Figure 2.4 displays a sample Auger spectrum taken before and after cleaning cycles on a Pt(111) crystal.

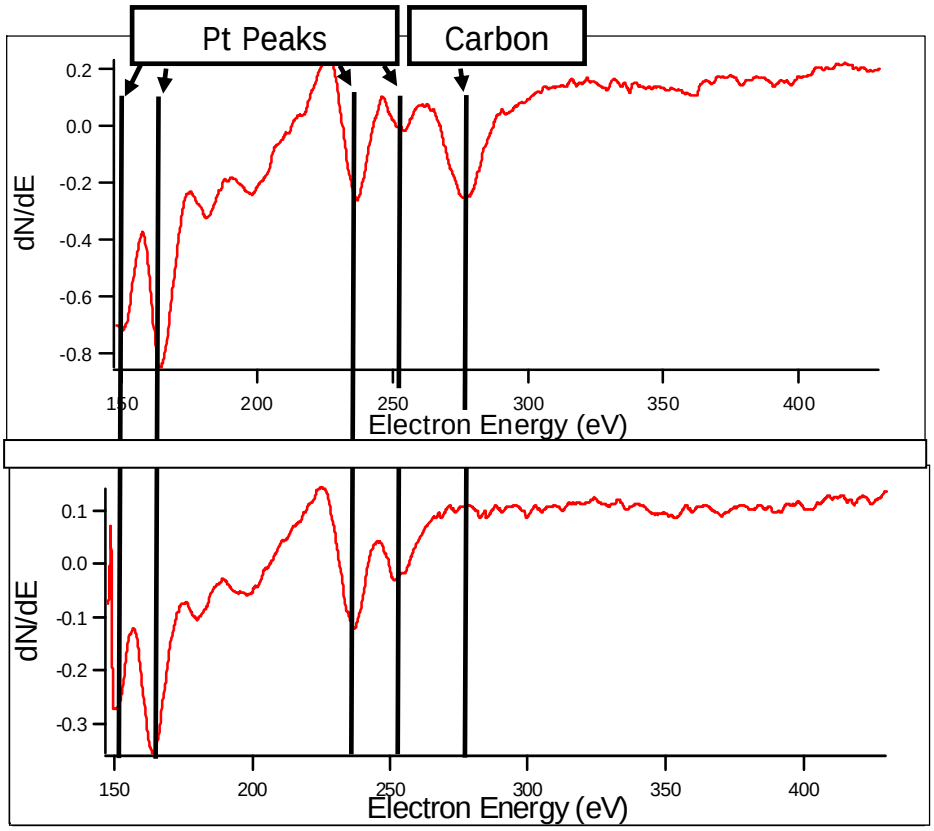

Figure 2.4. Sample Auger spectrum collected over Pt(111) both before (top) and after (bottom) a sputter/anneal cleaning cycle. After cleaning there is no detectable carbon left on the surface.

2.4 Nanoparticle Reaction Cell

Nanoparticle catalytic studies of furan hydrogenation were carried out in a cell depicted schematically in figure 2.5.

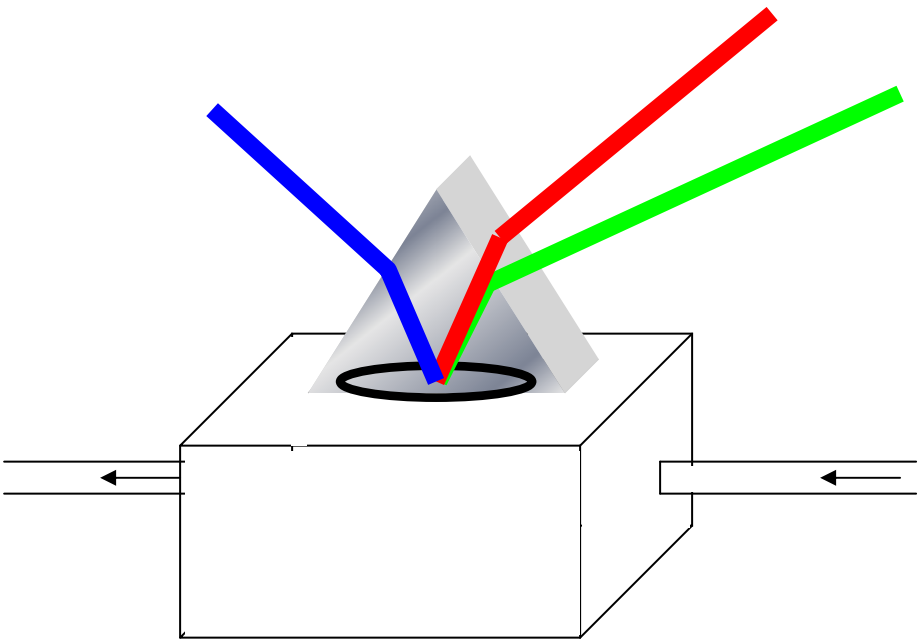

Figure 2.5. Schematic of the nanoparticle reaction cell. An o-ring sealed the silica prism to the stainless steel reaction cell which was surrounded in heat tape for temperature studies. The nanoparticles were deposited on the bottom of the prisms either by the drop cast or Langmuir Blodgett technique.

Similar to the single crystal studies, the gases were recirculated via a recirculation pump and connected to a GC (Hewlett Packard 6890). The reactant and products were separated in a 5% Carbowax 20M 15' stainless steel column and detected by flame ionization detection. For the uv-ozone cleaning of the nanoparticles, the exact procedure outlined by Aliaga et al[3] was used. A Bulbtronics 16W low-pressure mercury lamp with emission at 185 and 257 nm was placed in a metallic enclosure and the silica prism with nanoparticles deposited was placed 5 mm from the lamp's surface and then removed and placed directly onto the mount shown in figure 2.5. The gas lines were pumped with a turbomolecular pump.

References

(1) Somorjai, G. *Introduction to Surface Science and Catalysis*; Wiley: New York, 1994.

(2) Biberian, J. P.; Somorjai, G. A. *Applied Surface Science* **1979**, *2*, 352.

(3) Aliaga, C.; Park, J. Y.; Yamada, Y.; Lee, H. S.; Tsung, C. K.; Yang, P. D.; Somorjai, G. A. *Journal of Physical Chemistry C* **2009**, *113*, 6150.

Chapter 3

Sum Frequency Generation

Sum-frequency generation vibrational spectroscopy (SFG-VS) is a nonlinear vibrational spectroscopy technique in which two high-energy pulsed laser beams are overlapped spatially and temporally on an interface of interest. Due to the properties of the nonlinear susceptibility tensor, media with inversion symmetry such as isotropic gases or bulk metal crystals cannot generate a SFG-VS signal. Thus, the entire signal is generated at the interface, and only those molecules adsorbed at the interface can contribute to the acquired signal. The infrared-visible SFG-VS process (figure 3.1) can be thought of as an infrared excitation followed by an antistokes Raman relaxation process, the result of which is emitted radiation at the sum of the two incoming frequencies.

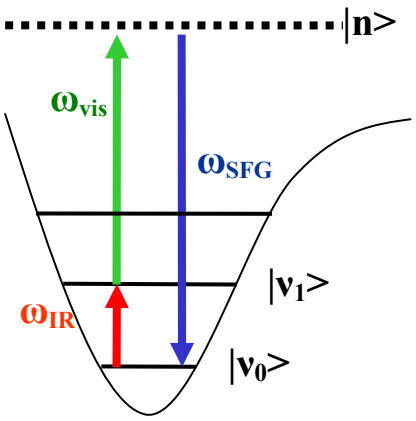

Figure 3.1. Schematic of the infrared-visible SFG-VS process. The term $v_0>$ refers to the vibrational ground state, $|v_1>$ the first vibrational level, and |n> refers to a virtual electronic state.

3.1 Theoretical Background to Sum Frequency Generation

The theory of sum frequency generation was first proposed by Bloembergen[1] in 1968, while the first experimental observation occurred a few years earlier in 1962[2]. However, it was not until the pioneering work of Y.R. Shen[3-5] throughout the 1980s that the technique was applied and shown to be surface specific. I give a brief description of the background here, but several excellent reviews of the topic and the application of SFG have been published.[6-12]

When light interacts with molecules, the electromagnetic field exerts a force on the electron clouds of the molecules it hits. This force induces a dipole as the electrons respond. The macroscopic average of molecular dipoles is a polarization, or a dipole moment per unit volume. Thus, the polarization on a material perturbed by a low energy electric field is given by equation 3.1.

$$\vec{P} \approx \vec{P}^{(0)} + \vec{P}^{(1)} = \vec{P}^{(0)} + \varepsilon_0 \vec{\chi}^{(1)} \vec{E}(r)\cos(\omega t) \qquad 3.1$$

where $\vec{P}^{(0)}$ refers to the static polarization of a material caused by the molecular average of static dipole moments, $\vec{P}^{(1)}$ is the first-order linear polarization, $\vec{\chi}^{(1)}$ is the linear susceptibility tensor, ε_0 is the permittivity of free space, t is time, and $\vec{E}(r)\cos(\omega t)$ describes the propagating electric field. As this equation indicates, the polarization will oscillate at the same frequency as the electric field. Thus, any radiation emitted in response to this effect will be at the same frequency as the incoming light.

Under strong electric fields, a linear response of the polarization is no longer adequate to fully describe the response, and higher order terms are added to the expansion in equation 3.1, as shown here in equation 3.2.

$$\vec{P} \approx \vec{P}^{(0)} + \vec{P}^{(1)} + \vec{P}^{(2)} + \vec{P}^{(3)} + \ldots \qquad 3.2$$

where $\vec{P}^{(2)}$ is the second order polarization given by equation 3.3.

$$P_i^{(2)} = \varepsilon_0 \sum_{j,k} \chi_{ijk}^{(2)} \vec{E}_j(r)\cos(\omega_1 t)\vec{E}_k(r)\cos(\omega_2 t) \qquad 3.3$$

where $\chi^{(2)}$ is the second-order nonlinear susceptibility tensor. Taking into account a simple trigonometric identity, equation 3.3 can be rearranged to give

$$P_i^{(2)} = \frac{1}{2}\varepsilon_0 \sum_{j,k} \chi_{ijk}^{(2)} \vec{E}_j(r)\vec{E}_k(r)\left[\cos(\omega_1 + \omega_2)t + \cos(\omega_1 - \omega_2)t\right] \qquad 3.4$$

In the case that $\omega_1 = \omega_2$ one can see that a component of the second-order polarization will be oscillating at 2ω, giving rise to the second harmonic generation first observed experimentally in 1961 by Franken et al[13]. However, when $\omega_1 \neq \omega_2$ equation 3.4 illustrates that there will be a component of the resulting second-order polarization which is oscillating at the sum of the two incoming frequencies (SFG) and the difference of the two incoming frequencies (DFG).

The intensity of SFG obtained in the laboratory will be proportional to the absolute square of $\chi^{(2)}$. Further, $\chi^{(2)}$ is composed of both a resonant and a nonresonant component. As seen in figure 3.1, the resonant ($\chi_R^{(2)}$) and nonresonant ($\chi_{NR}^{(2)}$) components correspond to when our infrared beam is on and off resonance respectively with a natural vibrational mode of a molecule being probed.

$$\chi^{(2)} = \chi_R^{(2)} + \chi_{NR}^{(2)} \qquad 3.5$$

$$I(\omega_{SFG}) \propto \left|\chi^{(2)}\right|^2 \propto \left|\sum_q \chi_{R,q}^{(2)} + \chi_{NR}^{(2)}\right|^2 \qquad 3.6$$

Where $\chi^{(2)}_{R,q}$ refers to the resonant non-linear susceptibility associated with the qth vibrational mode.

The reason why SFG was chosen as the tool to study surface catalyzed chemical reactions in this thesis is that it is an inherently surface-specific spectroscopy. Signal can only be created due to the presence of an interface. This is true because $\chi^{(2)}$ is a third rank tensor. In a centrosymmetric or isotropic medium such as a bulk metal crystal or isotropic gas phase molecules, there exists inversion symmetry. $\chi^{(2)}$ should be invariant under inversion symmetry as the nonlinear susceptibility in all directions should be equal. However, the electric field and the polarization must change signs as vectors upon the inversion operator. This necessitates that $\chi^{(2)} = -\chi^{(2)}$, which can only take place when $\chi^{(2)} = 0$. Since the SFG intensity is proportional to the absolute square of $\chi^{(2)}$ as seen in equation 3.6, no SFG signal will be obtained from any medium with inversion symmetry. Inversion symmetry has to be broken to order for $\chi^{(2)}$ to be nonzero, which is only necessarily true at an interface, such as the gas-solid interface encountered in heterogeneous catalysis.

The resonant susceptibility, which originates from vibrational modes on the surface, is described by equation 3.7.

$$\chi^{(2)}_R = N\chi^{(2)}_{i,j,k} \sum_{l,m,n} \left\langle (\hat{i}\cdot\hat{l})(\hat{j}\cdot\hat{m})(\hat{k}\cdot\hat{n}) \right\rangle \frac{A_q}{\omega_{IR} - \omega_q + i\Gamma_q} \Delta\rho_{gq} \qquad 3.7$$

where A_q is the strength of the qth vibrational mode, N is the number density of molecules on the surface, ω_{IR} is the frequency of the infrared laser beam, ω_q is the frequency of the qth vibrational mode, Γ_q is the damping constant of the qth vibrational

mode and $\Delta\rho_{gq}$ is the population difference between the ground and first excited states. The subscripts l,m, and n, refer to the axes for the molecular coordinate system and the average $\left\langle (\hat{i}\cdot\hat{l})(\hat{j}\cdot\hat{m})(\hat{k}\cdot\hat{n})\right\rangle$ is the coordination transformation from molecular fixed coordinates to laboratory fixed coordinates averaged over molecular orientations. One can see from equation 3.7 that when $\omega_{IR}=\omega_q$ a maximum is reached in $\chi_R^{(2)}$, therefore, as we scan the infrared laser beam frequency we obtain a vibrational spectrum of molecules adsorbed at the interface. Selection rules for the SFG process can be inferred from equation 3.8.

$$A_q = \frac{1}{2\omega_q}\frac{\partial\mu_n}{\partial q}\frac{\partial\alpha_{lm}^{(1)}}{\partial q} \qquad 3.8$$

where μ_n is the dipole moment and $\alpha_{lm}^{(1)}$ is the Raman polarizability. Therefore, in order for $\chi_{R,q}^{(2)}$ to be non-zero, the vibrational mode of interest must be both IR and Raman active. During the course of the vibrational motion, there must be both a change in dipole moment and a change in polarizability.

3.2 Sum Frequency Generation from a Surface

The nonlinear susceptibility tensor $\chi^{(2)}$ is a third rank tensor with 27 elements. However, due to symmetry constraints many of these elements vanish. An interface contains C_∞ symmetry as it is entirely symmetric in the x-y plane. These concerns reduce the 27-element tensor to seven non-vanishing components, of which only four are independent.

$$\chi_{xxz}^{(2)}=\chi_{yyz}^{(2)},\chi_{xzx}^{(2)}=\chi_{yzy}^{(2)},\chi_{zxx}^{(2)}=\chi_{zyy}^{(2)},\chi_{zzz}^{(2)} \qquad 3.9$$

where the x and y axes are in the plane of the surface, and the z axis perpendicular to the interface surface. If we consider x to be the axis pointing towards the incoming laser beam, we see that p-polarized laser light will interact with dipoles with some projection in the x-z plane while s-polarized light will interact with dipoles with a projection on the x-y plane of the surface. Therefore, using different polarization combinations will probe different components of the $\chi^{(2)}$ tensor. However, only some polarization combinations will probe non-zero components of $\chi^{(2)}$. Four possible combinations of polarization are available to probe the non-zero components of $\chi^{(2)}$: ppp, ssp, sps and pss, where the polarizations are listed in order of decreasing frequency (SFG, visible beam, IR).

By changing the polarization combinations used in an experiment, one can glean information about the molecular orientation of molecules at an interface.[14] However, over a metal surface such as those used in this thesis, these methods do not apply as we are limited by the metal-surface-selection-rule (MSSR). Any time a dipole is created over metal surface, the electrons within the metal instantaneously create an "image dipole". The process is depicted in figure 3.2. As can be seen, if a vibrational mode is excited parallel to a metal surface, the image dipole instantly cancels the vibrational dipole. Hence infrared spectroscopies (and thus SFG) are blind to any mode with an oscillating dipole perfectly parallel to the metal surface. However, if there is any component of a vibrational mode dipole which is perpendicular to the metal surface, the image dipole actually enhances the overall dipole created.

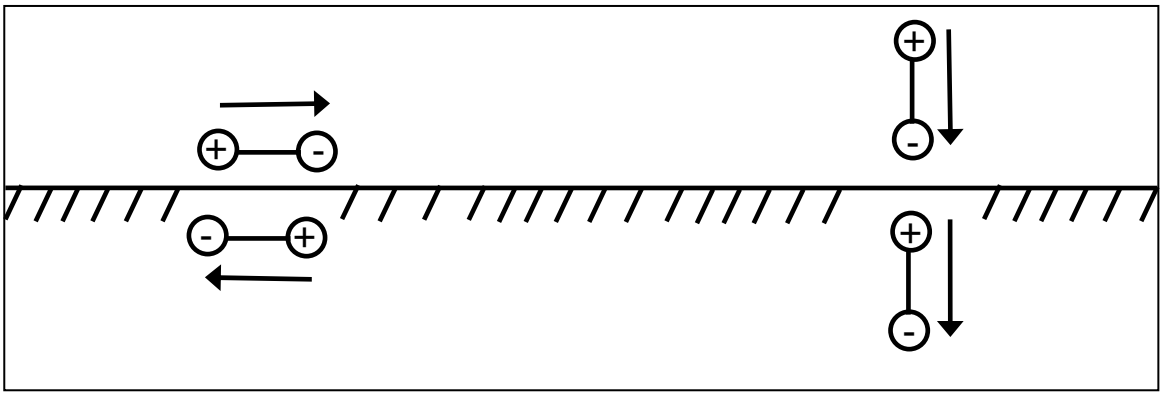

Figure 3.2. The image dipole created in a metal surface in response to a parallel dipole (left) and a perpendicular dipole (right)

The concept of the metal surface selection rule can be used in certain circumstances to elucidate if a hydrocarbon is adsorbed to a metal surface in an "upright" or "parallel" orientation. The use of this technique has been applied in this thesis at times and is documented in the literature[15]. The symmetric and asymmetric vibrations of methylene and methyl group have orthogonal dipoles. This is depicted in figure 3.3 for a methyl group.

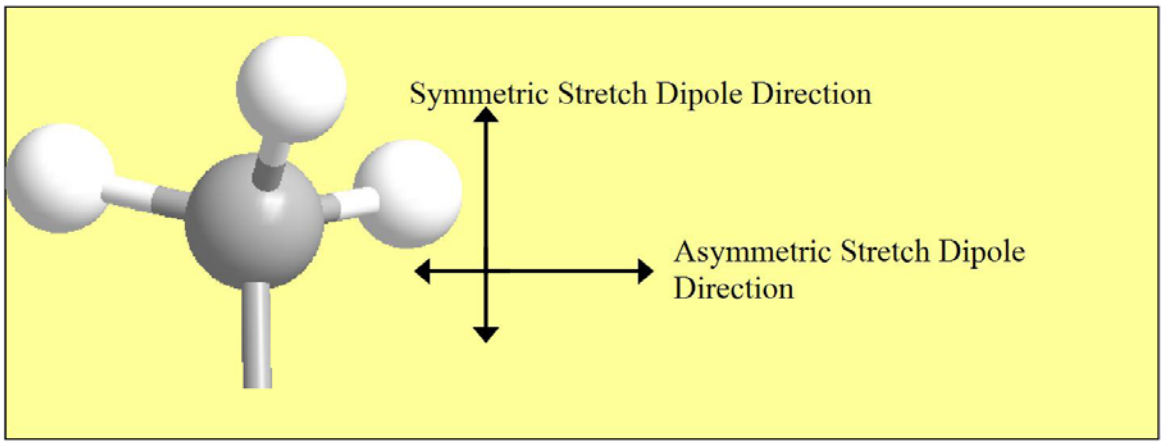

Figure 3.3. Schematic of a methyl group with its associated symmetric and asymmetric stretch dipole directions.

If one assumes that the molecular axis of the methyl group in figure 3.3 is perpendicular to a metal surface, a vibrational spectrum would yield a very strong methyl symmetric stretch peak, but a vanishing asymmetric peak. Similar arguments can be used for methylene groups. If one assumes that the molecular axis of the methyl group in figure 3.3 is parallel to a metal surface, a vibrational spectrum of this species would yield a very strong methyl asymmetric stretching mode, but no symmetric peak. In this way, a careful examination of the peak intensities in a vibrational spectrum over a metal surface can often lead towards a qualitative understanding of the molecular orientation.

3.3 Sum Frequency Generation Laser System

A commercial laser system was employed for all research done for this thesis. It is a mode-locked Nd:YAG laser (Leopard D20, Continuum) which creates radiation with a 20 picosecond long pulse at a 20 Hz repetition rate at 1064 nm. The 1064 light is beam-split. Some of the 1064 nm beam enters a KTP crystal where it frequency doubles to generate a 532 nm beam. This 532 nm beam is also beam-split, with half of it being sent out to the sample for SFG experiments, and the other half sent into an optical parametric generator (OPG) stage using two simultaneously tuning KTP crystals to prevent beam-walk to generate tunable light at ~800 nm and ~1200 nm. The ~800 nm light is sent to an optical parametric amplification stage where it combines with the residual 1064 nm light in two KTA crystals doing difference frequency generation to yield infrared light which we can tune from ~2000 cm^{-1} to 4500 cm^{-1} by tuning the ~800 nm beam leaving the OPG.

Typically, beam energies of roughly 200 μJ for both the visible 532 nm beam and the IR beam were used. The IR and VIS beams were intentionally collimated at about 1

cm^2 beam spot size so as to avoid ablating the metal surface. The VIS beam and IR beam were spatially and temporally overlapped on the catalyst surface of interest with incident angles of 55° and 60° with respect to the surface normal respectively for single crystal catalyst studies. For nanoparticle studies, the two laser beams were overlapped inside a fused silica prism and the evanescent wave was used to interrogate the nanoparticle surfaces. The resulting SFG beam was directed through a motorized monochromator to filter out any unwanted noise, and the signal-to-noise ratio was further enhanced by using a gated integrator to acquire and average the signal.

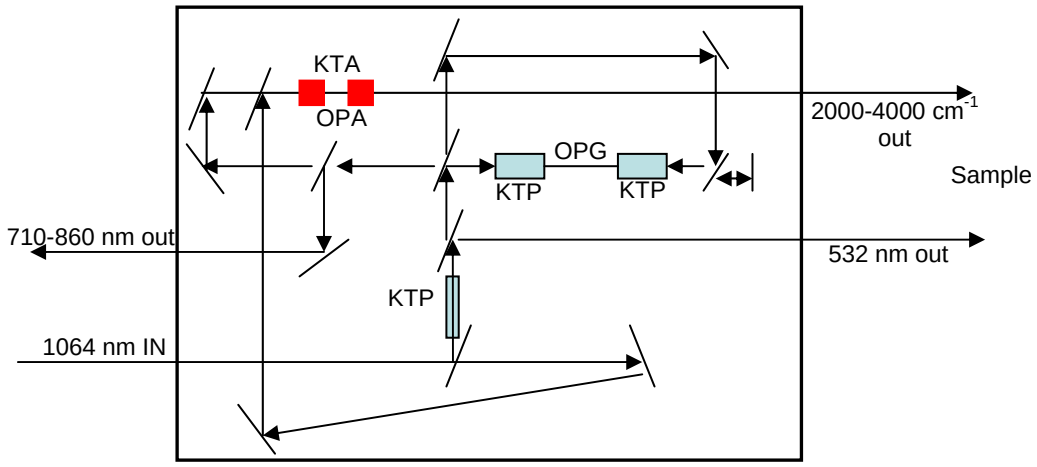

Figure 3.4. Schematic of the LaserVision OPG/OPA system for generating the 532 nm and tunable infrared beams for use in experiment.

References

(1) Bloember.N; Chang, R. K.; Jha, S. S.; Lee, C. H. *Physical Review* **1968**, *174*, 813.

(2) Bass, M.; Hill, A. E.; Franken, P. A.; Peters, C. W.; Weinreich, G. *Physical Review Letters* **1962**, *8*, 18.

(3) Hunt, J. H.; Guyotsionnest, P.; Shen, Y. R. *Chemical Physics Letters* **1987**, *133*, 189.

(4) Zhu, X. D.; Suhr, H.; Shen, Y. R. *Physical Review B* **1987**, *35*, 3047.

(5) Zhu, X. D.; Suhr, H. J.; Shen, Y. R. *Journal of the Optical Society of America B-Optical Physics* **1986**, *3*, P252.

(6) Lambert, A. G.; Davies, P. B.; Neivandt, D. J. *Applied Spectroscopy Reviews* **2005**, *40*, 103.

(7) Shen, Y. R. *Annual Review of Physical Chemistry* **1989**, *40*, 327.

(8) Shen, Y. R. *Nature* **1989**, *337*, 519.

(9) Shen, Y. R. *Surface Science* **1994**, *299*, 551.

(10) Shen, Y. R. *The Principles of Nonlinear Optics*; John Wiley & Sons: New Jersey, 2003.

(11) Du, Q.; Superfine, R.; Freysz, E.; Shen, Y. R. *Physical Review Letters* **1993**, *70*, 2313.

(12) Johal, M. S.; Ward, R. N.; Davies, P. B. *Journal of Physical Chemistry* **1996**, *100*, 274.

(13) Franken, P. A.; Weinreich, G.; Peters, C. W.; Hill, A. E. *Physical Review Letters* **1961**, *7*, 118.

(14) Hirose, C.; Yamamoto, H.; Akamatsu, N.; Domen, K. *Journal of Physical Chemistry* **1993**, *97*, 10064.

(15) Yang, M.; Somorjai, G. A. *Journal of the American Chemical Society* **2004**, *126*, 7698.

Chapter 4

Pyrrole Hydrogenation over Rh(111) and Pt(111) Single-Crystal Surfaces and Hydrogenation Promotion Mediated by 1-Methylpyrrole: A Kinetic and Sum-Frequency Generation Vibrational Spectroscopy Study

Sum frequency generation surface vibrational spectroscopy and kinetic measurements using gas chromatography have been used to study the adsorption and hydrogenation of pyrrole over both Pt(111) and Rh(111) single-crystal surfaces at Torr pressures (3 Torr pyrrole, 30 Torr H_2) to form pyrrolidine and the minor product butylamine. Over Pt(111) at 298K it was found that pyrrole adsorbs in an upright geometry cleaving the N-H bond to bind through the nitrogen as evidenced by SFG data. Over Rh(111) at 298K pyrrole adsorbs in a tilted geometry relative to the surface through the π-aromatic system. A pyrroline surface reaction intermediate, which was not detected in the gas phase, was seen by SFG during the hydrogenation over both surfaces. Significant enhancement of the reaction rate was achieved over both metal surfaces by adsorbing 1-methylpyrrole prior to reaction. SFG vibrational spectroscopic results indicate that reaction promotion is achieved by weakening the bonding between the N-containing products and the metal surface due to lateral interactions on the surface between 1-methylpyrrole and the reaction species, reducing the desorption energy of the

products. It was found that the ring-opening product butylamine was a reaction poison over both surfaces, but this effect can be minimized by treating the catalyst surfaces with 1-methylpyrrole prior to reaction. The reaction rate was not enhanced with elevated temperatures, and SFG suggests desorption of pyrrole at elevated temperatures.

4.1. Introduction

Catalytic reactions involving aromatic cyclic and heterocyclic molecules are important for the chemical industry for both fuel reforming and environmental concerns.[1] Due to the importance of surface interactions for heterogeneous catalysis, the adsorption of six-membered molecules, e.g. benzene and pyridine, has been studied on various metal surfaces.[2-6] Although five-membered ring systems are reaction intermediates in a number of catalytically important processes, they have received comparatively much less attention in surface science related research. This is partly explainable by the reduced stability of five-membered ring systems as compared to their six-membered analogues which makes the former less attractive for model studies since surface chemistry is expected to become more complex upon or following adsorption.

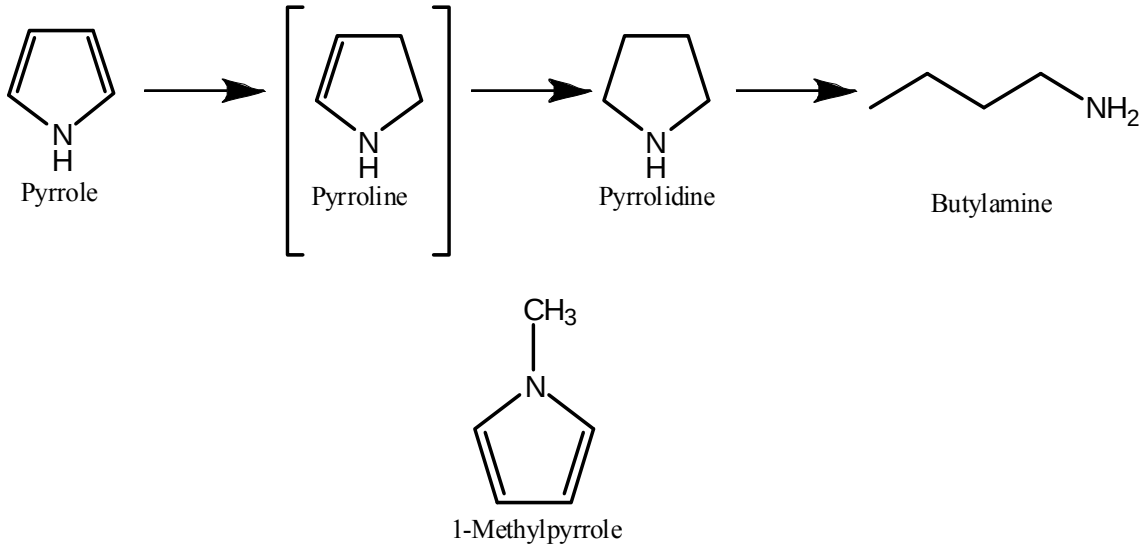

Scheme 4.1. (Top) Reaction mechanism for pyrrole hydrogenation. The intermediate pyrroline is not detected in the gas phase. (Bottom) The structure of 1-methylpyrrole.

Pyrrole (C_4H_5N) is a five-membered aromatic ring system (Scheme 4.1) in which the lone pair of electrons of nitrogen is delocalized over the π-system of the ring. The adsorption of pyrrole on both Pt(111)[7] and Rh(111)[8] metal surfaces has been studied to provide some insight into the five-membered heterocyclic bonding characteristics. The studies mentioned above showed that the adsorption geometry of pyrrole is sensitive to the type of metal substrate. Based on a NEXAFS study it was concluded that pyrrole adsorbs normal to the Pt(111) surface with the nitrogen as the anchoring point, which results in cleavage of the N-H bond.[7] Annealing of the pyrrole ad-layer in the absence of hydrogen further resulted in the dissociation of pyrrole leaving N-containing species on the Pt(111) surface. In contrast, on Rh(111), a study using angle resolved UV photoelectron spectroscopy (ARUPS), indicates that pyrrole is adsorbed at low temperature with its ring parallel to the surface, but a fraction of molecules splits off the

N-hydrogen bond between 150 and 300 K allowing bonding interaction with the surface via the nitrogen.[8]

It has long been known that nitrogen-containing compounds have inhibiting effects on the catalysts used for hydrogenation, due to their unshared pair of electrons. These poisoning effects can be reduced over Pt catalysts by conversion of these reactants into a form in which the nitrogen atom is shielded, e.g. by adding protic acids.[9-13] The hydrogenation of pyrrole derivatives was kinetically studied by Adkins and co-workers[14-16] over Raney nickel and other catalysts and later studies report on hydrogenation over supported precious metal catalysts (Pd/C, Ru/C, Rh/C, and Rh/Al_2O_3) in liquid phase by Hegedűs et al.[17-22] Under relatively mild reaction conditions (25-80 °C) and by using non-acidic solvents the hydrogenation of pyrrole derivatives showed higher activities on Rh than on Pt supported catalysts.

In this study, SFG vibrational spectroscopy and initial reaction turnover rates monitored by gas chromatography (GC) were used for the first time to investigate and verify surface species present during pyrrole hydrogenation (3 Torr of pyrrole) in the presence of excess hydrogen (30 Torr) over Rh(111) and Pt(111) single-crystal surfaces. Linear spectroscopies, such as infrared absorption, Raman, as well as electron spectroscopies typically cannot be employed under relevant catalytic reaction conditions (high pressure) due to the absorption by bulk gases, which masks the relatively small amount of absorption generated by adsorbed species at the catalyst surface. Because SFG is a second order nonlinear optical process, media with centrosymmetry and isotropic gases do not appear in the SFG spectrum under the electric dipole approximation.[23] Since bulk Rh and Pt have a center of inversion, its contribution to the SFG signal is negligible.

Because the symmetry is broken at the Rh and Pt single-crystal surfaces, SFG signal arises solely from the adsorbates. For these reasons, SFG is an ideal tool to monitor surface species under reaction conditions.

It has previously been reported in the literature that the co-adsorption of a large organic molecule on a catalyst surface can lead to enhanced hydrogenation reaction rates.[24-26] If the additive has a basic component that can interact laterally with neighboring adsorbates, it has been suggested this lateral adsorbate interaction can play a role in this promotion.[24] It has also been suggested that the co-adsorbed molecules can act as a hydrogen transfer agent to neighboring molecules, or to the catalyst surface increasing the surface coverage of hydrogen.[25,26] In this study, we found that adsorbing 1-methylpyrrole on the Rh(111) and Pt(111) surfaces prior to pyrrole hydrogenation significantly promotes the reaction rate. Gas chromatography measurements indicate that the production of ring-cracking products that poison the catalyst surface is significantly reduced in the presence of 1-methylpyrrole. Furthermore, blue-shifts of the amine vibrational modes to higher energies indicate that the interaction between nitrogen containing moieties of the reaction species and the surface is weakened when treated with 1-methylpyrrole prior to reaction favoring the desorption of reaction products and thus enhancing the hydrogenation rates.

4.2. Experimental Section

Materials

Prior to use, pyrrole (98%, Sigma-Aldrich Inc.), pyrrolidine (99%, Sigma-Aldrich Inc.), 1-methylpyrrole (99+%, SAFC Supply Solutions) and butylamine (≥99.5%, Fluka) were subjected to several freeze-pump-thaw cycles and the purities were checked by means of gas chromatography.

The high-pressure/ultra-high vacuum system

All experiments reported here were carried out in a high-pressure/ultrahigh-vacuum (HP/UHV) system. The UHV chamber is operated at a base pressure of 2 x 10^{-10} Torr and is isolated from the HP cell by a gate valve. The UHV system is equipped with an Auger electron spectrometer (AES), a quadrupole mass spectrometer (Stanford Research Systems) and an ion bombardment gun (Eurovac). The HP cell consists of two CaF_2 conflat windows that allow transmission of infrared (IR), visible (VIS) and sum frequency radiation for sum frequency generation (SFG) experiments. The product gases in the HP cell are constantly mixed via a recirculation pump and kinetic data is acquired by periodically sampling the reaction mixture and analyzing the relative gas phase composition in a flame ionization detector (FID) of a gas chromatograph (Hewlett Packard HP 5890 on a 5% Carbowax 20M packed column). For the study of promotion effects mediated by 1-methylpyrrole, 100 millitorr 1-methylpyrrole was dosed into the HP cell and recirculated in the presence of the corresponding single-crystal for 5 min. The HP cell was then evacuated and the reactants were added to the HP cell.

Sample preparation

Prior to each experiment, the Rh(111) and Pt(111) crystal surfaces were cleaned in the UHV chamber by Ar^+ (700 eV for Rh and 1 keV for Pt) sputtering for 20 min at about 3 x 10^{-5} Torr of Ar. After sputtering, the crystals were heated to 1103 K in the presence of O_2 of 5 x 10^{-7} Torr and annealed at the same temperature for 2 min. The cleanliness of the crystal surfaces was verified by AES and the crystallographic structure verified with low energy electron diffraction (LEED). The samples were then transferred into the HP cell for SFG and kinetic studies.

Sum Frequency generation vibrational spectroscopy

For SFG measurements, an active/passive mode-locked Nd:YAG laser (Leopard D-20, Continuum) with a pulse width of 20 ps and a repetition rate of 20 Hz was used. The fundamental output at 1064 nm was sent through an optical parametric generation/amplification (OPA/OPG) stage where a tunable IR (2300—4000 cm^{-1}) and a second harmonic VIS (532 nm) beam were created. The IR (150 μJ) and VIS (200 μJ) beams were spatially and temporally overlapped on the crystal surface at angles of incidence of 55 and 60°, respectively, with respect to the surface normal. The generated SFG beam was collected and sent through a motorized monochromator equipped with a photomultiplier tube to detect the SFG signal intensity. The signal-to-noise ratio was further increased by using a gated integrator while the IR beam was scanned through the spectral region of interest. The SFG process is enhanced when the IR beam comes into resonance with a vibrational mode of a molecule adsorbed at the surface, giving rise to a vibrational spectrum of adsorbed species. More information on the HP/UHV system and SFG measurement can be found elsewhere.[23,27-31]

4.3. Results and Discussion

4.3.1. Pyrrole Hydrogenation on Pt(111) and Rh(111) Single-Crystals under 3 Torr Pyrrole and 30 Torr Hydrogen: Turnover Rates, Selectivities, Deactivation, and Reaction Promotion by 1-Methylpyrrole.

Figure 4.1 displays the production of pyrrolidine as turnover rates (TOR, pyrrolidine molecules formed per metal surface atom per second) for both the Pt(111) (—■—) and Rh(111) (—●—) surfaces as a function of time under 3 Torr pyrrole and 30 Torr hydrogen at room temperature. Over both surfaces the major product was the full

hydrogenation of the aromatic pyrrole ring to form pyrrolidine (see Scheme 4.1). Over Pt(111) the TOR at one hour reaction time at room temperature was found to be 0.049 (±0.003) and very little deactivation of the catalyst was observed, while over Rh(111) at room temperature and at one hour the TOR was 0.053 (±0.018) and the TOR deactivated by 54% during the first hour of reaction. The turnover rates over Pt(111) and Rh(111) in the gas phase were therefore very similar, with the only difference being that Rh(111) exhibits deactivation, while Pt(111) does not. Whereas, in the liquid phase work by Hegedűs et al,[17] Rh on carbon exhibited an initial rate 62.5 times faster than Pt on carbon for the hydrogenation of pyrrole derivatives. We further investigated the temperature dependence of this reaction ranging from 298-413 K over both surfaces, but the rate of formation of pyrrolidine was not enhanced with temperature, and at elevated temperatures reaction deactivation was observed.

Figure 4.1 demonstrates the significant effect adsorbing 1-methylpyrrole on the surface prior to reaction has on the rate of pyrrole hydrogenation over both surfaces. On the Rh(111) surface a 17 fold rate enhancement is achieved by exposing the crystal to 100 millitorr 1-methylpyrrole preceding the reaction (—▲—), and no deactivation was seen after six hours of reaction time. This is an indication that the 1-methylpyrrole does not leave the Rh(111) surface during the course of the reaction as the promotion does not deactivate. The Pt(111) (—♦—) surface also demonstrated a significantly enhanced initial rate, by a factor of 17 fold, when 1-methylpyrrole is first adsorbed on the surface, but the reaction rate slows down by more than 80% within the first hour of hydrogenation.

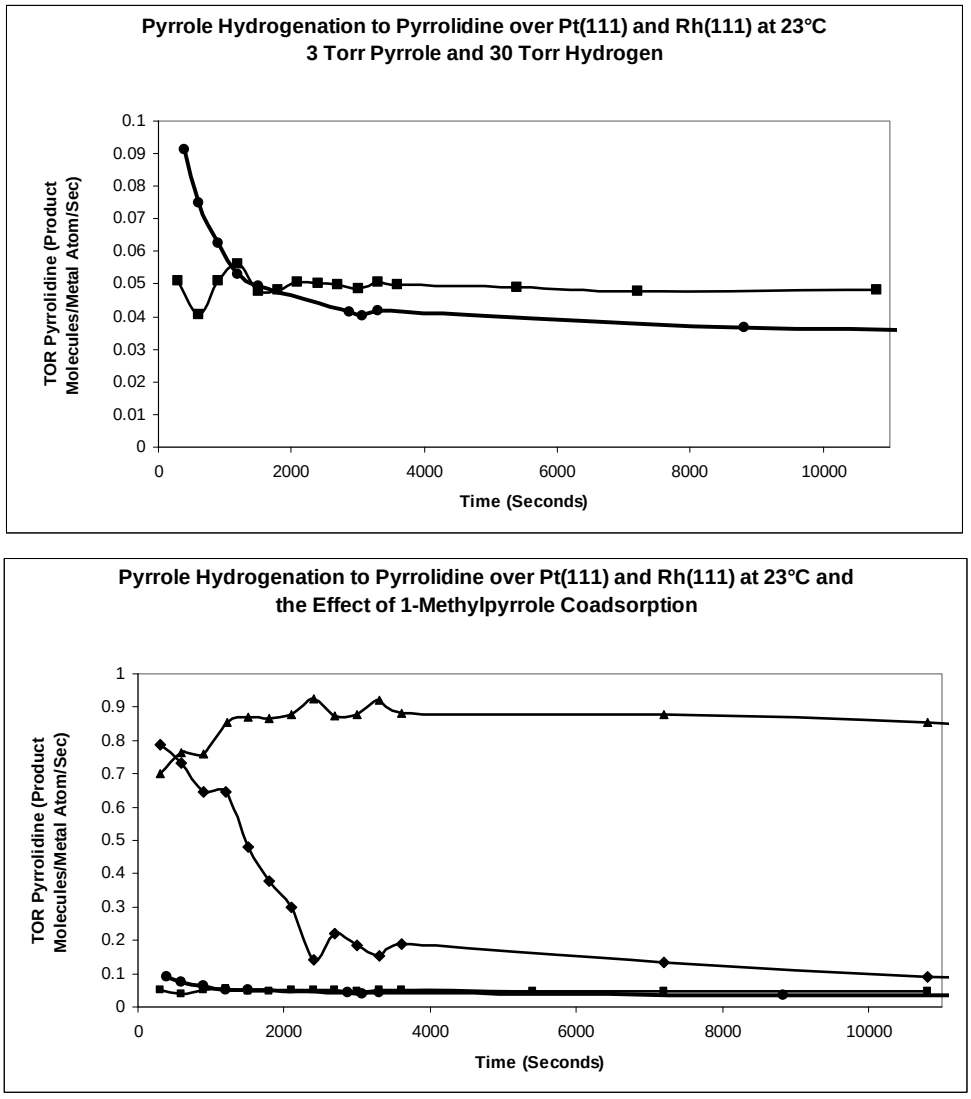

Figure 4.1. Turnover rates (pyrrolidine molecules formed per metal surface atom per second) for the formation of pyrrolidine as a function of time over Pt(111) (—■—) and Rh(111) (—●—) (included in both plots) as compared with Pt(111) dosed with 100 millitorr 1-methylpyrrole prior to reaction (—♦—) and Rh(111) dosed with 100 millitorr 1-methylpyrrole prior to reaction (—▲—) under 3 Torr pyrrole and 30 Torr H_2.

Table 4.1 shows the selectivities for this reaction over both catalyst surfaces at 298K observed with GC. As can be seen, by breaking a N-C bond, the pyrrolidine ring can crack on the surface to form the minor product butylamine. Further cracking to lighter compounds is seen only on Rh(111), while Pt(111) exhibits the highest tendency for ring opening. The adsorption of 1-methylpyrrole on the metal surfaces prior to reaction affects the reaction selectivities. Over both surfaces the selectivity for the formation of butylamine is greatly reduced. Once again the effect of elevated temperatures was studied for the 1-methylpyrrole promoted pyrrole hydrogenations, but it led to a significant deactivation of the reaction, not following Arrhenius type behavior.

Catalyst	pyrrolidine (%)	butylamine (%)	light cracking products (%)
Pt(111)	95.4	4.6	0
Rh(111)	97.7	1.5	0.8
Pt(111) pre-adsorbed with 1-methylpyrrole	99.3	0.7	0
Rh(111) pre-adsorbed with 1-methylpyrrole	99.9	0.1	0

Table 4.1. Selectivities of reaction products (given in %) after one hour of pyrrole hydrogenation (3 Torr pyrrole, 30 Torr H_2) over the corresponding catalyst surfaces.

4.3.2. Surface Species during Reaction on Unpromoted Pt(111) and Rh(111): Sum Frequency Generation Vibrational Spectroscopy Results.

The gas phase infrared spectrum for pyrrole exhibits only two vibrational resonances in the 2700-3600 cm^{-1} region, an aromatic N-H stretch at 3530 cm^{-1} and an aromatic C-H stretch at 3128 cm^{-1}.[32-34] Table 4.2 displays vibrational resonances for pyrrole,[32-35] pyrrolidine,[36] and butylamine[37,38] in the gas phase. The appearance of vibrational modes in the C-H region below 3000 cm^{-1} indicates hydrogenated products exist on the surface, as pyrrole has no such vibrational modes.

Assignment	Pyrrole	pyrrolidine	Butylamine
$\nu_{sym}(CH_2)$		2825 and 2882	2858
$\nu_{sym}(CH_3)$			2868
$\nu_{asym}(CH_2)$		2967	2908
$\nu_{asym}(CH_3)$			2960
$\nu_{aromatic}(CH)$	3128		
$2\delta(NH_2)$			3180
$\nu_{sym}(NH_2)$			3340
N (NH)		3367	
$\nu_{asym}(NH_2)$			3403
$\nu_{aromatic}(NH)$	3530		

Table 4.2. Summary of gas-phase vibrational modes (given in cm^{-1}) of pyrrole,[32,34,35] pyrrolidine,[36] and butylamine[37,38] in the spectral region between 2700 and 3600 cm^{-1}.

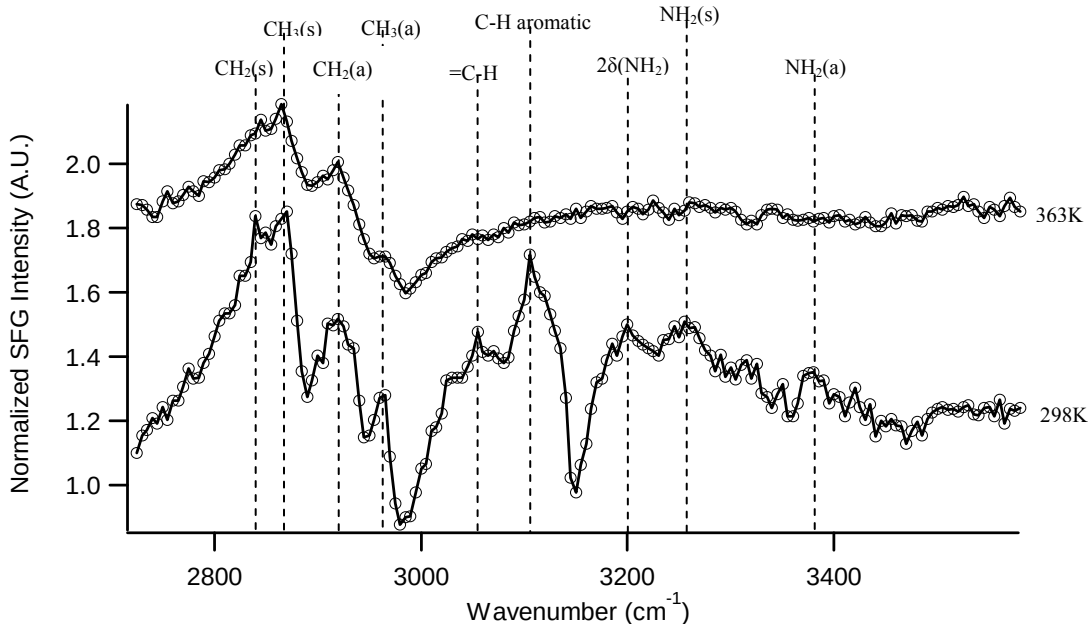

Figure 4.2 SFG vibrational spectra recorded during pyrrole hydrogenation (3 Torr pyrrole, 30 Torr H_2) over Pt(111). The spectrum depicted at the bottom was recorded at 298 K and the one depicted on top at 363 K.

Figure 4.2 shows the SFG vibrational spectra of 3 Torr pyrrole and 30 Torr hydrogen over Pt(111) at both 298 and 363K. The spectrum recorded at room temperature is characterized by nine vibrational resonances. The aromatic stretch at 3105 cm^{-1} indicates that an intact aromatic ring is adsorbed on the surface. The metal surface selection rule (MSSR)[39,40] states that vibrational modes parallel to a metal surface do not appear in the SFG vibrational spectrum, whereas vibrational modes with a component perpendicular to the surface are enhanced by the metal surface. Due to the appearance of the aromatic stretch in the spectrum we conclude that the aromatic ring must be standing with some component normal to the surface. Interestingly, there is no aromatic N-H stretch seen in this spectrum, but a strong C-H aromatic vibrational band. From this we can conclude that the pyrrole molecule adsorbs to the Pt(111) surface by cleaving the N-H bond,

standing perpendicular to the surface, maintaining the aromaticity of the ring as can be seen in Figure 4.3.

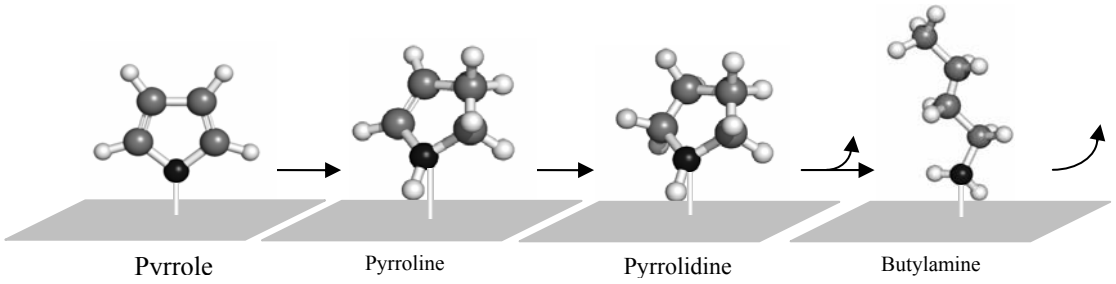

Figure 4.3 Proposed molecular adsorption and reaction pathway over Pt(111). Pyrrole adsorbs perpendicularly by cleaving the N-H bond. Once the aromaticity is broken by the hydrogenation of one of the double bonds, the molecule binds to the Pt(111) surface through the lone pair of electrons on the nitrogen. The subsequent hydrogenation of the ring yields pyrrolidine molecules, some fraction of which may undergo ring-opening and hydrogenation to yield butylamine before desorption.

This adsorption mode is an agreement with a previous NEXAFS work done by Tourillon et al.[7] The symmetric and asymmetric stretch of both the CH_3 and CH_2 groups can be seen for pyrrole hydrogenation on Pt(111). Firstly, this indicates that the hydrogenated products exist on the surface. Secondly, this is proof of the existence of the ring-opening product butylamine on the surface due to the clear presence of the CH_3 modes, which do not exist in the ring structure of pyrrolidine. A stretch also appears at 3055 cm^{-1} which is assigned to the vinylic stretch of pyrroline (Figure 4.3), which arises on the surface due to the hydrogenation of one of the double bonds in the pyrrole ring. Pyrroline is thus a surface reaction intermediate seen only in the SFG vibrational spectrum, as this product was not evolved in detectable amounts by GC during reaction.

The N-H peaks seen from 3200 cm^{-1} to 3400 cm^{-1} on Pt(111) are all quite broad and do overlap with each other. However, three peaks are distinguishable at 3200 cm^{-1}, 3258 cm^{-1}, and 3380 cm^{-1}. The presence of these three peaks suggests a primary amine and agrees well with the vibrational spectrum of butylamine, and we assign these peaks to $2\delta(NH_2)$ = 3200 cm^{-1}, $\nu_{sym}(NH_2)$ = 3258 cm^{-1}, and $\nu_{asym}(NH_2)$ = 3380 cm^{-1}. The broadness of the features in this region suggests that there may be more N-H species present on the surface, such as the N-H stretch of pyrrolidine, but this cannot be elucidated from these studies. Spectra of pyrrole in the absence of excess hydrogen were also taken, but were identical to those recorded in the presence of excess hydrogen.

To investigate why this reaction shows deactivation upon heating rather than Arrhenius rate enhancement, the SFG vibrational spectrum was taken on Pt(111) at 363K (see Figure 4.2, top spectrum). Upon heating the Pt(111) to 363K, all peaks except those corresponding to CH_3 and CH_2 groups vanish. An explanation for this is that the pyrrole ring itself is not strongly bound and desorbs from the surface, and the other reactive intermediates on the surface (pyrroline, pyrrolidine, and butylamine) must either then be desorbed or become bound in such a way that nitrogen contains no hydrogen bonds, such as forming a relatively strong N=Pt bond. In either case, desorption or the formation of an N=Pt bond, this helps to explain the non-Arrhenius behavior of this reaction.

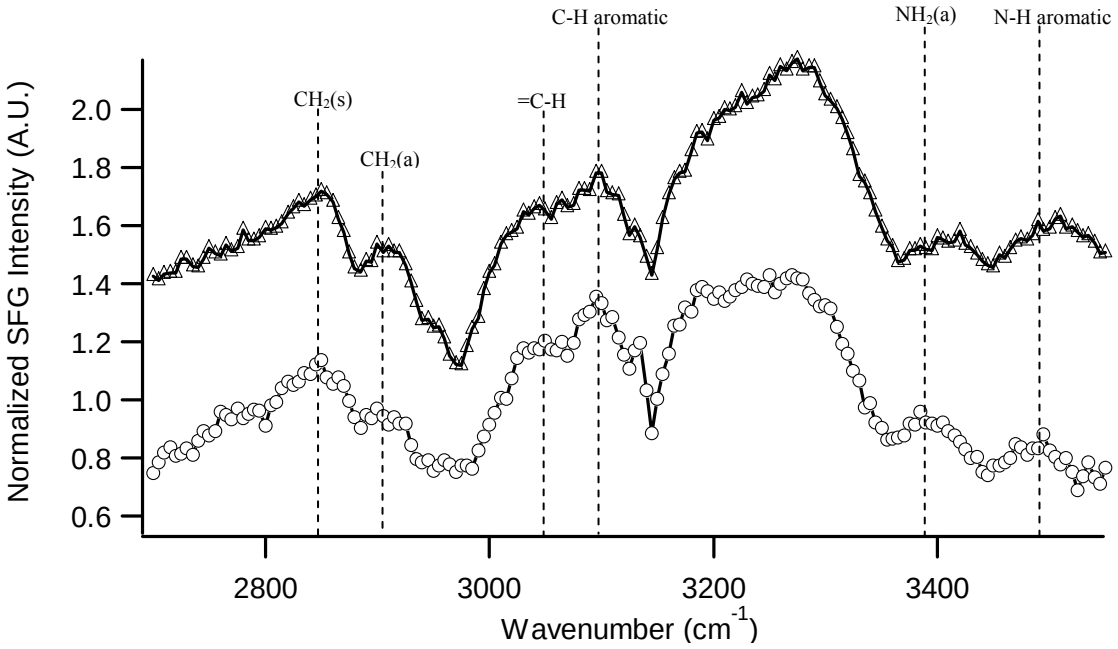

Figure 4.4 The bottom spectrum (—○—) is the SFG vibrational spectrum of 3 Torr pyrrole and 30 Torr hydrogen on Rh(111). The top spectrum (—△—) is of 3 Torr pyrrole and 30 Torr hydrogen on Rh(111) that was dosed with 100 millitorr 1-methylpyrrole prior to reaction.

Figure 4.4 displays the SFG vibrational spectrum (bottom) of 3 Torr pyrrole and 30 Torr hydrogen on Rh(111). The CH_2 stretches are clearly seen at $\nu_{sym}(CH_2) = 2850$ cm^{-1} and $\nu_{asym}(CH_2) = 2905$ cm^{-1}. Similarly to Pt(111), a ν(=CH) peak can be seen at 3048 cm^{-1}, indicating the presence of the partially hydrogenated ring. The aromatic C-H stretch is seen at 3095 cm^{-1} indicating an intact aromatic ring adsorbed to the surface with a component perpendicular to it. This mode is 10 cm^{-1} further red-shifted than the aromatic C-H seen on Pt(111), which suggests a more electron donating interaction between the π-aromatic system and the Rh(111) surface than on the Pt(111) surface. The N-H modes on Rh(111) are very pronounced (see Figure 4.4), however the region from 3180 cm^{-1} to

3300 cm^{-1} becomes one broad feature comprised of several strong N-H vibrational modes. However, two bands are clearly visible at 3385 cm^{-1} and 3495 cm^{-1}. These are assigned to $\nu_{asym}(NH_2)$ = 3385 cm^{-1} and an aromatic N-H at 3495 cm^{-1}. Due to the fact that both the aromatic C-H and the aromatic N-H modes are seen on Rh(111) the proposed adsorption mode is tilted with respect to the surface bonding through the π-aromatic system (Figure 4.5).

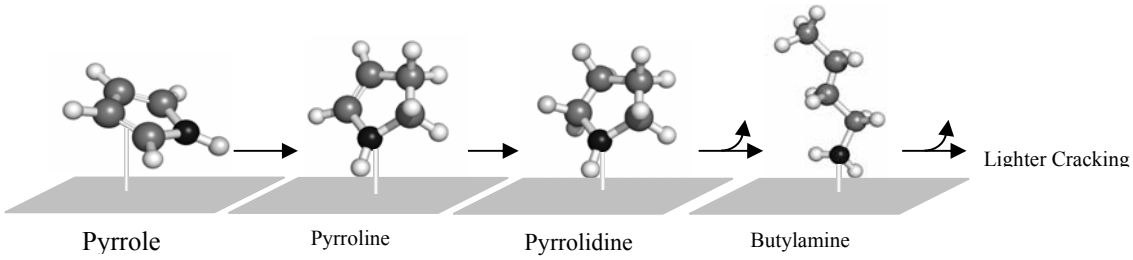

Figure 4.5. Proposed molecular adsorption and reaction pathway over Rh(111). Pyrrole adsorbs in a tilted geometry to the surface bonding through the aromatic π system. Once the aromaticity is broken by hydrogenating one of the ring double bonds, the molecule binds to the Rh(111) surface through the lone pair of electrons on nitrogen, which is followed by ring saturation. The molecule may either then desorb to form pyrrolidine, or crack the ring to form butylamine and desorb. On Rh(111) a very small fraction of molecules further decomposes to lighter products.

This suggested adsorption mode is also in agreement with work by Netzer et al.[8] which suggested the coexistence of both parallel and tilted pyrrole molecules on Rh(111) at room temperature. Though we can say with certainty that the tilted mode exists, we cannot rule out the possibility of a coexistence of a parallel adsorption mode based on the SFG vibrational results as such a molecule would not yield any SFG vibrational signature over a metal surface.

4.3.3. Surface Species During the Pyrrole Hydrogenation Reaction on Pt(111) and Rh(111) Promoted by the Adsorption of 1-Methylpyrrole Prior to Reaction: Sum Frequency Generation Vibrational Spectroscopy Results.

The adsorption of 1-methylpyrrole over Pt(111) has been studied by Tourillon et al.[7] with NEXAFS, and it was found that 1-methylpyrrole is stable against dissociation on the surface, and was likely to desorb intact at elevated temperatures, while pyrrole was found to dissociate into N-containing species as the temperature was increased. The SFG vibrational spectrum of 5 Torr 1-methylpyrrole on Pt(111) was taken and can be seen in Figure 4.6.

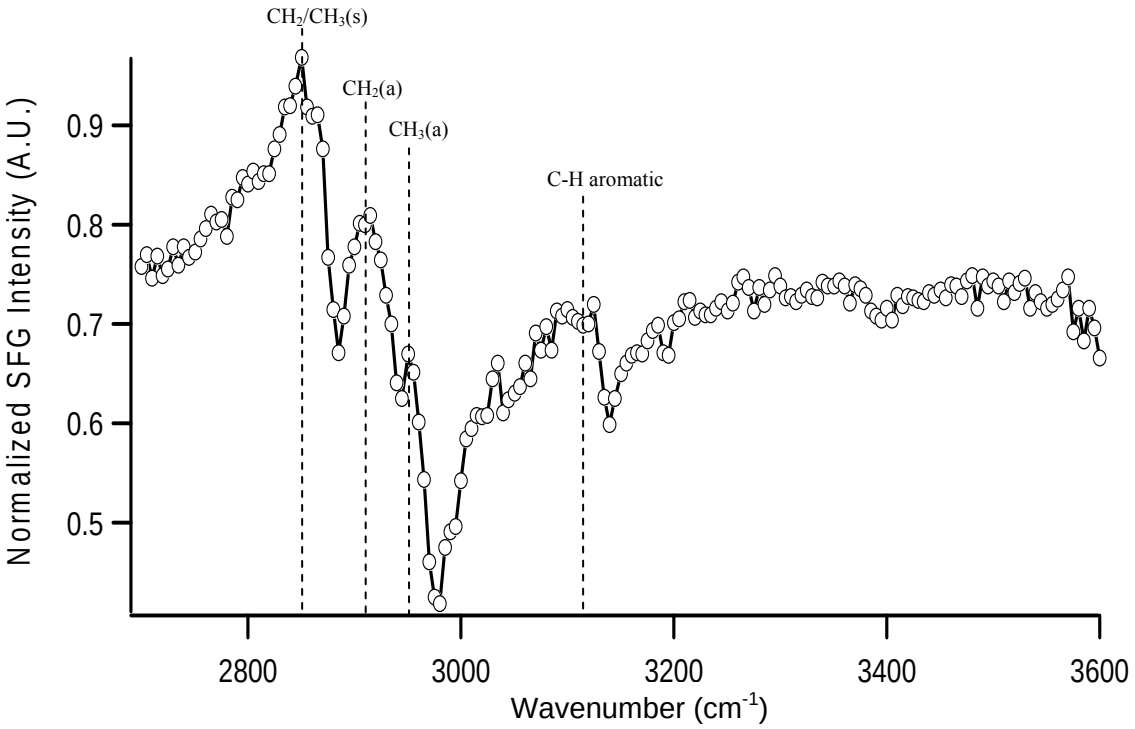

Figure 4.6. SFG vibrational spectrum recorded under 5 Torr 1-methylpyrrole over Pt(111).

No N-H modes are seen in the spectrum, indicating that the molecule is much more stable on the Pt(111) surface than pyrrole towards ring opening. The aromatic C-H stretch is seen at 3130 cm^{-1}, and the corresponding CH_3 and CH_2 stretches are also seen.

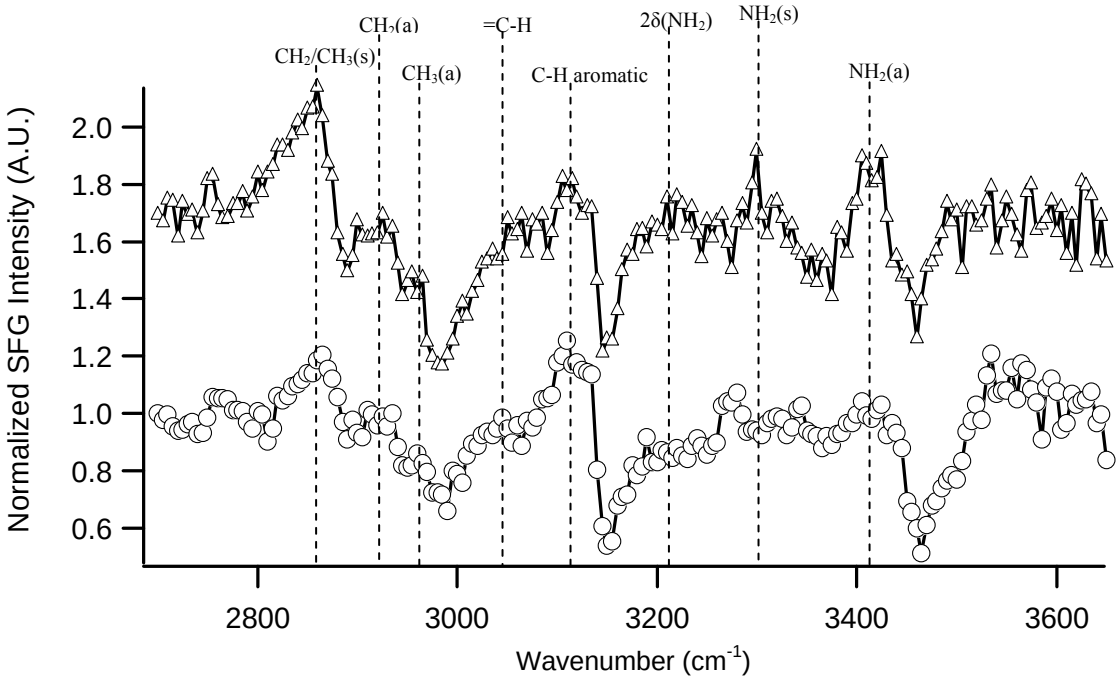

Figure 4.7. SFG vibrational spectra of 3 Torr pyrrole and 30 Torr hydrogen on Pt(111) after exposing the surface to 100 millitorr 1-methylpyrrole for five minutes. The bottom spectrum (—○—) was taken within one hour of reaction time. The top scpectrum (—△—) was taken from one to three hours.

Figure 4.7 displays the spectrum of pyrrole hydrogenation on Pt(111) following an exposure to 100 millitorr of 1-methylpyrrole. To investigate the significant deactivation seen kinetically over Pt(111) pre-treated with 1-methylpyrrole the bottom spectrum was taken during the first hour of reaction, and the top spectrum was averaged from one to three hours after initiating the reaction. In the top spectrum, all of the major peaks seen

for Pt(111) are once again present. However, the peaks corresponding to N-H modes are seen at $2\delta(NH_2)$ = 3220 cm^{-1}, $\nu_{sym}(NH_2)$ = 3300 cm^{-1}, and $\nu_{asym}(NH_2)$ = 3416 cm^{-1}. All of these vibrational modes are blue-shifted compared to unpromoted Pt(111) (see Table 3), indicating a weaker, less electron donating, interaction with the Pt(111) surface. This suggests that the co-adsorption with 1-methylpyrrole decreases the bonding interaction of the nitrogen containing portion of the product molecules with the surface, lowering the desorption energy, and reducing their residence time on the surface. In comparison with the bottom spectrum taken during the first hour of reaction, it is evident that that the intensities of the vibrational modes assigned to butylamine on the surface increase with time, as they are essentially absent in the bottom spectrum. Thus as the surface concentration of butylamine on Pt(111) increases, the rate of reaction for the formation of pyrrolidine decreases concomitantly. This suggests that butylamine is acting as a surface poison on Pt(111), being more strongly bound than reacting molecules, and using up the active sites.

The top spectrum in Figure 4.4 is that of 3 Torr pyrrole and 30 Torr hydrogen over Rh(111) which was recorded after exposing the surface to 100 millitorr 1-methylpyrrole prior to reaction. As can be seen, most of the stretches are identical to that of Rh(111) without the pre-treatment of 1-methylpyrrole except for those pertaining to the N-H stretches. The two distinguishable N-H bands are seen for $\nu_{asym}(NH_2)$ at 3410 cm^{-1} and for the aromatic N-H at 3510 cm^{-1}. This is a 25 cm^{-1} and 15 cm^{-1} blue shift in the wavenumber respectively (Table 3), when compared to pyrrole hydrogenation over Rh(111) without pre-adsorbed 1-methylpyrrole. This blue-shift is attributed to a weaker interaction between the Rh(111) surface and these N-H bonds.

Assignment	Pt(111)	Pt(111) with MP	Rh(111)	Rh(111) with MP
$\nu_{sym}(CH_2)$	2840		2850	2850
$\nu_{sym}(CH_3)$	2870	2860		
$\nu_{asym}(CH_2)$	2918	2918	2905	2905
$\nu_{asym}(CH_3)$	2962	2957		
ν(=CH)	3055		3048	3045
$\nu_{aromatic}$(CH)	3105	3110	3095	3095
$2\delta(NH_2)$	3200	3220	3180-3320	3180-3320
$\nu_{sym}(NH_2)$	3260	3300		
ν(NH)				
$\nu_{asym}(NH_2)$	3380	3416	3385	3410
$\nu_{aromatic}$(NH)			3495	3510

Table 4.3. Summary and assignments of SFG vibrational modes observed during pyrrole hydrogenation (3 Torr pyrrole, 30 Torr H_2, see Figs. 2,4,6 and 7) over the corresponding catalyst surface. "MP" refers to the surface pre-adsorbed with 1-methylpyrrole. Vibrational frequencies are given in cm^{-1}.

The SFG vibrational spectroscopy results over both Rh(111) and Pt(111) suggest that the adsorption of 1-methylpyrrole on the surface prior to the pyrrole hydrogenation reaction promotes the reaction rate by weakening the interaction of the nitrogen containing portion of the product molecules with the surface, allowing them to desorb more readily. This would allow pyrrolidine to desorb before continuing on to form the ring-cracking product more frequently.

4.3.4. Reaction Deactivation by Butylamine. Clearly, a good catalyst should not be bound too strongly to reaction products, or competitive adsorption between reactants and products will reduce the reaction rate. In the case of pyrrole hydrogenation, the lone pair of electrons on the nitrogen atom is delocalized over the pyrrole molecule, but once one of the double bonds in the ring is hydrogenated, the nitrogen lone pair orbital is free to interact and bond with the metal surface. It was shown (Table 1) that the promotion of pyrrole hydrogenation by the adsorption of 1-methylpyrrole prior to reaction significantly reduced the ring-opening tendency to form butylamine. To test the poisoning properties of butylamine, a reaction mixture of 3 Torr pyrrole, 0.3 Torr butylamine, and 30 Torr hydrogen was reacted over a Rh(111) surface that had been dosed with 100 millitorr 1-methylpyrrole prior to reaction. This resulted in a TOR at one hour which was 62% slower than that of the reaction without the butylamine additive. To gain a more complete picture of the deactivation kinetics in this reaction the conversion of pyrrolidine to butylamine was also studied. 4 Torr pyrrolidine and 40 Torr hydrogen were reacted over Rh(111). In one hour, the Rh(111) converted 7.4% of the pyrrolidine to butylamine. When the same reaction was carried out over Rh(111) that was exposed to 100 millitorr 1-methylpyrrole prior to reaction, 0.7% of the pyrrolidine had been converted to

butylamine after one hour. Thus, the adsorption of 1-methylpyrrole on the surface before the reaction resulted in a near 10 fold decrease in the ring-opening of pyrrolidine over Rh(111).

The SFG results during pyrrole hydrogenation indicated that over Pt(111) as the surface concentration of butylamine increased the reaction rate decreased. We can see here kinetically that the presence of butylamine in the reaction mixture over Rh(111) promoted with 1-methylpyrrole significantly decreases the reaction rate. Further, the co-adsorption of 1-methylpyrrole significantly inhibits the ring-opening of pyrrolidine on the surface. This effect can also be seen when comparing the pyrrole hydrogenation reaction selectivities (Table 1), which show that the reaction promotion by 1-methylpyrrole is accompanied by a significant decrease in the selectivity for ring-opening to form butylamine. This may be attributed to a shorter residence time of the pyrrolidine product molecule on the surface, due to its weakened interaction with the surface, allowing it to desorb before cracking the ring more frequently.

4.4. Conclusions.

Using a combination of SFG vibrational spectroscopy and kinetic measurements, the adsorption geometry and hydrogenation pathway of pyrrole has been clarified over both Pt(111) and Rh(111) single-crystal surfaces during reaction at catalytically relevant pressures and temperatures. SFG results show that on Pt(111) the N-H bond of the pyrrole molecule is cleaved, and pyrrole binds through the nitrogen to the metal surface in an upright orientation. On Rh(111) a tilted adsorption geometry was found in which the pyrrole molecule binds to the metal surface through its aromatic π-electron system.

Further, it was found that pre-treating the metal surfaces with 1-methylpyrrole significantly promotes the pyrrole hydrogenation reaction over both metal surfaces. Rh(111) exhibited a 17 fold rate enhancement, and showed little reaction deactivation. Pt(111) exhibited rate enhancement but was quickly deactivated back to the rate seen without promotion. SFG vibrational spectroscopy results showed that as the pyrrole hydrogenation rate over Pt(111) pre-dosed with 1-methylpyrrole deactivated, its surface concentration of butylamine increased, acting as a surface poison. It was shown that the presence of co-adsorbed 1-methylpyrrole weakens the interaction of the N-H modes with the metal surfaces, indicating less electron donation from the nitrogen atom to the surface. This suggests that the rate enhancement observed by co-adsorbing 1-methylpyrrole during pyrrole hydrogenation is achieved by lowering the desorption energy of the N-containing products.

References

(1) Cooper, B. H.; Donnis, B. B. L. *Applied Catalysis a-General* **1996**, *137*, 203.

(2) Netzer, F. P.; Bertel, E.; Matthew, J. A. D. *Surface Science* **1980**, *92*, 43.

(3) Horsley, J. A.; Stohr, J.; Hitchcock, A. P.; Newbury, D. C.; Johnson, A. L.; Sette, F. *Journal of Chemical Physics* **1985**, *83*, 6099.

(4) Ogletree, D. F.; Vanhove, M. A.; Somorjai, G. A. *Surface Science* **1987**, *183*, 1.

(5) Weiss, P. S.; Eigler, D. M. *Physical Review Letters* **1993**, *71*, 3139.

(6) Bratlie, K. M.; Kliewer, C. J.; Somorjai, G. A. *Journal of Physical Chemistry B* **2006**, *110*, 17925.

(7) Tourillon, G.; Raaen, S.; Skotheim, T. A.; Sagurton, M.; Garrett, R.; Williams, G. P. *Surface Science* **1987**, *184*, L345.

(8) Netzer, F. P.; Bertel, E.; Goldmann, A. *Surface Science* **1988**, *199*, 87.

(9) Hamilton, T. S.; Adams, R. *Journal of the American Chemical Society* **1928**, *50*, 2260.

(10) Maxted, E. B.; Walker, A. G. *Journal of the Chemical Society* **1948**, 1093.

(11) Devereux, J. M.; Payne, K. R.; Peeling, E. R. A. *Journal of the Chemical Society* **1957**, 2845.

(12) Maxted, E. B.; Biggs, M. S. *Journal of the Chemical Society* **1957**, 3844.

(13) Freifelder, M. *Practical Catalytic Hydrogenation*; Wiley: New York, 1971.

(14) Signaigo, F. K.; Adkins, H. *Journal of the American Chemical Society* **1936**, *58*, 709.

(15) Rainey, J. L.; Adkins, H. *Journal of the American Chemical Society* **1939**, *61*, 1104.

(16) Adkins, H.; Wolff, I. A.; Palvic, A.; Hutchinson, E. *Journal of the American Chemical Society* **1944**, *66*, 1293.

(17) Hegedus, L.; Mathe, T.; Tungler, A. *Applied Catalysis a-General* **1996**, *147*, 407.

(18) Hegedus, L.; Mathe, T.; Tungler, A. *Applied Catalysis a-General* **1997**, *161*, 283.

(19) Hegedus, L.; Mathe, T.; Tungler, A. *Applied Catalysis a-General* **1997**, *153*, 133.

(20) Tungler, A.; Hegedus, L.; Hada, V.; Mathe, T.; Szepesy, L. *Chem. Ind.: Cat. Org. React.* **2001**, *82*, 425.

(21) Hegedus, L.; Mathe, T. *Applied Catalysis a-General* **2002**, *226*, 319.

(22) Hegedus, L.; Mathe, T.; Tungler, A. *Applied Catalysis a-General* **1996**, *143*, 309.

(23) Shen, Y. R. *The Principles of Nonlinear Optics*; John Wiley & Sons: New Jersey, 2003.

(24) Bond, G.; Meheux, P. A.; Ibbotson, A.; Wells, P. B. *Catalysis Today* **1991**, *10*, 371.

(25) Jackson, S. D.; Hardy, H.; Kelly, G. J.; Shaw, L. A. The effect of co-adsorbates on activity/selectivity in the hydrogenation of aromatic alkynes. In *Heterogeneous Catalysis and Fine Chemicals Iv*, 1997; Vol. 108; pp 305.

(26) Jackson, S. D.; Munro, S.; Colman, P.; Lennon, D. *Langmuir* **2000**, *16*, 6519.

(27) Bratlie, K. M.; Flores, L. D.; Somorjai, G. A. *Surface Science* **2005**, *599*, 93.

(28) Kung, K. Y.; Chen, P.; Wei, F.; Rupprechter, G.; Shen, Y. R.; Somorjai, G. A. *Review of Scientific Instruments* **2001**, *72*, 1806.

(29) Yang, M. C.; Tang, D. C.; Somorjai, G. A. *Review of Scientific Instruments* **2003**, *74*, 4554.

(30) Shen, Y. R. *Annual Review of Physical Chemistry* **1989**, *40*, 327.

(31) Shen, Y. R. *Nature* **1989**, *337*, 519.

(32) Klots, T. D.; Chirico, R. D.; Steele, W. V. *Spectrochimica Acta Part a-Molecular and Biomolecular Spectroscopy* **1994**, *50*, 765.

(33) Lord, R. C.; Miller, F. A. *Journal of Chemical Physics* **1942**, *10*, 328.

(34) Mellouki, A.; Lievin, J.; Herman, M. *Chemical Physics* **2001**, *271*, 239.

(35) Mellouki, A.; Georges, R.; Herman, M.; Snavely, D. L.; Leytner, S. *Chemical Physics* **1997**, *220*, 311.

(36) Evans, J. C.; Wahr, J. C. *Journal of Chemical Physics* **1959**, *31*, 655.

(37) Sokoll, R.; Hobert, H.; Schmuck, I. *Journal of the Chemical Society-Faraday Transactions I* **1986**, *82*, 3391.

(38) Teixeira-Dias, J. J. C.; de Carvalho, L. A. E. B.; da Costa, A. M. A.; Lampreia, I. M. S.; Barbosa, E. F. G. *Spectrochimica Acta Part A: Molecular Spectroscopy* **1986**, *42*, 589.

(39) Dignam, M. J.; Moskovit.M; Stobie, R. W. *Transactions of the Faraday Society* **1971**, *67*, 3306.

(40) Pearce, H. A.; Sheppard, N. *Surface Science* **1976**, *59*, 205.

Chapter 5

Furan Hydrogenation over Pt(111) and Pt(100) Single-Crystal Surfaces and 1 and 10 nm Pt Nanoparticles: A Kinetic and Sum-Frequency Generation Vibrational Spectroscopy Study

Sum frequency generation surface vibrational spectroscopy and kinetic measurements using gas chromatography have been used to study the adsorption and hydrogenation of furan over Pt(111) and Pt(100) single-crystal surfaces and size-controlled 1 and 10 nm Pt nanoparticles at Torr pressures (10 Torr furan, 100 Torr H_2) to form dihydrofuran (DHF), tetrahydrofuran (THF), and the ring-cracking product butanol. Over Pt(111) it was found that at 90°C the dominant product was THF, but upon heating to 150°C a complete reversal of the selectivity was seen and butanol was the dominant product. Over Pt(100) at 90°C, the product was a 50/50 mixture between THF and butanol, and upon heating butanol became the dominant product. DHF was a minor product over the single crystals, but it was the dominant product over the 1 and 10 nm nanoparticles. SFG-VS results indicate that on the single crystals the furan ring is parallel to the surface under hydrogenation conditions, while over the nanoparticles it is somewhat tilted.

5.1. Introduction

Catalytic reactions involving aromatic cyclic and heterocyclic molecules are important for the chemical industry for both fuel reforming and environmental concerns.[1] The adsorption of six-membered molecules, e.g. benzene and pyridine, has been extensively studied on various metal surfaces.[2-6] Five-membered ring systems, such as pyrrole, furan, and thiophene have received comparatively much less attention. This may be due in part to the more complex behavior of five-membered rings upon adsorption to catalytic surfaces, making them less attractive for fundamental surface science study. A thorough understanding of the adsorption and reactions of these five-membered aromatic molecules is not only important fundamentally as model systems for studying heterogeneous catalysis, but it is directly important to the petrochemical industry as it applies to the hydrodenitrogenation, hydrodesulfurization, and hydrodeoxygenation processes.

The use of single crystals to study surface chemical reactions over metal catalysts has been a mainstay of surface science and catalysis research for many years[7], and it provides the reference state needed to probe and compare more complex nanoparticle surfaces which are more closely related to what is used industrially. The technique of sum frequency generation vibrational spectroscopy, a surface specific vibrational spectroscopy, has proven to be a powerful surface analysis technique over single crystal catalysts to reveal both adsorption modes and reaction intermediates *in situ* from UHV to atmospheric reactant pressures[6,8-12]. SFG-VS has now been applied to the study of size-controlled nanoparticle systems[13], which was not possible until recently due to the fact that the capping or stabilizing agent used in the synthesis of the nanoparticles interfered with the surface spectra of adsorbed reaction intermediates. However, Aliaga et al[13]

solved this problem by applying a UV-ozone cleaning treatment in the presence of oxygen to combust capping hydrocarbons from the surface of Pt nanoparticles deposited on a fused silica prism. In this study, this technique was applied so that the results over the single crystals could be compared to those from 1.0 and 10 nm platinum nanoparticles.

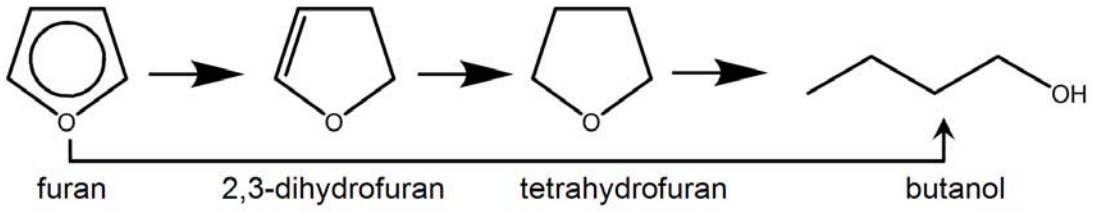

Scheme 5.1. Reaction scheme for the hydrogenation of furan.

Furan (C_4H_4O) is a five-membered aromatic ring system (Scheme 5.1) in which one of the two lone pairs of electrons of the oxygen is delocalized over the π-system of the ring. The adsorption of furan on various single crystal surfaces has been studied. Sexton et al[14] investigated the adsorption of furan on a Cu(100) surface using EELS and TDS determining that furan adsorbed to the surface at 85K with a monolayer of furan molecules π-bonded and lying parallel to the surface, while a second "bi-layer" builds on top of this which is tilted with respect to the surface. Gui et al[15] studied the adsorption of the 5-membered heterocycles, including furan, on Pt(111) electrodes using EELS *ex-situ* after immersion in a solution of furan at a given pH. In this case the furan underwent hydrolysis on the Pt(111) surface. While the conditions are quite different than gas phase hydrogenation, it is interesting to note the ring-cracking over Pt(111). The adsorption structure of furan on Pd(111) was investigated by Knight et al[16] using NEXAFS and

scanned-energy mode photoelectron diffraction (PhD), with the conclusion being that the furan molecule is adsorbed close to parallel (within 10°) to the Pd(111) surface. This is in agreement with STM images taken by Loui and Chiang[17] which demonstrate furan adsorbed nearly parallel to the Pd(111) surface. Solomon and Madix[18] determined both furan and dihydrofuran (DHF) adsorb to Ag(110) at a 22 (+/- 7)° angle using NEXAFS.

Limited work has been performed over Pt surfaces as to the adsorption and reaction of furan. Hlavathy et al[19] studied furan and tetrahydrofuran (THF) adsorption to a Pt foil using work function changes and Auger electron spectroscopy. Their determination was that furan adsorbs to a Pt foil via a surface π-complex, which would necessitate a near-parallel adsorption scheme. They determine further that THF is adsorbed to Pt via a C-Pt σ-bond and that the addition of hydrogen may increase C-O dissociation (bond scission) within the reactants.

The catalytic study of furan hydrogenation was first carried out in 1949 by Smith and Fuzek[20] over Adams platinum. It was observed that furan hydrogenation yielded one product, butanol. By using kinetic arguments, it was argued that over Adams platinum the reaction mechanism proceeded along one of two pathways. The furan ring could hydrogenate to yield dihydrofuran and tetrahydrofuran sequentially, or the furan ring could break to form butanol once desorbed, but the conversion of DHF or THF to butanol was not observed.

In this study the hydrogenation of furan to form the observed products DHF, THF, and butanol (Scheme 5.1) was carried out over Pt(111) and Pt(100) single crystals to help elucidate the effect catalyst structure has on the reaction mechanism and selectivity, and these results are compared to the reaction carried out over 1.0 and 10 nm Pt nanoparticles

to help determine the effect of catalyst size. Further, sum frequency generation vibrational spectroscopy was carried out *in-situ* to elucidate the surface species over all of the model catalysts in the temperature range of 300K to 420K under 10 Torr furan and 100 Torr hydrogen.

5.2. Experimental

Materials

Prior to use, furan (>99%, Sigma-Aldrich), 2,3-dihydrofuran (99%, Aldrich), tetrahydrofuran (>99%,Sigma-Aldrich) and 1-butanol (99.8%,Sigma-Aldrich) were subjected to several freeze-pump-thaw cycles and the purities were checked by means of gas chromatography.

The high-pressure/ultra-high vacuum system

All single crystal experiments reported here were carried out in a high-pressure/ultrahigh-vacuum (HP/UHV) system. The UHV chamber is operated at a base pressure of 2 x 10^{-10} Torr and is isolated from the HP cell by a gate valve. The UHV system is equipped with an Auger electron spectrometer (AES), a quadrupole mass spectrometer (Stanford Research Systems) and an ion bombardment gun (Eurovac). The HP cell consists of two CaF_2 conflat windows that allow transmission of infrared (IR), visible (VIS) and sum frequency radiation for sum frequency generation (SFG) experiments. The product gases in the HP cell are constantly mixed via a recirculation pump and kinetic data is acquired by periodically sampling the reaction mixture and analyzing the relative gas phase composition in a flame ionization detector (FID) of a gas chromatograph (Hewlett Packard HP 5890 on a 5% Carbowax 20M packed column).

Single Crystal Sample preparation

Prior to each experiment, the Pt(111) and Pt(100) crystal surfaces were cleaned in the UHV chamber by Ar^+ (1 keV) sputtering for 20 min at about 3 x 10^{-5} Torr of Ar. After sputtering, the crystals were heated to 1103 K in the presence of O_2 of 5 x 10^{-7} Torr and annealed at the same temperature for 2 min. The cleanliness of the crystal surfaces was verified by AES and the crystallographic structure verified with low energy electron diffraction (LEED). The samples were then transferred into the HP cell for SFG and kinetic studies.

Nanoparticle Preparation

The synthesis and characterization of these nanoparticles in this laboratory has been previously reported and is not the focus of this work.[13,21-24] Further, the stability of the 10 nm nanoparticles against agglomeration during the uv-ozone cleaning treatment has been previously reported.[13] Briefly, for the PVP capped nanoparticles, 0.1 mmol of ammonium hexachloroplatinate(IV), 1.5 mmol of trimethyl(tetradecyl)ammonium bromide, and 2 mmol of poly(vinylpyrrolidone) were added to 20 mL of ethylene glycol in a 50 mL three-necked flask at room temperature. The stock solution was heated to 80 °C in a Glas-Col electromantle (60 W, 50 mL) with a Cole-Parmer temperature controller (Diqi-sense) and was evacuated at this temperature for 20 min to remove water and oxygen under magnetic stirring. The flask was then heated to 180 at 10 °C/min and was maintained at this temperature for 1 h under Ar. When the reaction was complete, excess acetone was added at room temperature to form a cloudy black suspension. This suspension was separated by centrifugation at 4200 rpm for 10 min, and the black product was collected by discarding the colorless supernatant. The precipitated platinum

nanocrystals were washed twice by precipitation/dissolution (redispersed in 7.5 mL of ethanol with sonication and then precipitated by adding 37.5 mL of hexanes).

For the 1.0 nm nanoparticles, fourth generation hydroxyl terminated polyamidoamine (PAMAM) dendrimers were used as the templating and capping agent.[21] Synthesis and characterization of the 1.0 nm particles have been published.[21] The average number of metal atoms per nanoparticle is controlled by the Pt ion to dendrimer ratio. Since the particles were too small to successfully image with TEM, sizes were calculated from the average number of metal ions added per dendrimer, and this method has been verified using X-ray absorption.[25]

The 1.0 nm Pt nanoparticles were then drop cast onto a fused silica prism for catalytic and SFG-VS study. The 10 nm cubic Pt nanoparticles were deposited onto the fused silica prism using the Langmuir-Blodgett technique as described previously[13]. The particles were uv-ozone treated on the fused silica prism as described previously[13] to remove the organic capping layer. The removal of the capping layer (PVP in the case of the 10 nm particles and dendrimer in the case of the 1.0 nm particles) was verified by observing the disappearance of the C-H stretching vibrations in the SFG-VS spectrum. It is quite possible that there is left a carbon layer on the particles as this would yield no SFG-VS peak in the C-H region. Further, the oxidation of the surface metal atoms under such treatment has yet to be investigated.

Sum Frequency generation vibrational spectroscopy

For SFG measurements, an active/passive mode-locked Nd:YAG laser (Leopard D-20, Continuum) with a pulse width of 20 ps and a repetition rate of 20 Hz was used. The fundamental output at 1064 nm was sent through an optical parametric

generation/amplification (OPA/OPG) stage where a tunable IR (2300—4000 cm^{-1}) and a second harmonic VIS (532 nm) beam were created. The IR (150 μJ) and VIS (200 μJ) beams were spatially and temporally overlapped on the crystal surface at angles of incidence of 55 and 60°, respectively, with respect to the surface normal for the single crystal studies. In the case of the nanoparticle studies, the beams were directed into a fused silica prism on top of which the nanoparticles had been deposited. The generated SFG beam was collected and sent through a motorized monochromator equipped with a photomultiplier tube to detect the SFG signal intensity. The signal-to-noise ratio was further increased by using a gated integrator while the IR beam was scanned through the spectral region of interest. The SFG process is enhanced when the IR beam comes into resonance with a vibrational mode of a molecule adsorbed at the surface, giving rise to a vibrational spectrum of adsorbed species. More information on the HP/UHV system and SFG measurement can be found elsewhere.[26-31]

5.3. Results and Discussion

5.3.1. Furan Hydrogenation over Pt(111): Kinetic and SFG-VS Results

Furan hydrogenation was carried out over Pt(111) with 10 Torr furan, 100 Torr hydrogen, and 550 Torr argon in the temperature range of 22° C to 170° C.

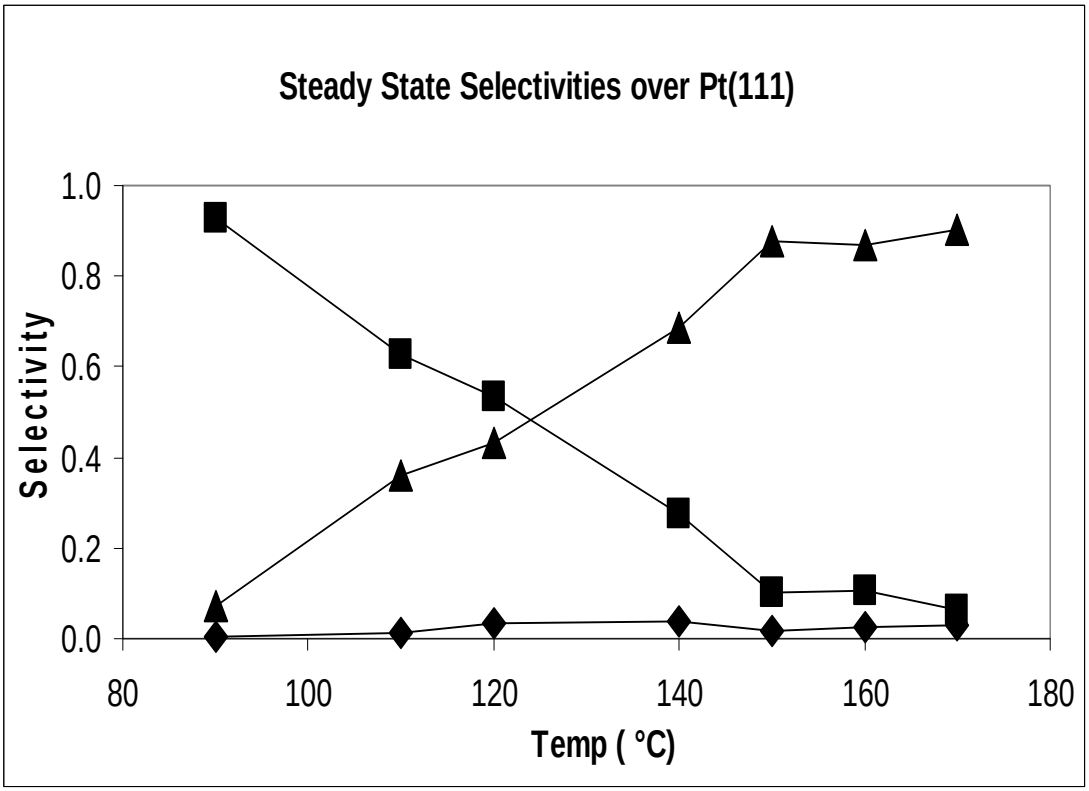

Figure 5.1. Temperature dependence of the hydrogenation of furan over Pt(111) using 10 Torr furan and 100 Torr hydrogen. The products are dihydrofuran (-♦-), tetrahydrofuran (-■-), and butanol (-▲-). There is a complete selectivity flip from 90°C to 150°C from tetrahydrofuran to the ring-cracking product butanol.

Figure 5.1 displays the reaction product distribution as a function of temperature as measured by GC. Dihydrofuran, tetrahydrofuran and butanol were all detectable products. As can be seen, up to 90°C the dominant product is THF, the saturated ring product. As the temperature is raised however, we see a complete reversal of the selectivity and the dominant product (~90%) becomes the ring-cracking product butanol. DHF is a minor product (< 4%) at all temperatures. It is interesting to note that Smith

and Fuzek[20] report only butanol as the reaction product over an Adams platinum catalyst whereas all three products are observed over Pt(111).

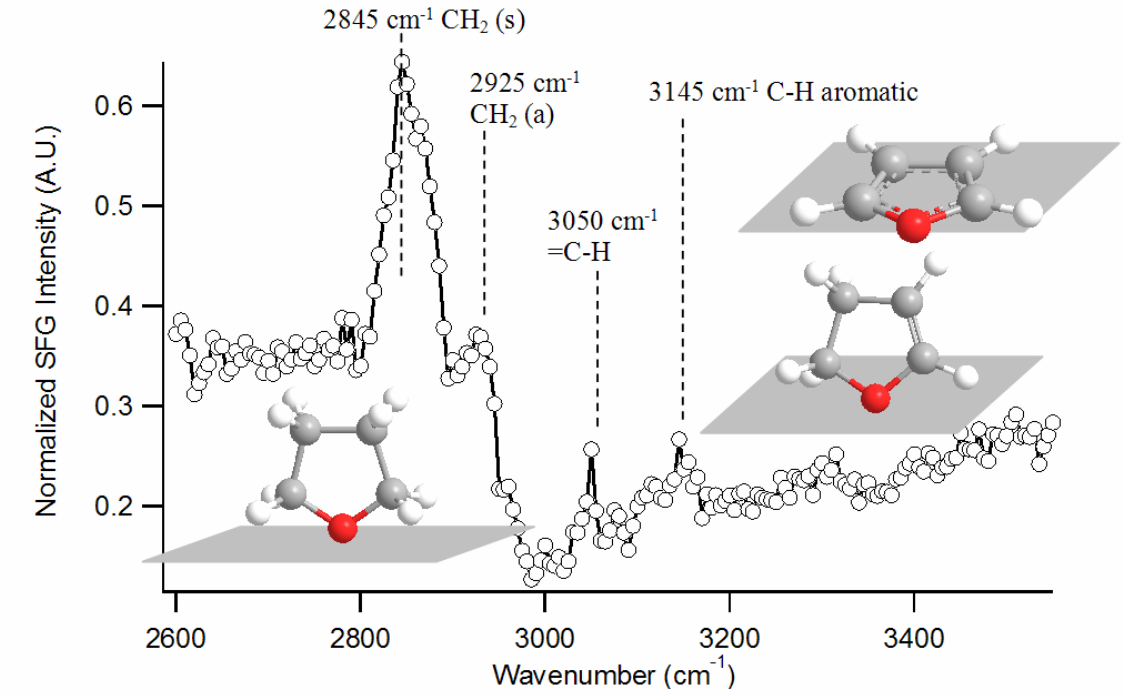

Figure 5.2. SFG-VS spectrum of 10 Torr furan over Pt(111) in the absence of excess hydrogen. Stretches are seen for the C-H aromatic stretch of furan, the C-H vinylic stretch of DHF, and the CH_2 symmetric and asymmetric stretches of the THF ring. In the molecule representations, oxygen is red, carbon is gray, and hydrogen is white.

Figure 5.2 shows the SFG-VS spectrum of 10 Torr furan over Pt(111) in the absence of excess hydrogen. Four major vibrational stretches are observed. The strongest two stretches are clearly seen at 2845 cm^{-1} and 2925 cm^{-1} corresponding to the CH_2 symmetric and asymmetric stretch of the THF ring respectively. It is possible that DHF

on the surface could contribute to the CH_2 stretches as well. A third stretch is seen at 3145 cm^{-1} which we can attribute to the aromatic C-H stretch of the furan ring. A thorough description of the vibrational modes of furan was done by Klots et al and the gas phase aromatic C-H stretch of furan arises at 3160 cm^{-1}. Thus, a 15 cm^{-1} redshift of this mode takes place upon the adsorption of furan to Pt(111). Lastly, a C-H stretch is observed at 3040 cm^{-1} which we assign to the vinylic C=C-H stretch of the DHF ring. Clearly, some hydrogenation is taking place on the surface species prior to the addition of excess hydrogen to the reaction mixture. This could be due to either the small background pressure of hydrogen in the high pressure cell or due to intermolecular hydrogen transfer.

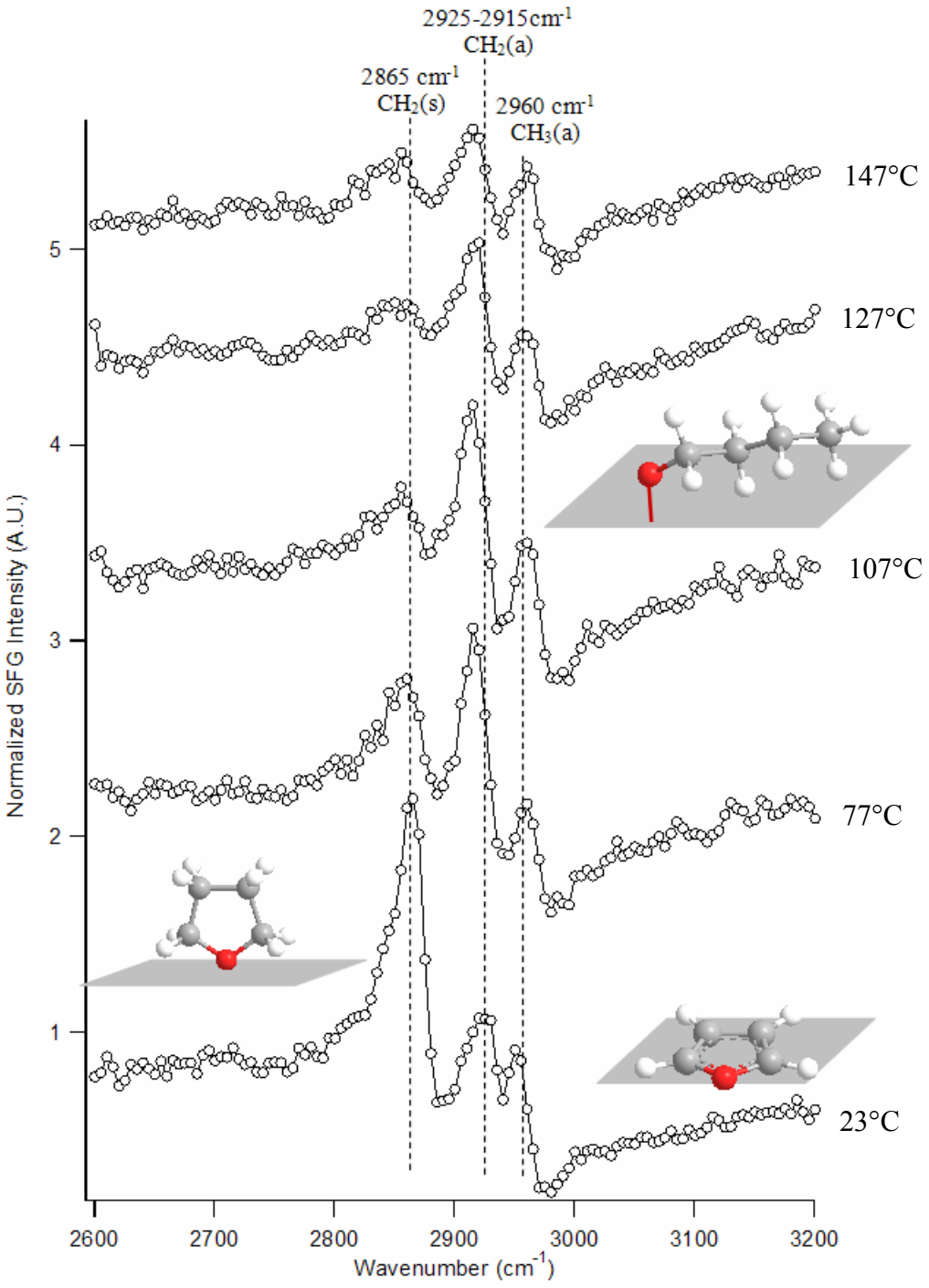

Figure 5.3. SFG-VS spectra of 10 Torr furan and 100 Torr hydrogen over Pt(111) from 23°C to 147°C.

Figure 5.3 displays the temperature dependent spectra of 10 Torr furan in the presence of 100 Torr hydrogen over Pt(111). The spectra are characterized by three peaks at 2860 cm^{-1}, 2925 cm^{-1}, and 2960 cm^{-1}. The peak at 2860 cm^{-1} can be attributed to the CH_2(s) stretch of the saturated ring, THF. The peak at 2960 cm^{-1} is very clearly indicative of the CH_3(a) stretch of the ring-cracking product, butanol. The peak at 2925 cm^{-1} red-shifts to 2915 cm^{-1} upon heating and may be attributed to a CH_2(a) stretch. The CH_2(s) stretch seen at 2860 cm^{-1} is blue-shifted slightly from standard hydrocarbon CH_2(s) stretches, due to the electron withdrawing effects of the O atom in the molecule. Further, the dominance of the CH_2(s) stretch relative to the CH_2(a) stretch at 23°C is indicative of a "standing up" THF species with respect to the metal surface[32]. No C-H aromatic stretch is seen once hydrogen is added to the reaction mixture, not even at room temperature when the gas phase is still >99.9% furan. This indicates that the furan ring is lying parallel to the Pt(111) surface upon the coadsorption of furan and hydrogen.

The three peaks undergo a general trend made clear by Figure 5.4 upon heating the crystal. In Figure 5.4 I have subtracted the spectrum of 10 Torr furan and 100 Torr hydrogen at 23° from the spectrum at 107°C to highlight the trend observed as the crystal is heated to 107°C. First, a very strong negative peak, or "loss peak", at 2860 cm^{-1} is seen. This occurs concomitantly with a gain in intensity at 2915 cm^{-1} and 2965 cm^{-1}. The gain observed in the peak at 2965 cm^{-1} can be attributed to an increasing surface concentration of butanol, the ring-cracking product, with increasing temperature.

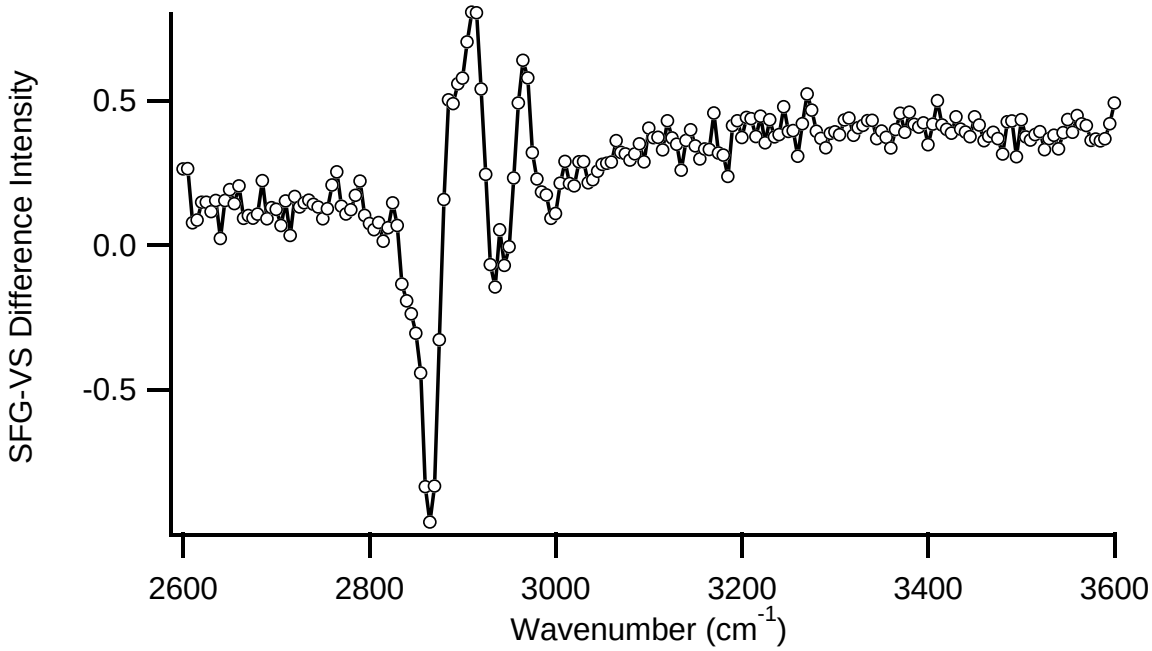

Figure 5.4. This is the difference spectrum of 10 Torr furan and 100 Torr hydrogen over Pt(111) at 107°C as compared with 10 Torr furan and 100 Torr hydrogen at 23°C to clarify the trends observed as the temperature is raised. A "loss" peak is observed at 2865 cm^{-1} upon heating corresponding to the CH_2 (s) stretch, while two positive peaks are seen at 2915 cm^{-1} and 2965 cm^{-1}.

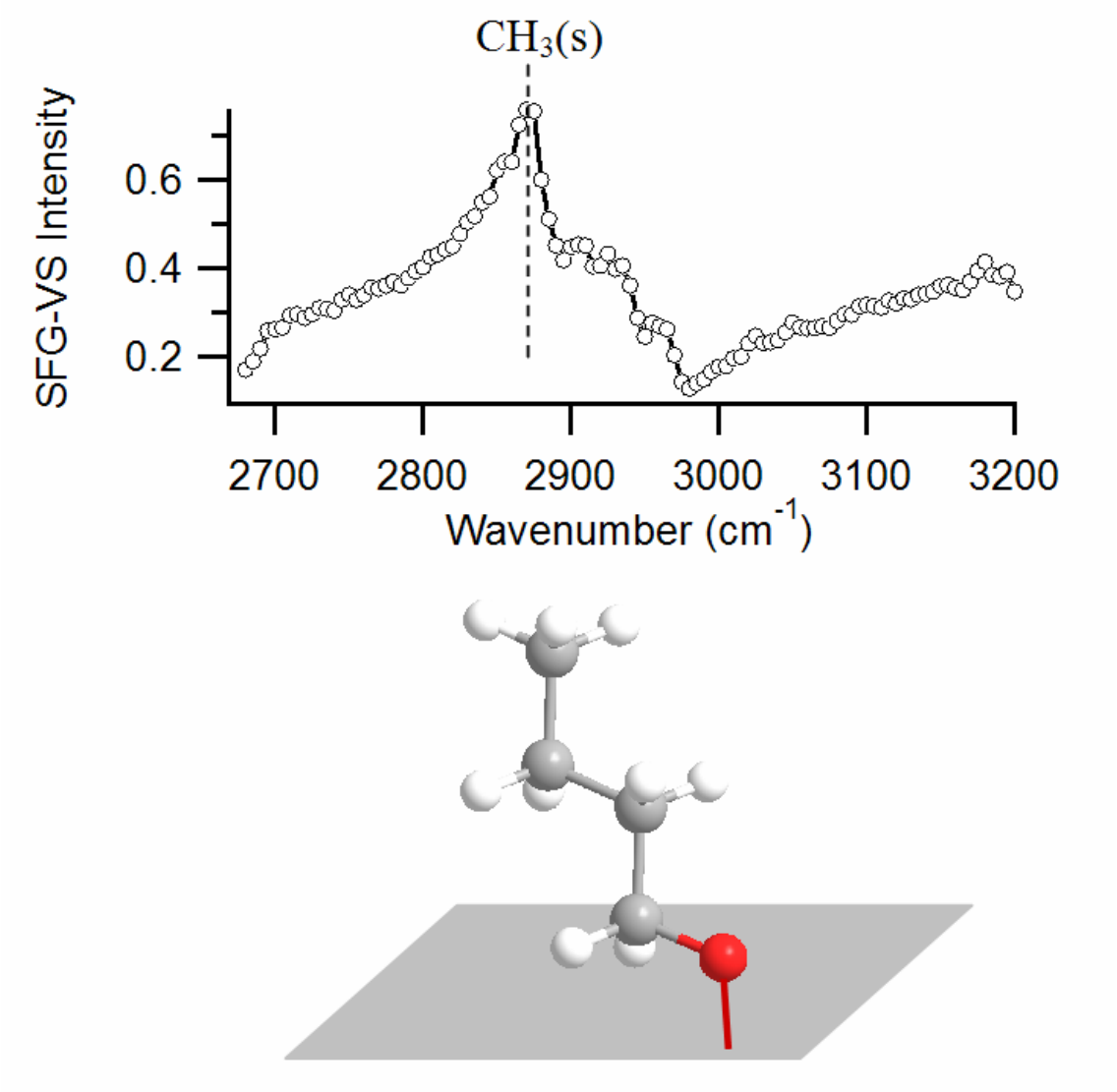

Figure 5.5. SFG-VS reference spectrum of 1 Torr butanol over Pt(111) at 23°C. The dominant CH_3(s) peak at 2875 cm^{-1} indicates that the butanol is standing upright on the surface.

Clearly, the desorption of the products is the rate limiting step for this reaction as the surface builds up an appreciable concentration. SFG-VS is not a suitable technique to quantify the relative surface coverages. The presence of the methyl asymmetric stretch and the absence of the methyl symmetric stretch, which would appear at 2875 cm^{-1}, indicate that the butanol molecule is adsorbed to the surface with the chain parallel to the surface. Further, there is no evidence of an O-H bond anywhere in the 3200-4000 cm^{-1} range which leads us to conclude that butanol is adsorbed to the surface through an O-Pt bond. Figure 5.5 displays the SFG-VS spectrum of 1 Torr butanol over Pt(111) as a reference. As can be seen, without the presence of coadsorbates the spectrum for butanol on Pt(111) is dominated by the methyl symmetric stretch at 2875 cm^{-1} indicating that the molecular axis of the methyl must be aligned nearly perpendicular to the metal surface; the methyl asymmetric stretch is very weak. This is in contrast to the what is observed for the butanol product on the Pt surface during the course of furan hydrogenation, for which the asymmetric methyl stretch is the visible one, indicating a different adsorption mode in the presence of coadsorbates (furan, hydrogen, etc.).

The strong increase of the stretch observed at 2915 cm^{-1}, which occurs concomitantly as the 2865 cm^{-1} vanishes, has three possible interpretations. It is either due to the THF ring adsorption going from an "upright" geometry to a more "flat lying" geometry, the formation of an oxametallacycle intermediate as the ring cracks, or due to a parallel lying butanol product on the surface (Figure 5.3). In the case of the oxametallacycle, the 2915 cm^{-1} stretch would be interpreted as the CH_2(s) stretch off of the C which is bound to the Pt surface (Figure 5.6).

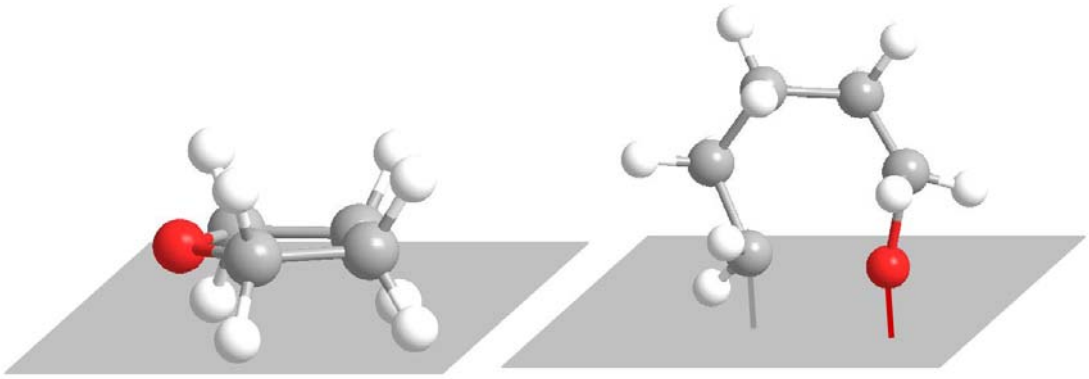

Figure 5.6. Two possible intermediates on Pt(111) during furan hydrogenation at 107°C and higher. On the left is a parallel THF molecule and on the right is an oxametallacycle.

This type of shift in the symmetric shift has been observed before with RAIRS[33] upon the formation of a C6 metallacycle on Pt(111) and appeared around ~2910 cm^{-1}. Over Ag(110), a 2 carbon oxametallacycle was prepared by thermally treating 2-iodoethanol, and resulted in a a single band at 2922 cm^{-1}.[34] However, in the case of furan hydrogenation over Pt(111), one would expect to see a nearly equivalent peak intensity associated with the CH_2(s) stretch of the carbon connected to the oxygen (Figure 5.6), which is not observed, as by 107-127°C there is significantly more intensity at the 2915 cm^{-1} peak than at the 2865 cm^{-1} peak. Thus, the oxametallacycle intermediate cannot fully explain the spectrum.

In the case of the orientational change in the THF ring interpretation, the 2915 cm^{-1} peak would be attributed to the CH_2(a) stretch off of the THF ring. This is further evidenced in that the stretch red-shifts by 10 cm^{-1} upon heating, indicating more interaction with the metal surface. As the ring goes from more perpendicular to the surface to more parallel to the surface, we would expect the methylene symmetric stretch

to vanish and the methylene asymmetric stretch to become dominant due to the metal surface selection rule. This is in fact what we observe.

Finally, as discussed above, the third interpretation is simply an increasing presence of parallel butanol bound to the surface as we raise the temperature. In fact, the presence of the asymmetric peak at 2965 cm^{-1} informs us that this is in fact occurring.

Thus there are several conclusions for the interpretation of the SFG-VS results during furan hydrogenation on Pt(111). First, furan lies parallel to the Pt(111) surface during hydrogenation. Second, at 23°C in the presence of 10 Torr furan and 100 Torr hydrogen we have predominantly an "upright" THF molecule on the surface. Third, we know that we have butanol bound to the Pt(111) surface in the parallel orientation growing in with temperature bound though the oxygen atom. Last we may have either a "parallel" lying THF as we raise the temperature or an oxametallacycle, neither of which can be ruled out or completely verified by the acquired spectra.

5.3.2 Furan Hydrogenation over Pt(100)

Figure 5.7 displays the steady state selectivity for furan hydrogenation over Pt(100) as a function of temperature for comparison to Pt(111) so as to help elucidate the effect that catalyst structure plays in this reaction. As can be seen, at 90°C we are close to a 50/50 product distribution between tetrahydrofuran and butanol. When compared to Pt(111) at 90°C, it is evident that there is significantly more ring-cracking on the Pt(100) surface at lower temperatures than on the (111) face. As the temperature is raised to 160°C, the selectivity becomes 86% for the cracking product butanol. This is the same general trend observed over Pt(111) in that butanol becomes the dominant product at high temperatures. The production of the partially saturated ring, which may

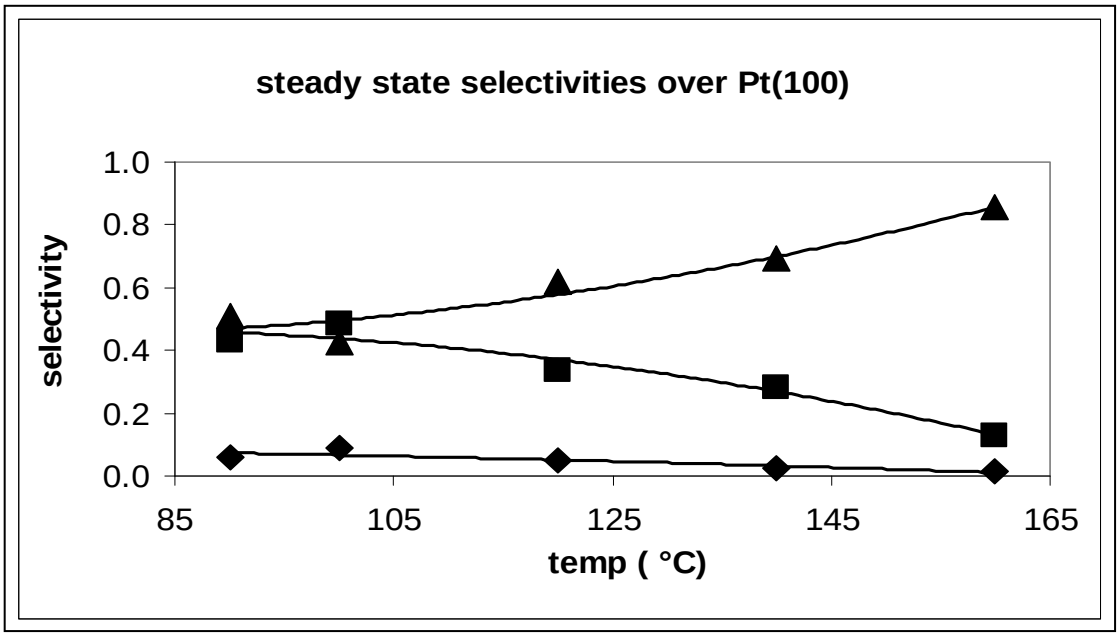

Figure 5.7. Steady state product distribution (selectivity) as a function of temperature on Pt(100) under 10 Torr furan and 100 Torr hydrogen. The products are dihydrofuran (-♦-), tetrahydrofuran (-■-), and butanol (-▲-).

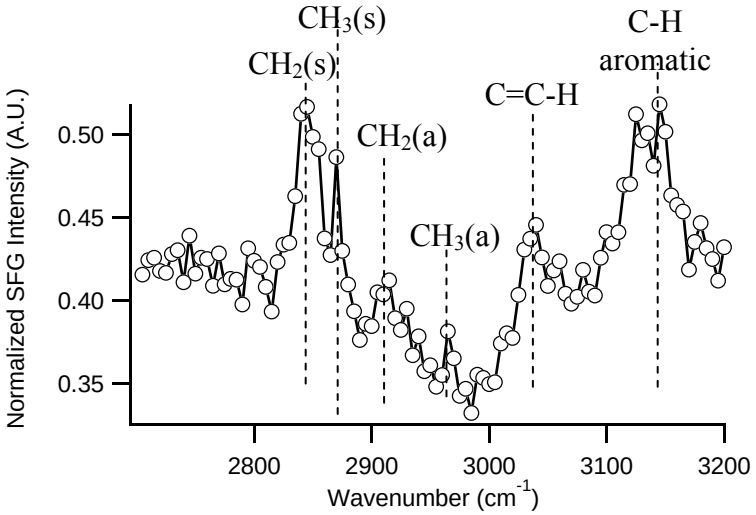

Figure 5.8. SFG-VS spectrum of 10 Torr furan over Pt(100) at 23°C. No excess hydrogen was added. Four resonances are seen. At 3145 cm^{-1} is the C-H aromatic stretch indicating a furan ring which is not parallel to the surface. At 3040 cm^{-1} is observed a vinylic C=C-H stretch of the partially saturated DHF ring. At 2915 cm^{-1} and 2850 cm^{-1} the methylene asymmetric and symmetric stretches are seen respectively. A narrow peak at 2870 cm^{-1} is seen which would correspond to the methyl symmetric stretch of the ring cracking product butanol.

be a desirable intermediate for synthetic applications, is very low as in the case over Pt(111). DHF is 8.9% of the product at 90°C over Pt(100) and it is 0.9% of the product at 90°C over Pt(111). Although it is a minor product, Pt(100) does create ten times more DHF than Pt(111).

Figure 5.8 displays the SFG-VS spectrum of 10 Torr furan over Pt(100) in the absence of excess hydrogen. At 3145 cm^{-1} a strong C-H aromatic stretch is seen for the furan ring, which is quite different than the very weak C-H aromatic seen on Pt(111) under the same conditions. This indicates that the furan ring is significantly tilted upward with respect to the Pt(100) surface. A vinylic C=C-H stretch is observed at 3040 cm^{-1} corresponding to the vinylic portion of the partially saturated ring of dihydrofuran. The methylene symmetric and asymmetric stretches are observed at 2845 cm^{-1} and 2915 cm^{-1} respectively with the symmetric stretch significantly more dominant. The methyl symmetric and asymmetric stretches are also observed at 2870 cm^{-1} and 2965 cm^{-1} respectively, also exhibiting much stronger symmetric intensity. This spectrum implies that upon the adsorption of furan to Pt(100) at room temperature there exists vertically oriented furan, THF, DHF, and butanol on the surface.

Figure 5.9 displays the spectra of 10 Torr furan and 100 Torr hydrogen over the Pt(100) surface as a function of temperature. Similarly to Pt(111) the aromatic and vinylic resonances disappear upon the addition of 100 Torr hydrogen. This is an indication that under reactive conditions the furan ring lies parallel to the surface. The absence of the DHF peak may be due to a parallel orientation, but more likely due to this part of the reaction having a fast reaction rate constant forward to THF, i.e. the double bond is quickly hydrogenated. The methylene and methyl symmetric stretching

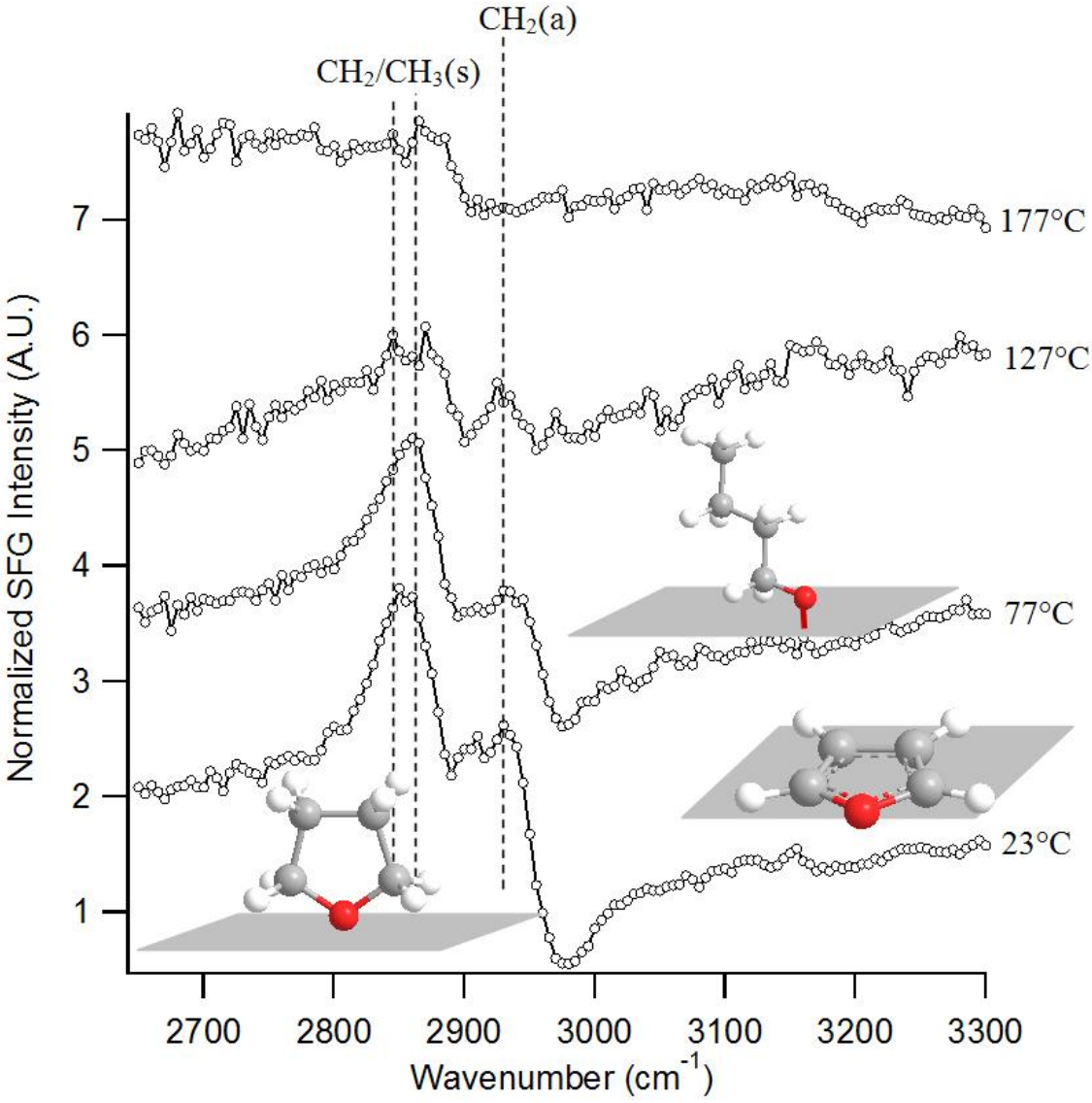

Figure 5.9. SFG-VS spectra of 10 Torr furan and 100 Torr hydrogen over Pt(100). The structures indicated are upright THF, upright butanol, and parallel furan molecules.

vibrations are seen very close together at 2850 cm^{-1} and 2860 cm^{-1} at 23°C, appearing as one wide peak with a doublet at the top. As the reaction mixture is heated to 127°C however, the peaks resolve a little more and are seen at 2845 cm^{-1} and 2870 cm^{-1} respectively. By 147°C nearly all resonant signal is lost with just a small peak seen at 2870 cm^{-1} for the methyl symmetric stretch. The methylene asymmetric stretch is seen at 2930 cm^{-1} whereas the methyl asymmetric stretch is not visible. These spectra indicate that both THF and butanol are present on the surface in upright geometries (Figure 5.9) and as the surface is heated to 147°C the adsorbates become less ordered (less SFG-VS signal). The lack of a major peak around ~2910 cm^{-1} rules out the presence of an oxametallacycle as a major surface species during furan hydrogenation over Pt(100). This does not eliminate the oxametallacycle as a transient intermediate between the ring and ring-cracked structures of furan and butanol, but if present it must nevertheless be short-lived enough as to not build up any appreciable surface concentration.

5.3.3. Furan Hydrogenation over 1.0 and 10 nm Pt Nanoparticles

To elucidate the effect that catalyst size has on this reaction, the hydrogenation of furan was also carried out over 1 nm and 10 nm Pt nanoparticles. The synthesis and characterization of these nanoparticles in this laboratory has been previously reported and is not the focus of this work.[13,21-24] Further, the stability of the 10 nm nanoparticles against agglomeration during the UV-Ozone cleaning treatment has been previously reported[13].

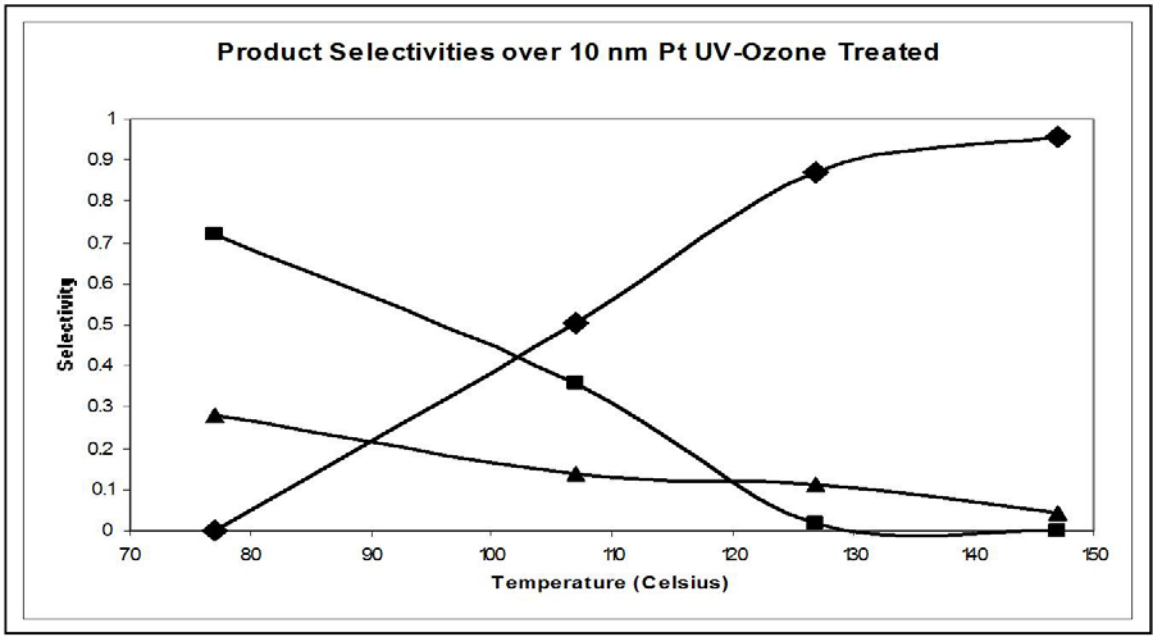

Figure 5.10. Product selectivities during furan hydrogenation on 10 nm Pt cubic nanoparticles (10 Torr furan, 100 Torr hydrogen). The particles had been UV-Ozone treated to remove the PVP capping layer. The products are dihydrofuran (-♦-), tetrahydrofuran (-■-), and butanol (-▲-).

Figure 5.10 displays the reaction selectivity as a function of temperature during furan hydrogenation carried out over 10 nm Pt cubic nanoparticles which had been UV-Ozone cleaned until no C-H modes were present in the SFG-VS spectrum. A significant difference is seen in the product selectivities as compared with the single crystals. The partially saturated ring, DHF, was always a minor product over the single crystals, with Pt(100) having the highest selectivity of ~9% at 90°C. At 77°C, the 10 nm cubic nanoparticles have a selectivity of 72% for the formation of THF, but as the temperature is raised to 147°C the dominant product becomes DHF, with a selectivity of 96%.

Butanol is always present in the product distribution, starting at 28% of the product at 77°C and trending downward until at 147°C it is 4% of the product distribution.

Figure 5.11 displays the SFG-VS spectra of 10 Torr furan and 100 Torr hydrogen over a Langmuir Blodgett film of 10 nm Pt cubic nanoparticles deposited onto a fused silica prism. At 23°C, a weak C-H aromatic stretch is observed at 3145 cm^{-1}, indicating a non-parallel adsorption mode of furan, and the vinylic DHF C=C-H stretch is seen at 3060 cm^{-1}. These stretches are not observed over the single crystals under hydrogenation conditions. The methyl asymmetric peak is observed at 2955 cm^{-1}, but this peak vanishes by 107°C. This along with the disapprearance of the methyl symmetric stretch by 147°C indicates the surface concentration of butanol is decreasing with increasing temperature, a trend which agrees with the observed selectivity in figure 5.11. By 147°C only the methylene symmetric stretch is present in the spectrum. The dominance of this methylene symmetric stretch over the asymmetric stretch is indicative of an upright ring geometry.

The selectivity of furan hydrogenation as a function of temperature over the 1.0 nm Pt nanoparticles is displayed in figure 5.12. As can be seen, the 1.0 nm nanoparticles exhibit a selectivity trend completely different than the single crystals and also different from the 10 nm cubic nanoparticles. At all temperatures, the dominant product is DHF, the partially saturated ring. Further, butanol is never produced as a product over these cleaned 1.0 nm particles. The SFG-VS spectra displayed in figure 5.13 of furan hydrogenation (1 Torr furan, 100 Torr hydrogen) over the 1.0 nm nanoparticles display no methyl asymmetric stretch at all and there is no peak intensity at 2870 cm^{-1}, the location of the methyl symmetric stretch on all other catalysts studied. Thus, no butanol

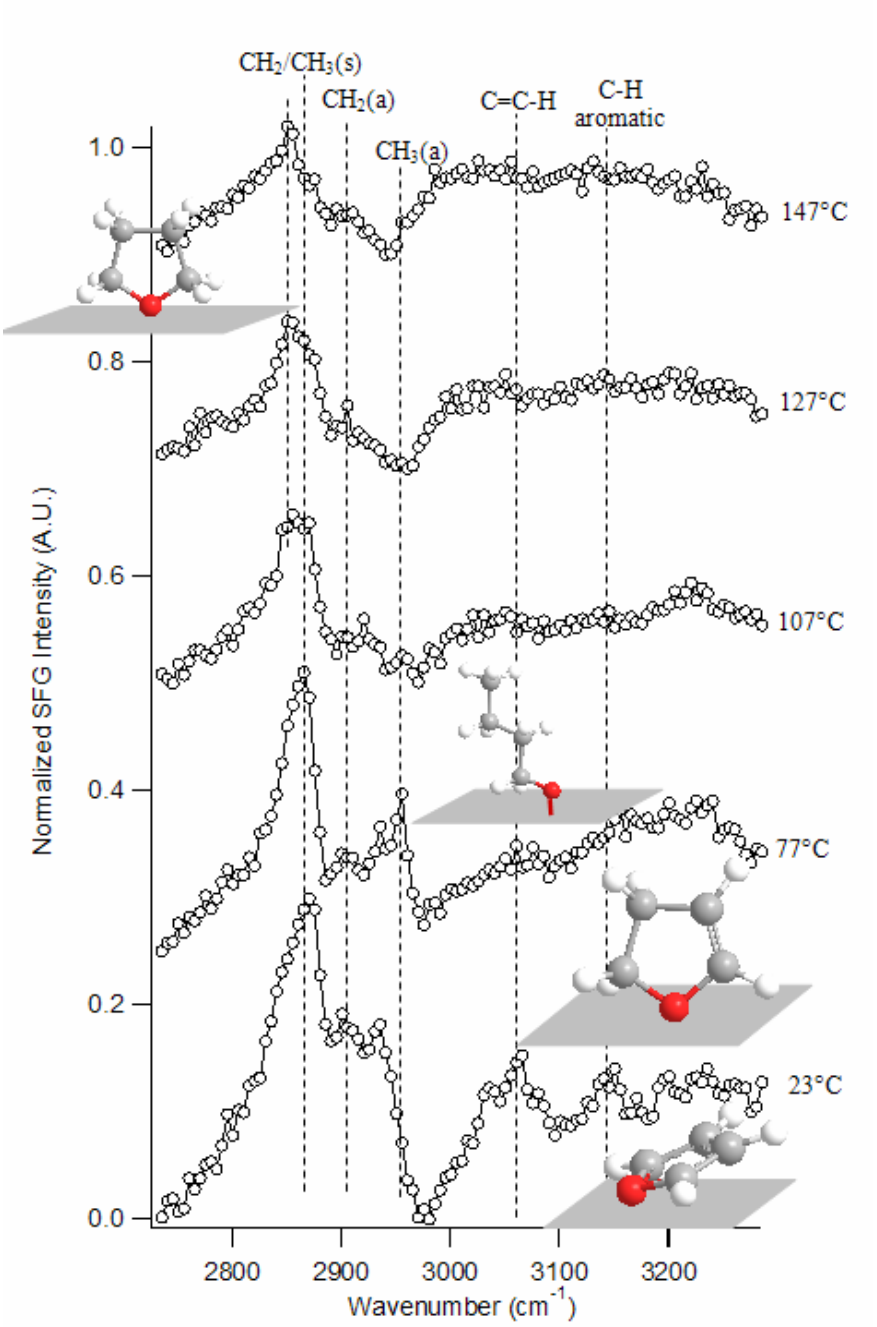

Figure 5.11. SFG-VS spectra of 10 Torr furan and 100 Torr hydrogen over UV-Ozone cleaned 10 nm Pt cubic nanoparticles. The presence of the aromatic mode indicates a tilted adsorption geometry for furan. Also observed are DHF, upright butanol, and upright THF molecules. The butanol stretch disappears by 107°C. The furan ring goes parallel by 77°C.

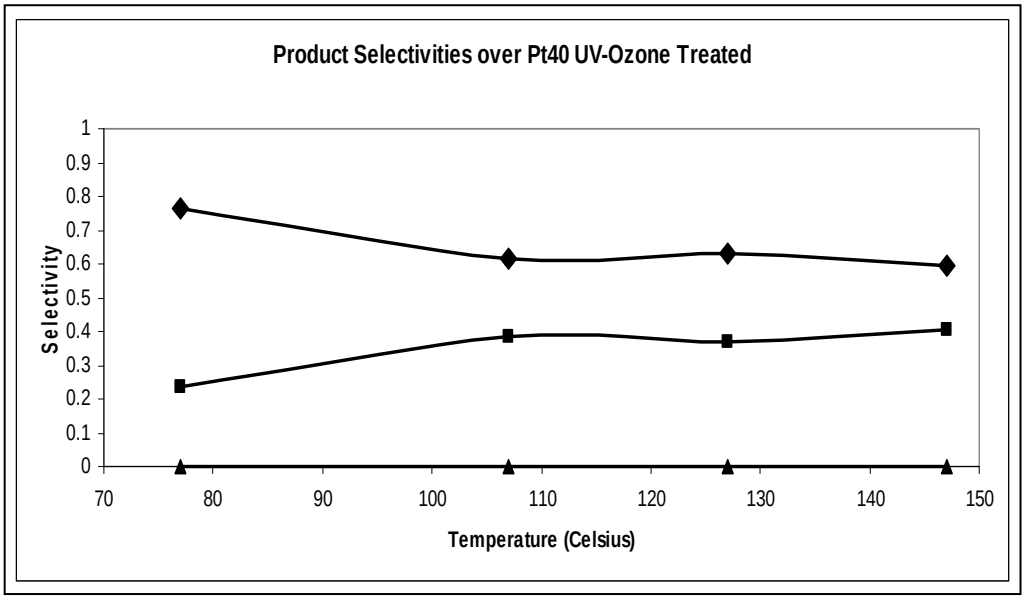

Figure 5.12. Reaction selectivity as a function of temperature during the hydrogenation of furan (10 Torr furan, 100 Torr hydrogen) over 1.0 nm Pt nanoparticles. The dendrimer layer was cleaned using the UV-Ozone cleaning method. The products are dihydrofuran (-♦-), tetrahydrofuran (-■-), and butanol (-▲-).

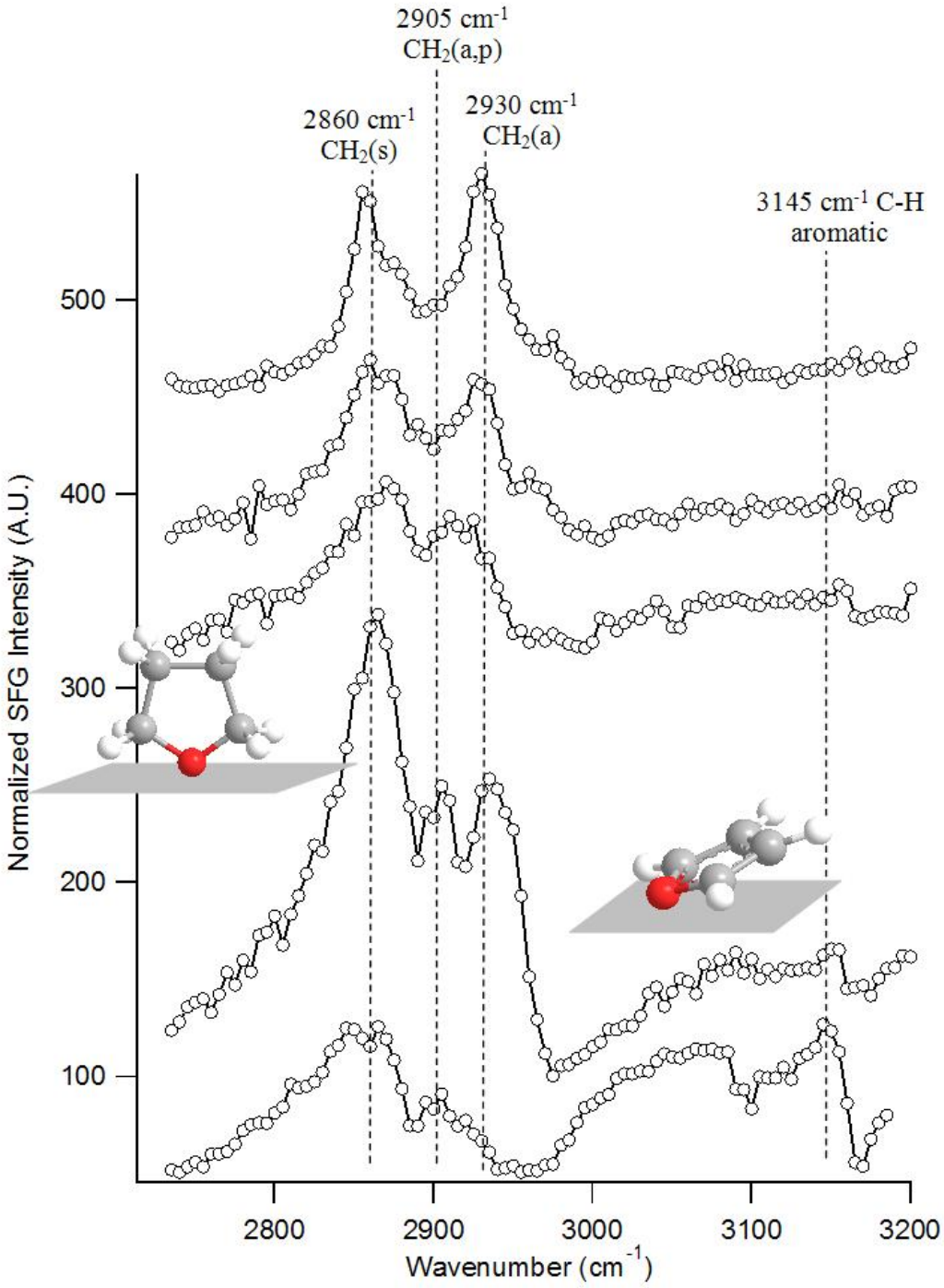

Figure 5.13. SFG-VS spectra of 1 Torr furan and 100 Torr hydrogen over 1.0 nm Pt nanoparticles. The nanoparticles were initially coated in a dendrimer as part of the synthesis, but this was removed using the uv-ozone treatment.

is observed on the surface of the 1.0 nm nanoparticles, in agreement with the observed selectivity, in which this is the only catalyst which did not produce ring-cracking product.

The cleaning of these nanoparticles has a very large effect on the selectivity of the reaction. Furan hydrogenation over the 1.0 and 10 nm nanoparticles prior to cleaning yielded only butanol as a reaction product. This is a complete reversal of the selectivity reported over the uv-ozone cleaned nanoparticles. XPS studies are underway to determine the exact oxidation state of the surface atoms in these catalysts following the uv-ozone treatment. It has been previously shown that as nanoparticles get smaller, the proportion of surface atoms in higher oxidation states increases.[35] Thus the oxidation state following the uv-ozone treatment is very likely higher on the smaller nanoparticles, and certainly higher than on the single crystals. The oxidation state of the surface before, during, and after the reaction are needed to determine the stability of the surface oxide under reducing conditions at these temperatures.

5.4. Conclusions

In this study, sum frequency generation vibrational spectroscopy and gas chromatography have been applied to systematically study the surface species present on the Pt(111) and Pt(100) single crystal surfaces *in-situ* during furan hydrogenation as well as the product selectivities as a function of catalyst temperature. These results are then compared to those obtained over uv-ozone cleaned 1.0 and 10 nm Pt nanoparticles. The SFG-VS data indicates that on Pt(111) under furan hydrogenation conditions the planar furan ring lies parallel to the metal surface. Butanol is bound to the surface through the O atom, adsorbed in a parallel orientation. The surface concentration of butanol increases with increasing temperature over Pt(111), and THF is bound to the surface in an upright

binding geometry. Over Pt(100) the SFG-VS spectra also indicate a parallel furan adsorption under hydrogenation conditions. Both butanol and THF are seen bound to the Pt(100) surface in upright geometries. Over the 10 nm Pt cubic nanoparticles butanol is seen bound only at lower temperatures, and vanishes at higher temperatures, while over the 1.0 nm Pt nanoparticles it is not seen at all. This is in agreement with the observed selectivities.

A clear selectivity trend is observed, the larger the nanoparticle, and the expression of more <100> facets, the higher the selectivity for ring-cracking. This is the same trend observed for pyrrole hydrogenation and ring-cracking over Pt nanoparticles by Kuhn et al[22]. The smaller the nanoparticle, the higher the production of the partially saturated ring. These finding are summarized in figure 5.14. The surface species over all surfaces correlated well with the product distributions.

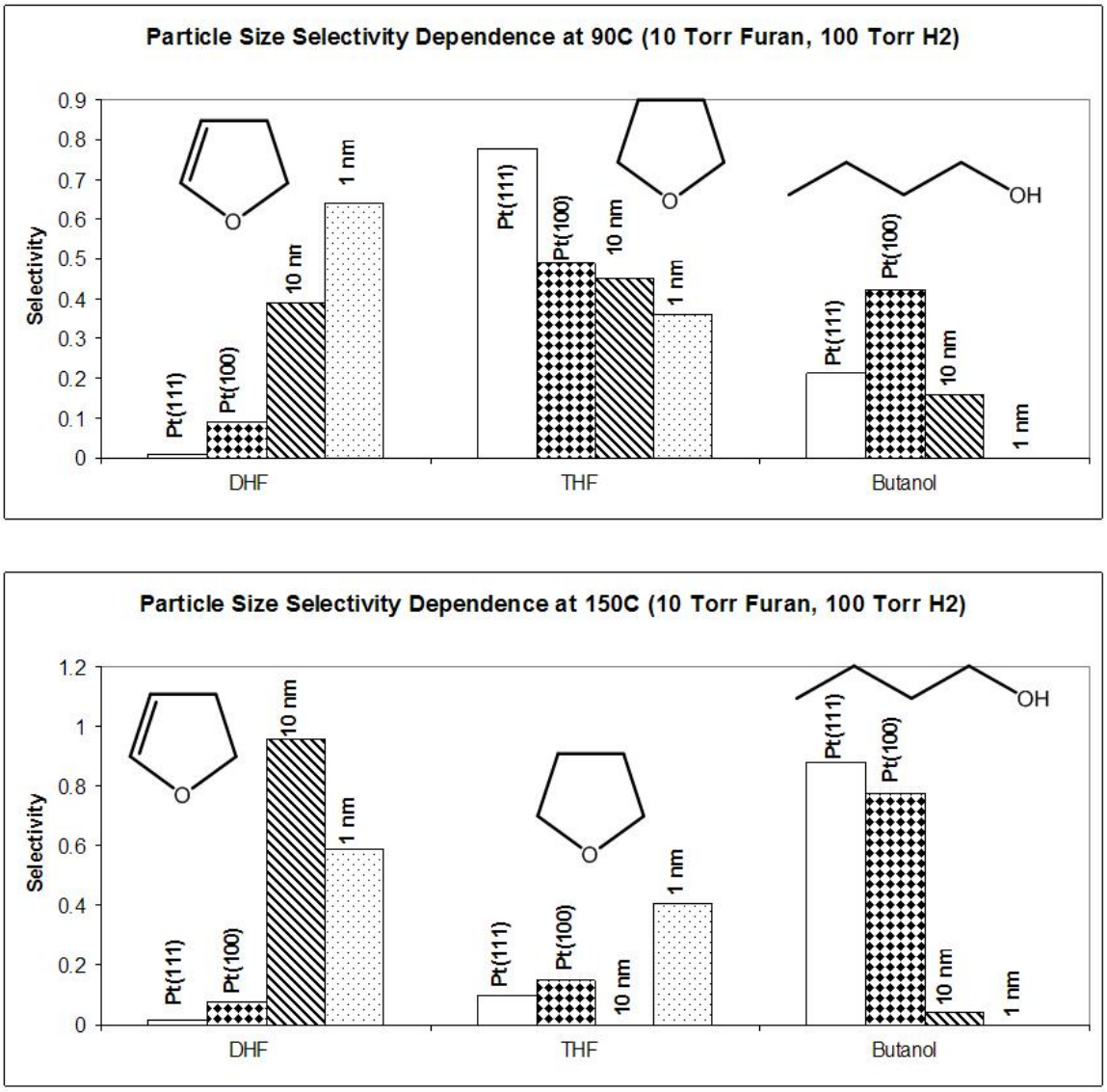

Figure 5.14. A comparison of the product selectivities during furan hydrogenation as a function of catalyst size and structure at 90°C (top) and 150°C (bottom).

References

(1) Cooper, B. H.; Donnis, B. B. L. *Applied Catalysis a-General* **1996**, *137*, 203.

(2) Netzer, F. P.; Bertel, E.; Matthew, J. A. D. *Surface Science* **1980**, *92*, 43.

(3) Horsley, J. A.; Stohr, J.; Hitchcock, A. P.; Newbury, D. C.; Johnson, A. L.; Sette, F. *Journal of Chemical Physics* **1985**, *83*, 6099.

(4) Ogletree, D. F.; Vanhove, M. A.; Somorjai, G. A. *Surface Science* **1987**, *183*, 1.

(5) Weiss, P. S.; Eigler, D. M. *Physical Review Letters* **1993**, *71*, 3139.

(6) Bratlie, K. M.; Kliewer, C. J.; Somorjai, G. A. *Journal of Physical Chemistry B* **2006**, *110*, 17925.

(7) Somorjai, G. *Introduction to Surface Science and Catalysis*, 1994.

(8) Cremer, P. S.; McIntyre, B. J.; Salmeron, M.; Shen, Y. R.; Somorjai, G. A. *Catalysis Letters* **1995**, *34*, 11.

(9) Cremer, P. S.; Su, X. C.; Shen, Y. R.; Somorjai, G. *Journal of the Chemical Society-Faraday Transactions* **1996**, *92*, 4717.

(10) Cremer, P. S.; Su, X. C.; Shen, Y. R.; Somorjai, G. A. *Journal of the American Chemical Society* **1996**, *118*, 2942.

(11) Kliewer, C. J.; Bieri, M.; Somorjai, G. A. *Journal of Physical Chemistry C* **2008**, *112*, 11373.

(12) McCrea, K.; Parker, J. S.; Chen, P. L.; Somorjai, G. *Surface Science* **2001**, *494*, 238.

(13) Aliaga, C.; Park, J. Y.; Yamada, Y.; Lee, H. S.; Tsung, C. K.; Yang, P. D.; Somorjai, G. A. *Journal of Physical Chemistry C* **2009**, *113*, 6150.

(14) Sexton, B. A. *Surface Science* **1985**, *163*, 99.

(15) Gui, J. Y.; Stern, D. A.; Lu, F.; Hubbard, A. T. *Journal of Electroanalytical Chemistry* **1991**, *305*, 37.

(16) Knight, M. J.; Allegretti, F.; Kröger, E. A.; Polcik, M.; Lamont, C. L. A.; Woodruff, D. P. *Surface Science* **2008**, *602*, 2524.

(17) Loui, A.; Chiang, S. "Investigation of furan on vicinal Pd(111) by scanning tunneling microscopy", 2004.

(18) Solomon, J. L.; Madix, R. J.; Stohr, J. *Journal of Chemical Physics* **1991**, *94*, 4012.

(19) Hlavathy, Z.; Tetenyi, P. *Surface Science* **2007**, *601*, 2026.

(20) Smith, H. A.; Fuzek, J. F. *Journal of the American Chemical Society* **1949**, *71*, 415.

(21) Huang, W.; Kuhn, J. N.; Tsung, C. K.; Zhang, Y.; Habas, S. E.; Yang, P.; Somorjai, G. A. *Nano Letters* **2008**, *8*, 2027.

(22) Kuhn, J. N.; Huang, W. Y.; Tsung, C. K.; Zhang, Y. W.; Somorjai, G. A. *Journal of the American Chemical Society* **2008**, *130*, 14026.

(23) Lee, H.; Habas, S. E.; Kweskin, S.; Butcher, D.; Somorjai, G. A.; Yang, P. D. *Angewandte Chemie-International Edition* **2006**, *45*, 7824.

(24) Zhang, Y. W.; Grass, M. E.; Kuhn, J. N.; Tao, F.; Habas, S. E.; Huang, W. Y.; Yang, P. D.; Somorjai, G. A. *Journal of the American Chemical Society* **2008**, *130*, 5868.

(25) Alexeev, O. S.; Siani, A.; Lafaye, G.; Williams, C. T.; Ploehn, H. J.; Amiridis, M. D. *Journal of Physical Chemistry B* **2006**, *110*, 24903.

(26) Bratlie, K. M.; Flores, L. D.; Somorjai, G. A. *Surface Science* **2005**, *599*, 93.

(27) Kung, K. Y.; Chen, P.; Wei, F.; Rupprechter, G.; Shen, Y. R.; Somorjai, G. A. *Review of Scientific Instruments* **2001**, *72*, 1806.

(28) Yang, M. C.; Tang, D. C.; Somorjai, G. A. *Review of Scientific Instruments* **2003**, *74*, 4554.

(29) Shen, Y. R. *The Principles of Nonlinear Optics*; John Wiley & Sons: New Jersey, 2003.

(30) Shen, Y. R. *Annual Review of Physical Chemistry* **1989**, *40*, 327.

(31) Shen, Y. R. *Nature* **1989**, *337*, 519.

(32) Yang, M.; Somorjai, G. A. *Journal of the American Chemical Society* **2004**, *126*, 7698.

(33) Ilharco, L. M.; Garcia, A. R.; Hargreaves, E. C.; Chesters, M. A. *Surface Science* **2000**, *459*, 115.

(34) Jones, G. S.; Mavrikakis, M.; Barteau, M. A.; Vohs, J. M. *Journal of the American Chemical Society* **1998**, *120*, 3196.

(35) Grass, M. E.; Zhang, Y. W.; Butcher, D. R.; Park, J. Y.; Li, Y. M.; Bluhm, H.; Bratlie, K. M.; Zhang, T. F.; Somorjai, G. A. *Angewandte Chemie-International Edition* **2008**, *47*, 8893.

Chapter 6

Structure Effects on Pyridine Hydrogenation over Pt(111) and Pt(100) Studied with Sum Frequency Generation Vibrational Spectroscopy

Sum frequency generation vibrational spectroscopy was applied *in-situ* during pyridine hydrogenation (10 Torr pyridine and 100 Torr hydrogen) over two well-defined platinum single crystals, Pt(100) and Pt(111). The surface reaction intermediates were clarified. Pyridine adsorbs to both crystals as the α-pyridyl intermediate. Over Pt(100) 1,4-dihydropyridine was observed as a reaction intermediate, while over Pt(111) this was not detected. Upon heating the crystals from 300K to 350K, the pyridine ring lies down flat on the catalyst surfaces. Over Pt(111) a tilted piperidine product is bound to the surface. No evidence was found for the pyridinium cation intermediate over either of these surfaces.

6.1. Introduction

Catalytic reactions involving aromatic cyclic and heterocyclic molecules are important for the chemical industry for both fuel reforming and environmental concerns.[1] Hydrodenitrogenation chemistry is vitally important to the fuel reforming industry as nitrogen-containing compounds inhibit the downstream catalysts used for hydrodesulfurization through competitive adsorption[2] and act as a poison to acid

catalysts.[3] Several recent works have focused on the understanding of the fundamental molecular level details of the adsorption and reaction of nitrogen-containing aromatics on model platinum catalysts.[4-7] In general, molecular level studies of surface reactions are of paramount importance and is the subject of much current research.[8] Pyridine is a six-membered aromatic ring with one nitrogen heteroatom. The lone pair of electrons on the nitrogen atom are localized, meaning they do not take part in the aromaticity. This means that pyridine is an electron donor, having the ability to donate electron density to a catalyst surface through either its π-aromatic orbitals or through σ-donation of the N lone pair to the surface.

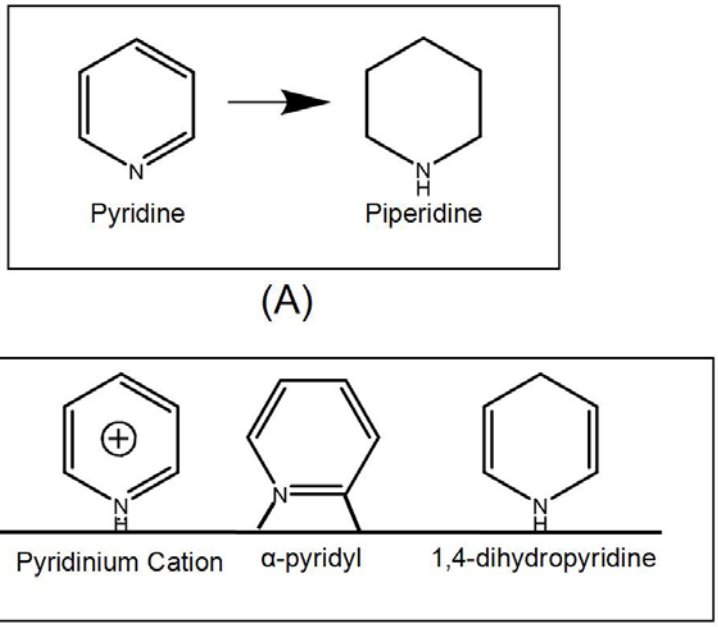

Scheme 6.1. Panel A displays the hydrogenation of pyridine to form the product piperidine. Panel B displays the possible surface bound reaction intermediates proposed in the literature, pyridinium, α-pyridyl, and 1,4-dihydropyridine. In addition all three of these intermediates displayed as upright, could be tilted with respect to the surface.

One of the fundamental questions in pyridine adsorption to catalyst surfaces is whether it will bind through the aromatic orbitals, creating a parallel lying structure to a catalyst surface, or through the lone-pair electron donation of the N atom creating a vertical structure on the surface.[5] Haq and King[5] propose based on RAIRS data that at 300K and higher over Pt(111) pyridine adsorbs at all coverages as an α-pyridyl surface intermediate by binding through the nitrogen atom, and cleaving the C-H bond from the α-carbon to create two bonds to the metal surface (Scheme 6.1). Looking at 12 nm cubic Pt nanoparticles coated with tetradecyltrimethylammonium bromide (TTAB), nanoparticles which express <100> facets selectively, Bratlie and Somorjai found that upon the coadsorption of pyridine and hydrogen on this catalyst surface, the pyridine was protonated at the nitrogen to create a pyridinium cation on the surface[4] as evidenced by a unique N-H stretching vibration at 3450 cm^{-1}. The formation of pyridinium has been demonstrated by Lee and Masel over a Pt(110) single crystal under UHV conditions using HREELS upon the coadsorption of pyridine and hydrogen.[7] Haq and King demonstrate that the adsorption geometry of pyridine is coverage dependent, in that higher coverages tend toward tilted or upright adsorption geometries, while low surface coverages lead to parallel lying pyridine on the Pt(111) surface.

In order to help clarify the effect of catalyst geometry in the coadsorption of pyridine and hydrogen, sum frequency generation vibrational spectroscopy (SFG-VS) is applied in this work during pyridine hydrogenation at Torr pressures over Pt(111) and Pt(100) with the goal of determining the surface intermediates present from 300K-400K.

6.2. Experimental Section

Materials

Prior to use, pyridine (99.9%, Sigma-Aldrich Inc.) was subjected to several freeze-pump-thaw cycles and the purity was checked by means of gas chromatography.

The high-pressure/ultra-high vacuum system

All experiments reported here were carried out in a high-pressure/ultrahigh-vacuum (HP/UHV) system. The UHV chamber is operated at a base pressure of 2 x 10^{-10} Torr and is isolated from the HP cell by a gate valve. The UHV system is equipped with an Auger electron spectrometer (AES), a quadrupole mass spectrometer (Stanford Research Systems) and an ion bombardment gun (Eurovac). The HP cell consists of two CaF_2 conflat windows that allow transmission of infrared (IR), visible (VIS) and sum frequency radiation for sum frequency generation (SFG) experiments. The product gases in the HP cell are constantly mixed via a recirculation pump and kinetic data is acquired by periodically sampling the reaction mixture and analyzing the relative gas phase composition in a flame ionization detector (FID) of a gas chromatograph (Hewlett Packard HP 5890 on a 5% Carbowax 20M packed column).

Sample preparation

Prior to each experiment, the Pt(111) and Pt(100) crystal surfaces were cleaned in the UHV chamber by Ar^+ (1 keV) sputtering for 20 min at about 5 x 10^{-5} Torr of Ar. After sputtering, the crystals were heated to 1103 K in the presence of O_2 of 5 x 10^{-7} Torr and annealed at the same temperature for 2 min. The cleanliness of the crystal surfaces was verified by AES and the crystallographic structure verified with low energy electron diffraction (LEED). The samples were then transferred into the HP cell for SFG and kinetic studies.

Sum Frequency generation vibrational spectroscopy

For SFG measurements, an active/passive mode-locked Nd:YAG laser (Leopard D-20, Continuum) with a pulse width of 20 ps and a repetition rate of 20 Hz was used. The fundamental output at 1064 nm was sent through an optical parametric generation/amplification (OPA/OPG) stage where a tunable IR (2300—4000 cm^{-1}) and a second harmonic VIS (532 nm) beam were created. The IR (150 μJ) and VIS (200 μJ) beams were spatially and temporally overlapped on the crystal surface at angles of incidence of 55 and 60°, respectively, with respect to the surface normal. The generated SFG beam was collected and sent through a motorized monochromator equipped with a photomultiplier tube to detect the SFG signal intensity. The signal-to-noise ratio was further increased by using a gated integrator while the IR beam was scanned through the spectral region of interest. The SFG process is enhanced when the IR beam comes into resonance with a vibrational mode of a molecule adsorbed at the surface, giving rise to a vibrational spectrum of adsorbed species. More information on the HP/UHV system and SFG measurement can be found elsewhere.[9-14]

6.3. Results and Discussion

Figure 6.1 displays the sum frequency generation vibrational spectrum of 10 Torr pyridine and 100 Torr hydrogen over Pt(100). Two very strong resonances are observed. At 3050 cm^{-1} the C-H aromatic stretch is seen. The high intensity of this peak indicates the pyridine ring is in an upright adsorption geometry with respect to the surface. A second dominant peak is observed at 2845 cm^{-1} corresponding to a CH_2 symmetric stretch off of the saturated pyridine ring, piperidine (Scheme 6.1). A much weaker peak is seen at 2905 cm^{-1} assigned to a CH_2 asymmetric surface perturbed species.

The spectrum displayed in figure 6.1 shows no evidence of the pyridinium cation on the Pt(100). In the work of Lee and Masel[7] on Pt(110) and Bratlie and Somorjai on cubic Pt nanoparticles, the pyridinium N-H stretch was observed at 3450 cm^{-1}. The work of Lee et al was done under UHV conditions, but the work of Bratlie et al was performed under identical reactant partial pressures as used in this experiment. As the Pt cubic nanoparticles used in that work express the <100> face of platinum dominantly, the

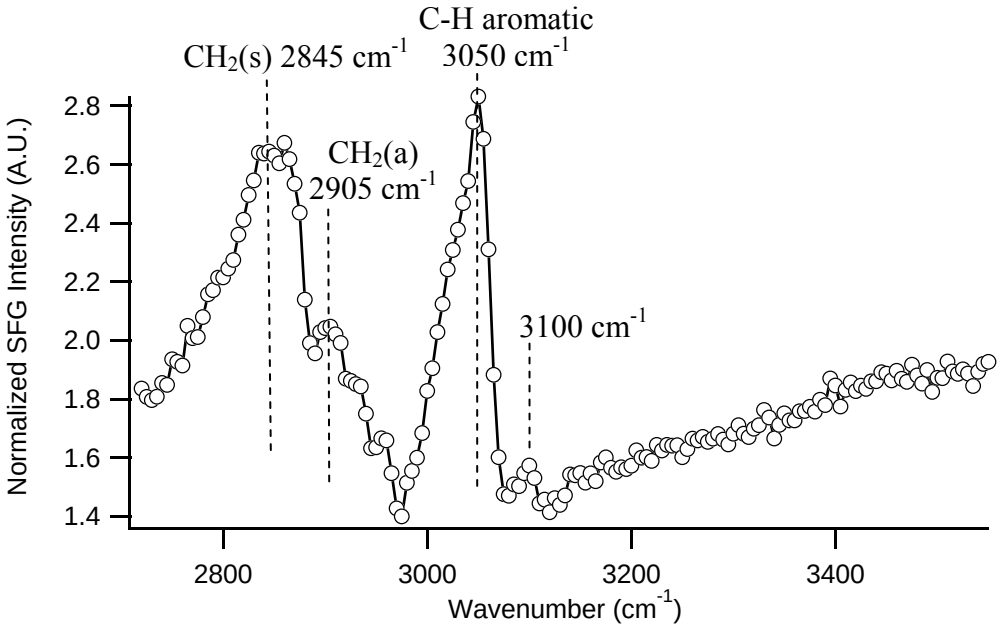

Figure 6.1. SFG-VS spectrum of 10 Torr pyridine and 100 Torr hydrogen over a Pt(100) crystal at 300K. Two stretches are quite dominant in the spectrum, the aromatic C-H and the symmetric methylene stretch indicating an upright structure on the Pt(100) surface. No evidence is obtained for the pyridinium cation over Pt(100).

difference in reaction intermediate must be due to a particle size effect or due to the capping agent stabilizing the protonated pyridine as TTAB (the capping agent used in said work) is a charged structure. No N-H modes of any type are observed in the spectrum at 300K.

In the work of Haq and King[5] for pyridine adsorption at 300K at all coverages they determined a vertical α-pyridyl surface structure. This assignment agrees with ARUPS results[15] also pointing towards a vertical α-pyridyl structure. This assignment agrees with the vertical structure we propose. It is clear from the spectrum that the hydrogenated product is also aligned perpendicular to the surface. In the work of Lee and Masel, several possible surface intermediates are explored using ab initio calculations at the B3LYP/6-311G-(d,p) level, and the respective reference spectra for the possible intermediates were calculated. Our spectrum is in near perfect agreement with the 1,4-dihydropyridine surface intermediate. The only peak missing is that of the N-H mode, which we postulate is because the intermediate is bound through the nitrogen to the Pt(100) surface replacing the hydrogen on the nitrogen atom.

Figure 6.2 displays the temperature dependent SFG-VS spectra of 10 torr pyridine and 100 torr hydrogen over Pt(100) from 300K-400K. Upon heating to 350K, the peak at 3050 cm^{-1} shrinks until it is comparable in size to a neighboring peak at 3100 cm^{-1}. A peak at 3100 cm^{-1} and 3050 cm^{-1} agrees with the C=C-H stretch at the α and β carbons respectively of 1,4-dihydropyridine.

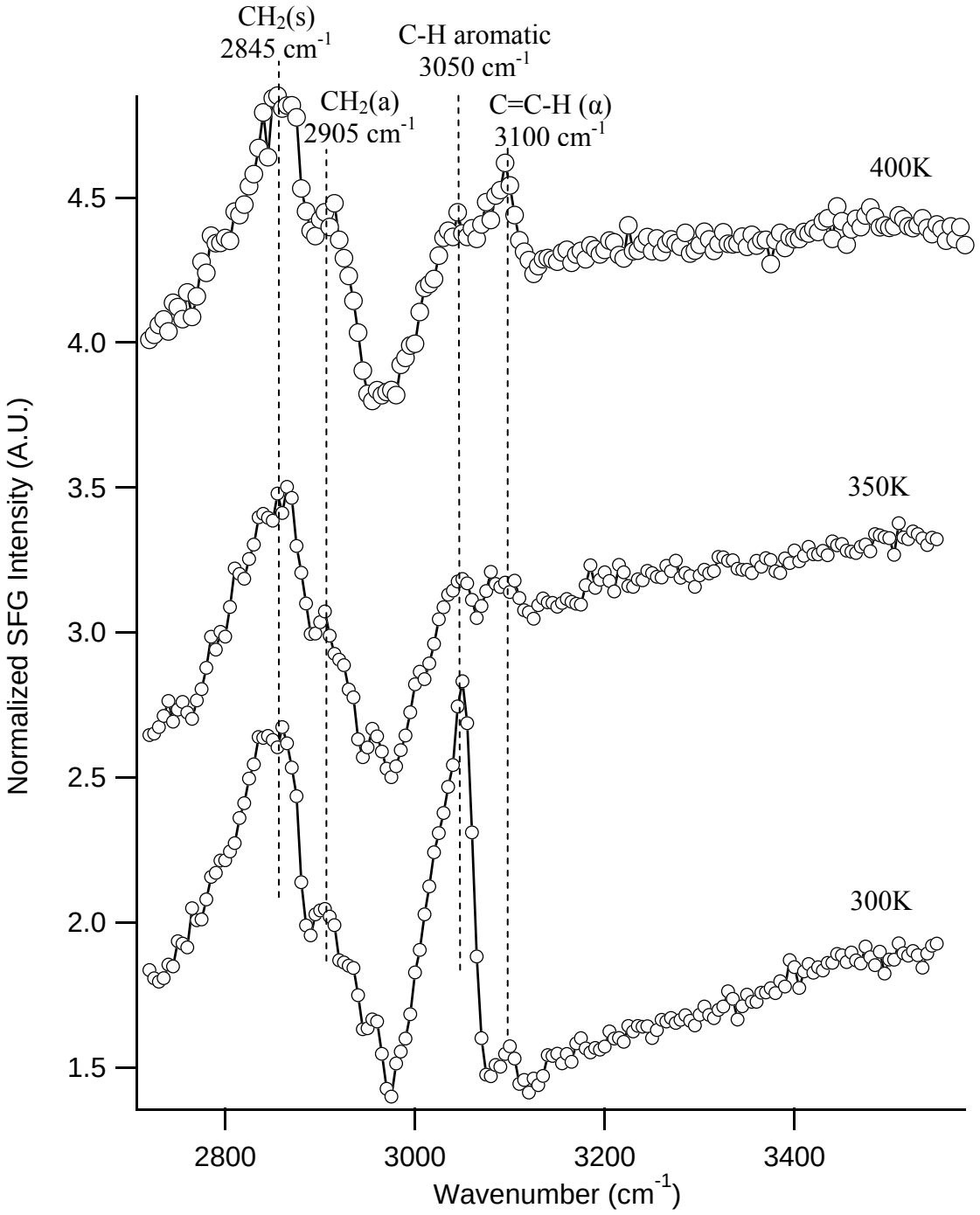

Figure 6.2. Temperature dependent SFG-VS spectra of 10 Torr pyridine and 100 Torr hydrogen over Pt(100). Evidence for the presence of a vertical α-pyridyl structure at 300K and 1,4-dihydropyridine as the sample is heated to 350K.

The rest of the spectrum remains unchanged up to 400K. The disappearance of the dominant peak at 3050 cm^{-1} indicates the pyridine ring becomes more parallel to the Pt(100) surface at elevated temperatures. This is in agreement with the general trend observed in the literature[5,7] that at lower coverages over platinum the pyridine ring adsorbs in a parallel fashion. Surface coverage σ by an adsorbate is defined as

$$\sigma = F\tau \tag{1}$$

where F is the incidenct flux of molecules and τ is the surface residence time given by

$$\tau = \tau_0 e^{(\frac{\Delta H_{ads}}{RT})} \tag{2}$$

where τ_0 is correlated to the surface atom vibration time (on the order of 10^{-12} s), ΔH_{ads} is the adsorption energy, T is the temperature, and R is the gas constant. Thus, as the temperature is raised the surface coverage goes down with temperature. This then agrees with the disappearance of the pyridine aromatic peak. As the temperature is raised, the surface coverage decreases, which has been previously observed to induce a parallel orientation of the pyridine ring. At the elevated temperatures the spectrum still agrees with the presence of vertical 1,4-dihydropyridine on the surface up to 400K on Pt(100).

To help elucidate the effect of catalyst structure, these results were compared to those acquired over a Pt(111) crystal. Figure 6.3 displays the temperature dependent SFG-VS spectra of 10 Torr pyridine and 100 Torr hydrogen over a Pt(111) crystal from 300K-400K. Once again, no evidence was found for pyridinium, nor any N-H modes on the surface. At 300K, a resonance is seen at 3060 cm^{-1} corresponding to the C-H aromatic stretch of the pyridine molecule. This stretch is not quite as dominant as the one

seen over Pt(100). Upon heating the crystal to 350K, only the methylene symmetric and asymmetric stretches are seen in the spectrum.

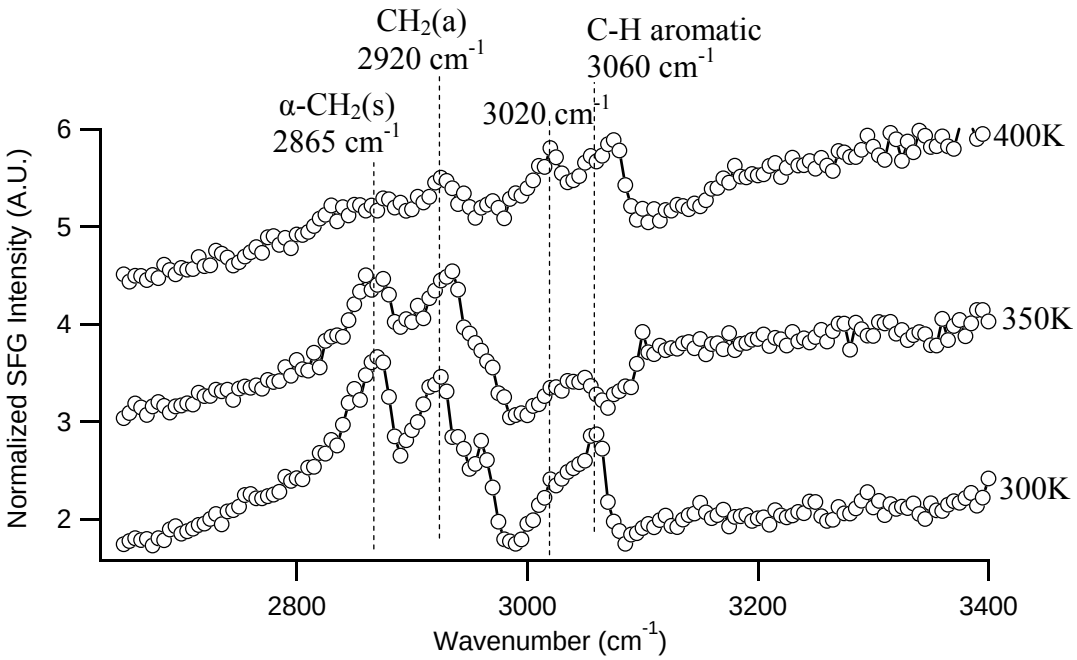

Figure 6.3. Temperature dependent SFG-VS spectra of 10 Torr pyridine and 100 Torr hydrogen over Pt(111) from 300K-400K.

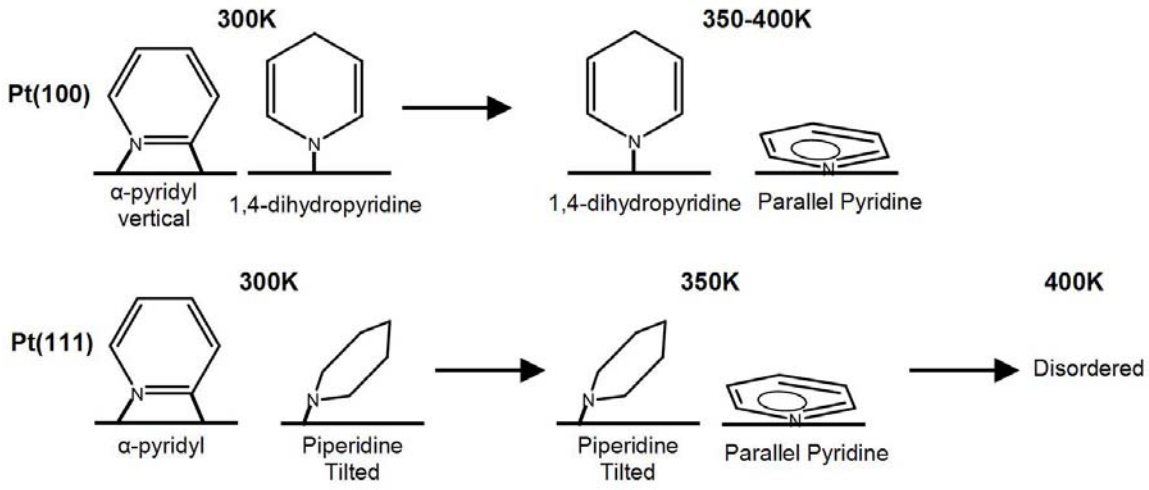

Scheme 6.2. Observed and proposed reaction intermediates for pyridine hydrogenation (10 Torr pyridine/100 Torr hydrogen) over Pt(100) (top) and Pt(111) (bottom) as a function of temperature from 300-400K.

Heating the crystal further to 400K results in all of the modes nearly vanishing altogether. Only a small C-H aromatic resonance is still seen. This is likely due to increasing disorder on the surface at elevated temperatures. SFG-VS requires dipoles to be ordered in order to generate a signal, thus as molecules disorder, SFG-VS signal diminishes. The presence of the α-carbon methylene stretch and the disappearance of all modes other than the methylene stretches at 350K indicates that we are seeing the saturated product piperidine on the surface, and that similarly to Pt(100), the pyridine ring lies more parallel at elevated temperatures. Scheme 6.2 summarizes the results for reaction intermediates found over Pt(100) and Pt(111).

6.4. Conclusions.

Sum frequency generation vibrational spectroscopy has been applied to the study of pyridine hydrogenation over two well-defined platinum single crystals, Pt(100) and Pt(111), to help elucidate the effect that catalyst structure has in the adsorption and reaction of pyridine. Relating this data to previously published work, the adsorption modes and reaction intermediates were clarified. Over Pt(100) the pyridine molecule adsorbs as an α-pyridyl intermediate perpendicular to the metal surface. Also present is the 1,4-dihydropyridine intermediate. Upon heating the crystal to 350K, the perpendicular α-pyridyl structure disappears, and the pyridine ring is adsorbed parallel to the metal surface while the 1,4-dihydropyridine remains. The intermediates remain constant upon heating further to 400K. No evidence of an N-H mode on the surface was found, thus the 1,4-dihydropyridine is adsorbed through the N with a σ-bond. Further, no evidence of the proposed pyridinium cation intermediate was found on this surface, as was found over Pt(110)[7].

Over the Pt(111) crystal the pyridine adsorbs as an α-pyridyl intermediate as well. The hydrogenated product piperidine is present on the surface in a tilted geometry at 300K. Upon heating the crystal to 350K, the α-pyridyl peak disappears indicating pyridine lies parallel on the surface at elevated temperature. Only the piperidine is visible at 350K. Upon heating the Pt(111) crystal to 400K the molecules disorder on the surface as all SFG resonant intensity vanishes.

References

(1) Cooper, B. H.; Donnis, B. B. L. *Applied Catalysis a-General* **1996**, *137*, 203.

(2) Girgis, M. J.; Gates, B. C. *Industrial & Engineering Chemistry Research* **1991**, *30*, 2021.

(3) Busca, G. *Chemical Reviews* **2007**, *107*, 5366.

(4) Bratlie, K. M.; Komvopoulos, K.; Somorjai, G. A. *Journal of Physical Chemistry C* **2008**, *112*, 11865.

(5) Haq, S.; King, D. A. *Journal of Physical Chemistry* **1996**, *100*, 16957.

(6) Kliewer, C. J.; Bieri, M.; Somorjai, G. A. *Journal of Physical Chemistry C* **2008**, *112*, 11373.

(7) Lee, I. C.; Masel, R. I. *Journal of Physical Chemistry B* **2002**, *106*, 368.

(8) Somorjai, G. A.; Kliewer, C. J. *Reaction Kinetics and Catalysis Letters* **2009**, *96*, 191.

(9) Bratlie, K. M.; Flores, L. D.; Somorjai, G. A. *Surface Science* **2005**, *599*, 93.

(10) Kung, K. Y.; Chen, P.; Wei, F.; Rupprechter, G.; Shen, Y. R.; Somorjai, G. A. *Review of Scientific Instruments* **2001**, *72*, 1806.

(11) Yang, M. C.; Tang, D. C.; Somorjai, G. A. *Review of Scientific Instruments* **2003**, *74*, 4554.

(12) Shen, Y. R. *The Principles of Nonlinear Optics*; John Wiley & Sons: New Jersey, 2003.

(13) Shen, Y. R. *Annual Review of Physical Chemistry* **1989**, *40*, 327.

(14) Shen, Y. R. *Nature* **1989**, *337*, 519.

(15) Connolly, M.; Somers, J.; Bridge, M. E.; Lloyd, D. R. *Surface Science* **1987**, *185*, 559.

Chapter 7

Hydrogenation of the α,β-Unsaturated Aldehydes Acrolein, Crotonaldehyde, and Prenal over Pt Single Crystals: A Kinetic and Sum-Frequency Generation Vibrational Spectroscopy Study

Sum-frequency generation vibrational spectroscopy (SFG-VS) and kinetic measurements using gas chromatography have been used to study the surface reaction intermediates during the hydrogenation of three α,β-unsaturated aldehydes, acrolein, crotonaldehyde, and prenal, over Pt(111) at Torr pressures (1 Torr aldehyde, 100 Torr hydrogen) in the temperature range of 295K to 415K. SFG-VS data showed that acrolein has mixed adsorption species of η_2-di-σ(CC)-trans, η_2-di-σ(CC)-cis as well as highly coordinated η_3 or η_4 species. Crotonaldehyde adsorbed to Pt(111) as η_2 surface intermediates. SFG-VS during prenal hydrogenation also suggested the presence of the η_2 adsorption species, and became more highly coordinated as the temperature was raised to 415K, in agreement with its enhanced C=O hydrogenation. The effect of catalyst surface structure was clarified by carrying out the hydrogenation of crotonaldehyde over both Pt(111) and Pt(100) single crystals while acquiring the SFG-VS spectra in situ. Both the kinetics and SFG-VS showed little structure sensitivity. Pt(100) generated more

decarbonylation "cracking" product while Pt(111) had a higher selectivity for the formation of the desired unsaturated alcohol, crotylalcohol.

7.1 Introduction

The selective hydrogenation of an unsaturated C=C bond in the presence of a C=O carbonyl group of the same molecule has been a subject of much research in recent years. Both experimental and theoretical work has been devoted to this topic and comprehensive reviews of the subject have been published[1-4]. One product of this reaction, the unsaturated alcohol, is an important intermediate in both the pharmaceutical and fragrance industries. However, it is quite difficult to achieve a high selectivity and activity for the unsaturated alcohol product because the hydrogenation of the C=C is thermodynamically preferred by roughly 35 kJ/mol[2].

The platinum group metals are the catalysts most frequently employed during this reaction, but the selectivity for the desired unsaturated alcohol is relatively low for these catalysts. Over platinum, the selectivity for unsaturated alcohol has been shown to improve upon alloying with another metal[5], for instance Fe[6] or Sn[7], as well as upon the addition of various promoters[3,8], such as potassium on the surface. Catalyst structure, such as the (111) or (100) crystal face of a metal, has also been suggested to play a role in the reaction selectivity[9].

Also effecting the selectivity in the hydrogenation of α,β-unsaturated aldehydes is the amount of steric hindrance to adsorption added to the C=C bond by the placement of bulky groups, such as phenyl or methyl groups, on this side of the molecule. Hoang-Van et al[10] reported on the hydrogenation of acrolein over various platinum catalysts. Each of

the widely used Pt based catalysts (Pt black, Pt-Al, Pt-Si) showed greater than 99% selectivity for the hydrogenation of the C=C to yield propionaldehyde (Scheme 7.1).

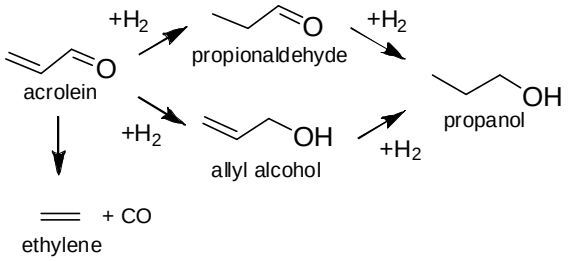

Scheme 7.1. The hydrogenation pathways for acrolein.

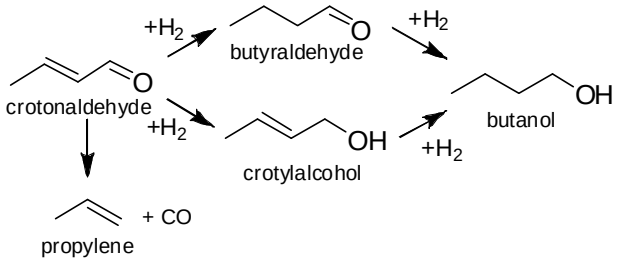

Scheme 7.2. The hydrogenation pathways for crotonaldehyde.

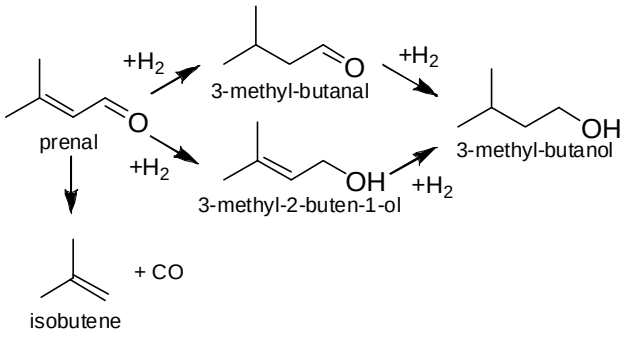

Scheme 7.3. The hydrogenation pathways for prenal.

In comparison, for the hydrogenation of prenal, the same molecule as acrolein with two methyl groups added to the C=C bond, Birchem et al[7,11] show at 353K the dominant product to be the unsaturated alcohol, a complete reversal of the selectivity seen for acrolein hydrogenation.

In this work, the hydrogenation of acrolein, crotonaldehyde, and prenal (Schemes 7.1-7.3) was carried out over Pt(111) while using sum frequency generation vibrational spectroscopy (SFG-VS) to monitor the surface reaction intermediates. These spectra are then compared to published gas phase IR spectra, HREEL spectra, and DFT calculations to assist in the interpretation. Crotonaldehyde, with a reaction selectivity which is between that of prenal hydrogenation and acrolein hydrogenation, was chosen to elucidate the effect that catalyst structure has on this reaction. Reaction kinetics using gas chromatography and SFG-VS spectra were taken for crotonaldehyde hydrogenation over Pt(111) and Pt(100) in the temperature range from 150K to 415K. Finally, prenal hydrogenation was studied kinetically over Pt(111) in the temperature range of 308K to 403K.

7.2. Experimental Section

Materials

Crotonaldehyde (99.5%, Fluka) and prenal (97%, Sigma-Aldrich Inc.) were subjected to several freeze-pump-thaw cycles prior to use and the purities were checked by means of gas chromatography and quadrupole mass spectrometry. Acrolein was obtained in gas phase from Airgas with balance of research grade argon and purity verified with quadrupole mass spectrometry to be 99%.

The high-pressure/ultra-high vacuum system

All experiments reported here were carried out in a high-pressure/ultrahigh-vacuum (HP/UHV) system. The UHV chamber is operated at a base pressure of 2 x 10^{-10} Torr and is isolated from the HP cell by a gate valve. The UHV system is equipped with an Auger electron spectrometer (AES), a quadrupole mass spectrometer (Stanford Research Systems) and an ion bombardment gun (Eurovac). The HP cell consists of two CaF_2 conflat windows that allow transmission of infrared (IR), visible (VIS) and sum frequency radiation for sum frequency generation (SFG) experiments. The product gases in the HP cell are constantly mixed via a recirculation pump and kinetic data is acquired by periodically sampling the reaction mixture and analyzing the relative gas phase composition in a flame ionization detector (FID) of a gas chromatograph (Hewlett Packard HP 5890 on a 5% Carbowax 20M packed column).

Sample preparation

Prior to each experiment, the Pt(111) and Pt(100) crystal surfaces were cleaned in the UHV chamber by Ar^+ (1 keV) sputtering for 20 min at approximately 3 x 10^{-5} Torr of Ar. After sputtering, the crystals were heated to 1103 K in the presence of O_2 of 5 x 10^{-7} Torr and annealed at the same temperature for 2 min. The cleanliness of the crystal surfaces was verified by AES and the crystallographic structure verified with low energy electron diffraction (LEED). The samples were then transferred into the HP cell for SFG and kinetic studies.

Sum Frequency generation vibrational spectroscopy

For SFG measurements, an active/passive mode-locked Nd:YAG laser (Leopard D-20, Continuum) with a pulse width of 20 ps and a repetition rate of 20 Hz was used. The fundamental output at 1064 nm was sent through an optical parametric

generation/amplification (OPA/OPG) stage where a tunable IR (2300-4000 cm^{-1}) and a second harmonic VIS (532 nm) beam were created. The IR (150 μJ) and VIS (200 μJ) beams were spatially and temporally overlapped on the crystal surface at angles of incidence of 55 and 60°, respectively, with respect to the surface normal. The generated SFG beam was collected and sent through a motorized monochromator equipped with a photomultiplier tube to detect the SFG signal intensity. The signal-to-noise ratio was further increased by using a gated integrator while the IR beam was scanned through the spectral region of interest. The SFG signal, I^{SFG}, is related to the incoming visible (I^{VIS}) and infrared (I^{IR}) beam intensities, and second-order susceptibility of the media ($\chi^{(2)}$), according to eq 7.1:

$$I^{SFG}(\omega_{SFG}) \propto \left|\chi^{(2)}\right|^2 I^{VIS}(\omega_{VIS}) I^{IR}(\omega_{IR}) \qquad (7.1)$$

($\chi^{(2)}$) is enhanced when ω_{IR} is at resonance with a vibrational mode of the molecules, q, according to eq 2:

$$I^{SFG} \propto \left|\chi_{NR}{}^{(2)} e^{i\phi_{NR}} + \sum_q \frac{A_q}{\omega_{IR} - \omega_q + i\Gamma_q} e^{i\gamma_q}\right|^2 \qquad (7.2)$$

where $\chi_{NR}{}^{(2)}$ is the nonresonant nonlinear susceptibility, $e^{i\phi_{NR}}$ is the phase associated with the nonresonant background, A_q is the strength of the qth vibrational mode, ω_{IR} is the frequency of the incident IR laser beam, ω_q is the frequency of the qth vibrational mode, Γ_q is the natural line width of the qth vibrational transition, and $e^{i\gamma_q}$ is the phase associated with the qth vibrational transition. All SFG-VS spectra reported are data fit to a form of eq 7.2.

Since the gas phase in the HP cell absorbs some small amount of the incoming IR radiation, the SFG signal was then normalized by using the following expression (eq 7.3):

$$I^{\mathrm{SFG,norm}} = \frac{I^{\mathrm{SFG}}}{\sqrt{I^{\mathrm{IR,before}} I^{\mathrm{IR,after}}}} \qquad (7.3)$$

where $I^{\mathrm{IR,before}}$ and $I^{\mathrm{IR,after}}$ define the IR beam intensities measured before and after the HP cell to correct for any infrared radiation absorbed between the HP cell window and the sample, which is mounted exactly halfway between the HP cell entrance and exit window. More information on the HP/UHV system and SFG measurement can be found elsewhere.[12-16]

7.3. Results and Discussion

7.3.1. Sum Frequency Generation Vibrational Spectroscopy of Acrolein, Crotonaldehyde, and Prenal Hydrogenation over Pt(111)

7.3.1.1. Acrolein Hydrogenation on Pt(111) – SFG-VS Results

Acrolein is the simplest α,β-unsaturated aldehyde which makes it attractive for surface science study. As can be seen in Scheme 7.1, it contains only the conjugated carbonyl and alkene groups with no side groups. Using density functional theory analysis, Loffreda et al[17] examined possible adsorption modes of acrolein on Pt(111) at various coverages and determined adsorption energies and predicted a vibrational spectrum for each of the possible stable structures. Experimental assignments of the gas phase modes of acrolein have been previously published.[18] Further, Murillo et al[19] examined the adsorption of acrolein to the Pt(111) surface at 110K using HREELS. Our spectra obtained in-situ during the catalytic hydrogenation reactions are compared to the published data.

There are seven stable adsorption modes presented in the theoretical work mentioned above. First, the η_1 adsorption mode has the oxygen atom as the only part of the acrolein molecule which interacts with the Pt(111) surface. The η_2-cis and η_2-trans modes involve

a di-σ bond to two Pt atoms originating from the C=C of the acrolein. Clearly, the cis conformer being the one with the oxygen of the carbonyl pointing back towards the acrolein molecule, while in the trans form it points away. The η_3-cis and η_3-trans are the same as the η_2 adsorption modes with the exception that the oxygen atom of the carbonyl is pointing down to and bonding with the metal surface. Finally the η_4-cis and η_4-trans adsorption modes are bound to the surface via two di-σ bonds, one originating from the C=C and one from the C=O.

Figure 7.1 shows the SFG vibrational spectrum of 1 Torr acrolein with no hydrogen added over a Pt(111) single crystal at 295K. Five vibrational resonances are seen in this C-H region. The vibrational resonance furthest to the red is present at 2785 cm^{-1} which can be assigned to the aldehyde C-H stretch. The aldehyde C-H in gas phase acrolein is at 2800 cm^{-1}, so a 15 cm^{-1} red-shift of this clearly identifiable mode occurs upon adsorption. Table 7.1 gives a direct comparison between the observed SFG-VS vibrational modes and those previously published for acrolein in the literature.

To gain deeper insight into the true bonding characteristics of the acrolein molecule to the Pt(111) surface the vibrational spectra are compared to those predicted with DFT. Although there are often several structures that correspond to a given vibrational frequency, one can only accept structures if the other peaks in the predicted spectrum also agree with the observed vibrational modes. In the DFT work of Loffreda et al[17], the only chemisorption mode of acrolein with a vibrational mode near this value is the η_2-trans species. The rest of the resonances are seen at 2850 cm^{-1}, 2930 cm^{-1}, 3020 cm^{-1}, and 3060 cm^{-1}. There is a possible shoulder at ~2865 cm^{-1} as well. The η_1 adsorption species, interacting with the Pt surface solely through the oxygen atom, may be ruled out

due to the absence of any modes above 3100 cm^{-1} in the SFG-VS spectrum, likewise the η_4-cis can be eliminated as an option. The mode observed at 2850 cm^{-1} corresponds best with the η_2-cis C-H aldehyde vibrational mode. The two lower frequency aldehyde peaks at 2850 cm^{-1} and 2785 cm^{-1} are quite indicative of the η_2 di-σ(CC) adsorption mode as none of the more highly coordinated surface species have C-H resonances that far to the red.

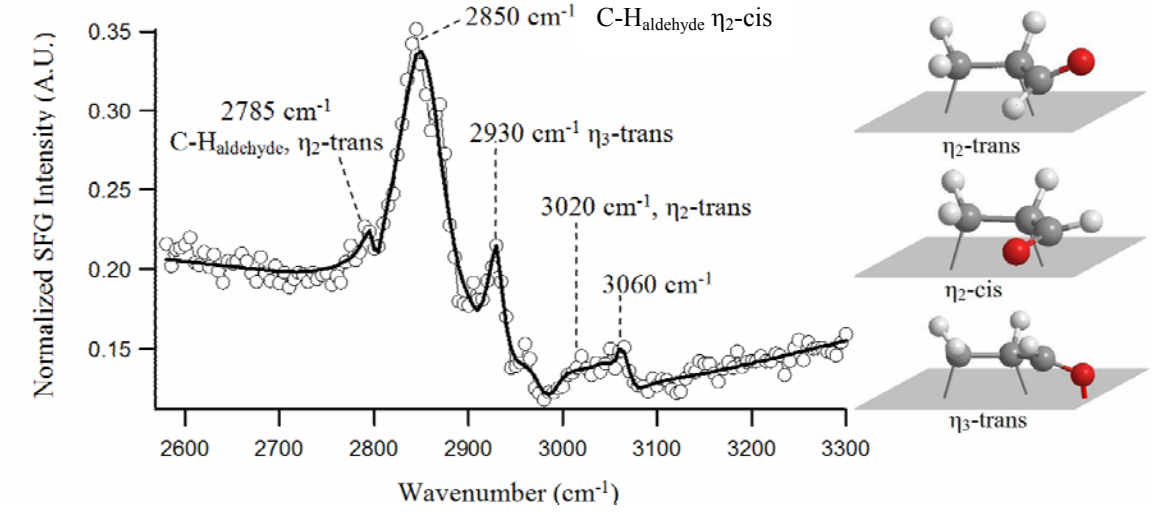

Figure 7.1. SFG-VS spectrum of 10 Torr furan over Pt(111) in the absence of excess hydrogen. Stretches are seen for the C-H aromatic stretch of furan, the C-H vinylic stretch of DHF, and the CH_2 symmetric and asymmetric stretches of the THF ring. In the molecule representations, oxygen is red, carbon is gray, and hydrogen is white.

Figure 7.2 displays the SFG spectra as 100 Torr hydrogen is added and the temperature is raised to 415K. Upon the addition of hydrogen at room temperature the spectrum

undergoes two changes. The small aldehyde peak at 2785 cm^{-1}, corresponding to the η_2-trans surface species, disappears as well as the peak at 3020 cm^{-1}.

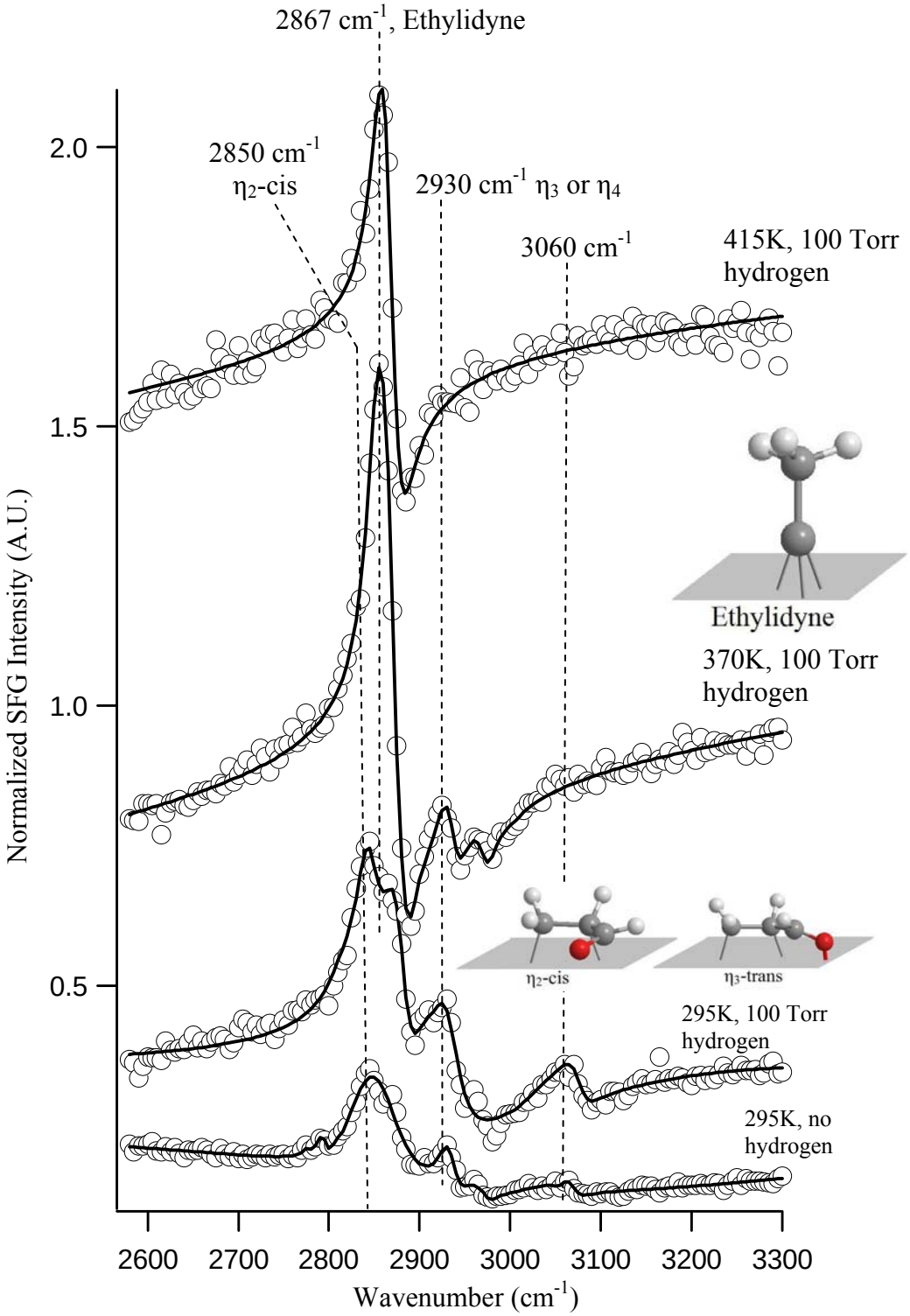

Figure 7.2. SFG-VS spectra of 1 Torr acrolein over the Pt(111) crystal surface. The bottom spectra was taken in the absence of hydrogen, then the subsequent spectra include the addition of 100 Torr hydrogen and heating the crystal to 415K. The acrolein peaks vanish and only ethylidyne remains as the crystal is heated.

Due to the fact that those two modes disappear together, as well as the fact that DFT predicts the η_2-trans adsorption mode to have absorptions in both those regions, the 3020 cm^{-1} peak is also assigned to a C-H vibration off of the di-σ bond of the η_2-trans species (Figs. 7.1,7.2) which agrees with the assignment made in the comparison to experimental values in Table 7.1.

Assignment	IR Gas Phase	HREELS 110K	SFG-VS 298K
$\nu_{asym}(=CH_2)$	3103	3098	3060
N(β)(CH)	3069	2997	3020
$\nu_{sym}(=CH_2)$	2998	2908	2930
$\nu_{aldehyde}(CH)$	2800	2854	2850/2785

Table 7.1. Summary of experimental acrolein vibrational modes (given in cm^{-1}) for gas phase acrolein[18], acrolein adsorbed onto Pt(111) at 110K using HREELS[19], and the observed SFG vibrational modes for 1 Torr acrolein on Pt(111) at 298K.

Upon heating the Pt(111) crystal to 370K, a strong new peak appears at 2867 cm^{-1}. The other resonances become very weak and the only one with appreciable signal remains at 2930 cm^{-1}. Upon further heating the Pt(111) crystal to 415K, the only remaining peak is the 2867 cm^{-1} resonance corresponding to ethylidyne on the surface resulting from the decarbonylation of acrolein. The ethylidyne is red-shifted by about 10 cm^{-1} from its usual location on a clean Pt(111) crystal, but the coadsorption of CO and ethylidyne on Pt(111) has been previously reported to cause a similar red-shift in the ethylidyne peak[20]. The observation of ethylidyne on Pt(111) after acrolein adsorption was also noted by de Jesus and Zaera[21] using RAIRS.

According to the Gibbs free adsorption energy curves reported by Loffreda et al[22] for acrolein adsorption to Pt(111) the experimental conditions used here (1 Torr acrolein, 295-415K) likely crosses the 0 Gibbs free adsorption energy line as the temperature is raised, thus favoring desorption of the acrolein molecule. This is in agreement with the SFG-VS spectra, as by 415K the only species remaining on the surface is ethylidyne. Lastly, the peak observed at 2930 cm^{-1} is indicative of a more highly coordinated η_3-trans or η_4-trans surface species. In relation to the DFT calculations, it is most closely matched with the η_3-trans species. Clearly, then, for acrolein adsorption and hydrogenation over Pt(111) there exists a mixed state of adsorption mode surface species.

In a later paper Loffreda et al[23] study the hydrogenation reaction pathway with DFT over the Pt(111) surface. Their conclusion was that the reaction actually favors the attack of the C=O carbonyl, but the desorption step of the resulting allyl alcohol has a very high barrier height compared to the reaction pathway involving the attack of the C=C and desorption of the propionaldehyde product. Thus, they conclude the surface will build up a high concentration of allyl alcohol, but the gas phase will show a high selectivity for the formation of propionaldehyde. In this work the frequency range from 2500-4000 cm^{-1} was studied and there was no evidence found for the unsaturated alcohol on the surface as was proposed by Loffreda et al[23], although a species with the OH bond perfectly parallel to the surface cannot be ruled out due to the metal surface selection rule[24,25].

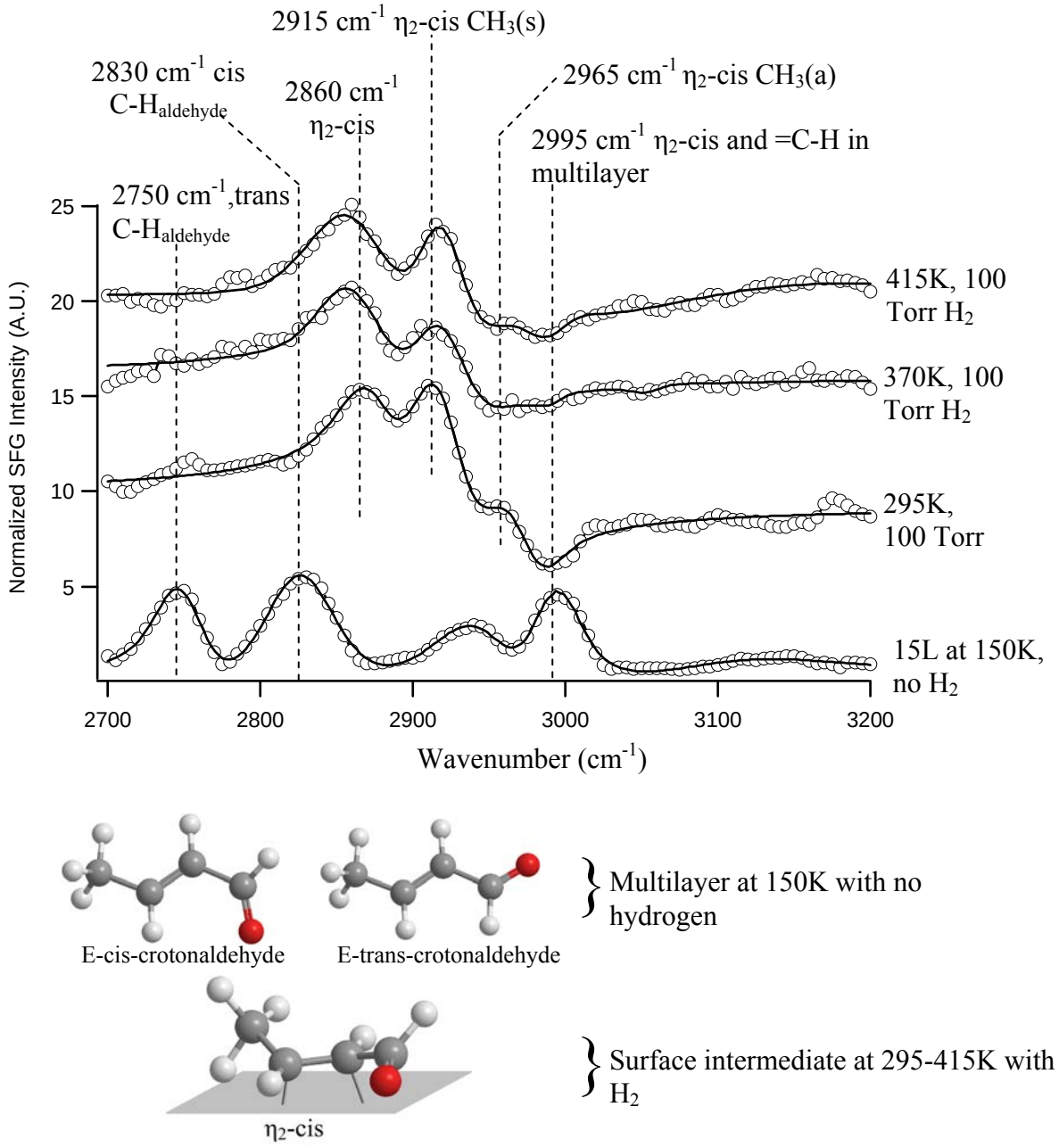

Figure 7.3. SFG-VS spectra of crotonaldehyde hydrogenation over Pt(111). The bottom spectrum was taken at 150K after exposing the crystal to 15L crotonaldehyde to form a multilayer. The top three spectra were taken with 1 Torr crotonaldehyde and 100 Torr hydrogen over the Pt(111) crystal at the temperatures listed.

7.3.1.2. Crotonaldehyde Hydrogenation on Pt(111)– SFG-VS Results

The hydrogenation of crotonaldehyde (Scheme 7.2) has selectivity for the desired unsaturated alcohol between that of acrolein and prenal hydrogenation (Sec. 7.3.2). The addition of the methyl group improves the selectivity for the unsaturated alcohol, but it also adds complexity to the vibrational spectrum, especially in the C-H region. Figure 7.3 shows the spectrum for a multilayer of crotonaldehyde on Pt(111) at 150K in the absence of hydrogen as a reference spectrum, followed by the temperature dependent spectra of 1 Torr crotonaldehyde and 100 Torr hydrogen reacting over a Pt(111) single crystal from 295 to 415K. In the multilayer (bottom) at 150K, four vibrational resonances are seen. At 2750 cm^{-1} a strong peak is seen for the trans aldehyde C-H vibration. The analysis of the other three peaks at 2830 cm^{-1}, 2935 cm^{-1}, and 2995 cm^{-1} can be made by comparison to gas phase IR (Table 7.2) and DFT calculations[26] for interpretation. In this context, the peak at 2830 cm^{-1} corresponds to the aldehyde C-H stretch of E-(s)-cis crotonaldehyde, the 2935 cm^{-1} corresponds to the symmetric stretching in the methyl side group and the 2995 cm^{-1} corresponds to both the asymmetric methyl stretch and the vinylic C-H stretches off the C=C bond.

Assignment	IR Gas Phase	SFG-VS 150K
ν_{asym}(=CH)	3058	2995
ν_{sym}(=CH)	2995	2995
$\nu_{asym}(CH_3)$	2963	2995
$\nu_{sym}(CH_3)$	2938	2935
$\nu_{aldehyde}$(CH)	2805/2728	2830/2750

Table 7.2. Summary of experimental crotonaldehyde vibrational modes (given in cm^{-1}) for gas phase crotonaldehyde[27], and 15L crotonaldehyde adsorbed to Pt(111) at 150K using SFG-VS.

The spectrum recorded at 295K in the presence of hydrogen in Figure 7.3 shows five vibrational resonances much different from the multilayer condensed onto Pt(111). First, the trans aldehyde C-H stretch around 2750 cm^{-1} disappears by 295K. Four more resonances are seen at 2865 cm^{-1}, 2915 cm^{-1}, 2965 cm^{-1}, and 2995 cm^{-1}. The 2995 cm^{-1} resonance has flipped from a positive going peak to a negative going peak due to a change in its relative phase as seen in the fit to eq. 7.2. Further, the absence of any peak at 2750 cm^{-1} or below suggests that the η_2-di-σ(CC)-E-(s)-trans species is not present in significant surface concentration at 295K in 100 Torr H_2. Although the trans adsorbed species disappears as the temperature is raised and hydrogen is added, this does not necessarily mean it is no longer participating in the reaction mechanism. The trans species could react more quickly than the cis surface species, in which case no appreciable surface concentration of the trans species would build up.

At 295K, once again in comparison to the DFT calculated frequencies[26,28], the frequencies agree quite well with the η_2-di-σ(CC)-E-(s)-cis crotonaldehyde species (Fig. 7.3). As the Pt(111) crystal is heated to 415K the only notable change is the disappearance of the negative going peak at 2995 cm^{-1}.

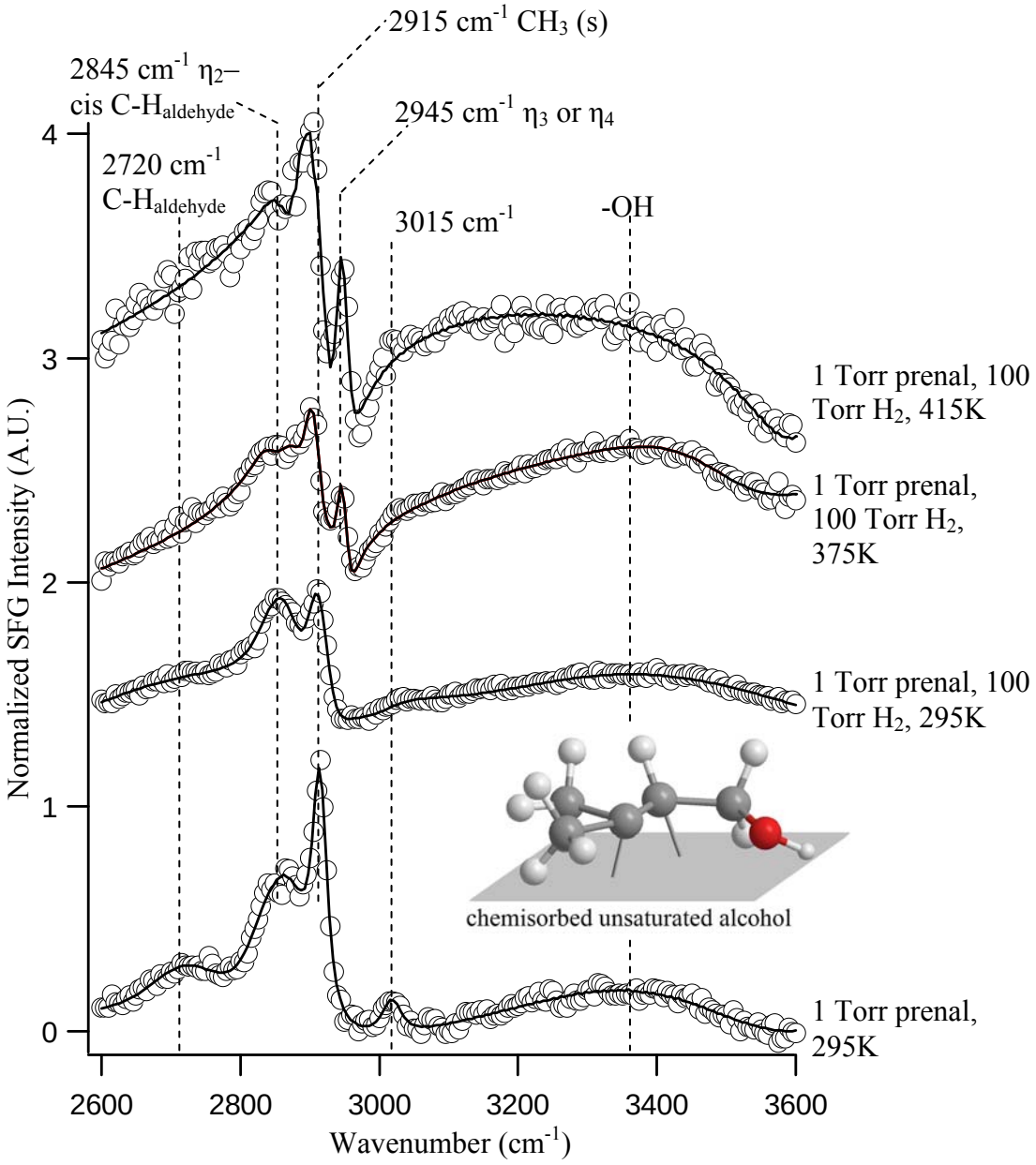

Figure 7.4. SFG-VS spectra of 1 Torr prenal over Pt(111) from 295K to 415K. The bottom one is before the addition of H_2, while the rest are with 100 Torr H_2. The –OH peak indicates alcohol on the surface at all temperatures. The "soft" modes at 2720 cm^{-1} and 2845 cm^{-1} are indicative of η_2 adsorption species. The 2945 cm^{-1} peak is indicative of more highly coordinated η_4 or possibly η_3 adsorbed prenal species.

7.3.1.3 Prenal Hydrogenation on Pt(111) – SFG-VS Results

Figure 7.4 displays the SFG-VS spectra of 1 Torr prenal both with and without 100 Torr hydrogen over Pt(111). A striking difference between these spectra and those discussed for acrolein and crotonaldehyde is the broad –OH hydrogen bonded peak centered around 3380 cm^{-1} present even before hydrogen is added to the system (made clearer in Figure 7.5). The hydrogenation of prenal has been shown to be more selective for the formation of the desired unsaturated alcohol both in previous work[6] and in this work (Sec. 7.3.3). The buildup of –OH on the surface would indeed indicate that the desorption step of the alcohol is a rate limiting step as was proposed for acrolein hydrogenation by Loffreda et al.[23,29] Upon heating, the –OH vibration is red-shifted, indicating a more electron donating interaction with the surface. This –OH stretch may indicate either the presence of the 3-methyl-2-buten-1-ol product bound to the surface or a hydroxyallyl type reaction intermediate as proposed by Loffreda et al[29] to be in equilibrium with the unsaturated aldehyde reactant. As reported by Haubrich et al[30], another possible reaction product in the hydrogenation of prenal is water in a dehydration to form the 3-methylbutane product. The –OH stretch of water cannot be eliminated as a possible source for this observed broad –OH stretch.

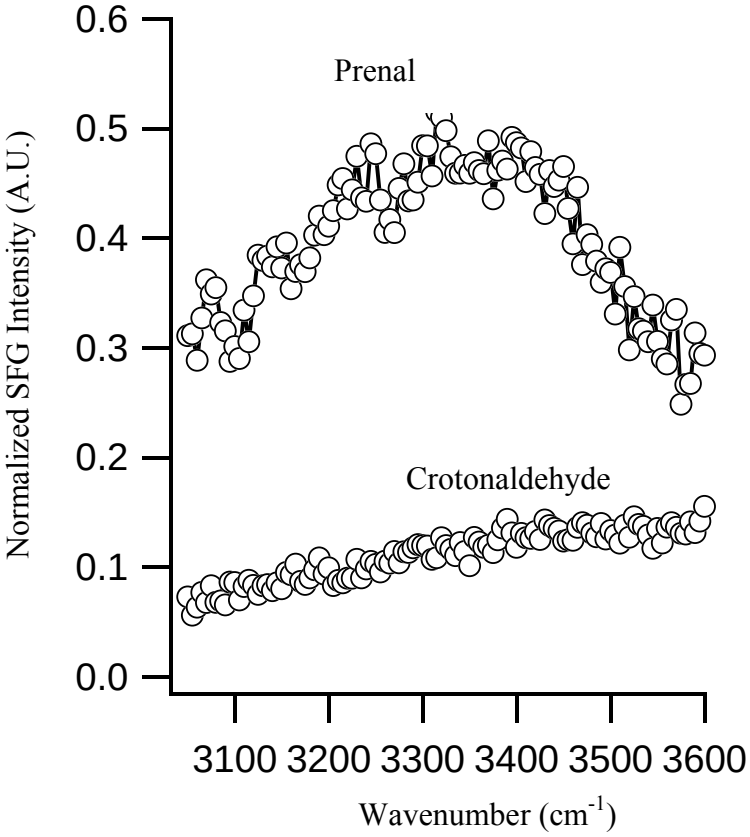

Figure 7.5. SFG-VS spectra of the –OH region of 1 Torr prenal on Pt(111) (top) and 1 Torr crotonaldehyde on Pt(111) (bottom) in the absence of excess hydrogen.

Once again, by comparing the observed spectra with the DFT calculated spectra for the various adsorption modes is informative[26,30,31]. For the spectra (Figure 7.4, bottom and Figure 7.5, top) taken prior to the addition of hydrogen, a peak is visible at 2720 cm^{-1} which should clearly correspond to an intact aldehyde C-H. Other than the –OH peak discussed, vibrational peaks are observed at 2845 cm^{-1}, 2915 cm^{-1}, and 3015 cm^{-1}. Upon the addition of 100 Torr hydrogen, the 2720 cm^{-1} peak vanishes and the 3015 cm^{-1} peak becomes much weaker. The only changes in the spectra as the crystal is heated to 415K is that the –OH band becomes more intense, and red-shifted, and a new peak grows in at 2945 cm^{-1}. The peak growing in at 2945 cm^{-1} agrees well with the growing presence of either the η_3-di-σ(CC)-σ(O)-(s)-cis, corresponding to the asymmetric stretching in one of the methyl groups, or to the aldehyde C-H stretch of the η_4-di-σ(CC)-di-σ(CO)-(s)-trans species on the surface at higher temperatures. The high temperature spectrum is reversible. After heating to 415K and then returning the crystal to 295K the peak at 2945 cm^{-1} disappears again. This is proof that it is not a cracking product or poison on the surface, but a reversible change in surface intermediate.

7.3.2. Hydrogenation of Crotonaldehyde over Pt(111) and Pt(100): Kinetic and SFG-VS Results

The hydrogenation of crotonaldehyde was carried out with 1 Torr crotonaldehyde and 100 Torr hydrogen over both the Pt(111) and Pt(100) crystal faces to elucidate the effect that catalyst structure plays in this reaction. The industrially desired product crotyl alcohol, the unsaturated alcohol, results from the hydrogenation of the C=O (Scheme 7.2), while the thermodynamically favored product, butyraldehyde, results from the

hydrogenation of the C=C. Further, the temperature range from 295K to 415K was used and apparent activation energies calculated for the reaction products over both surfaces.

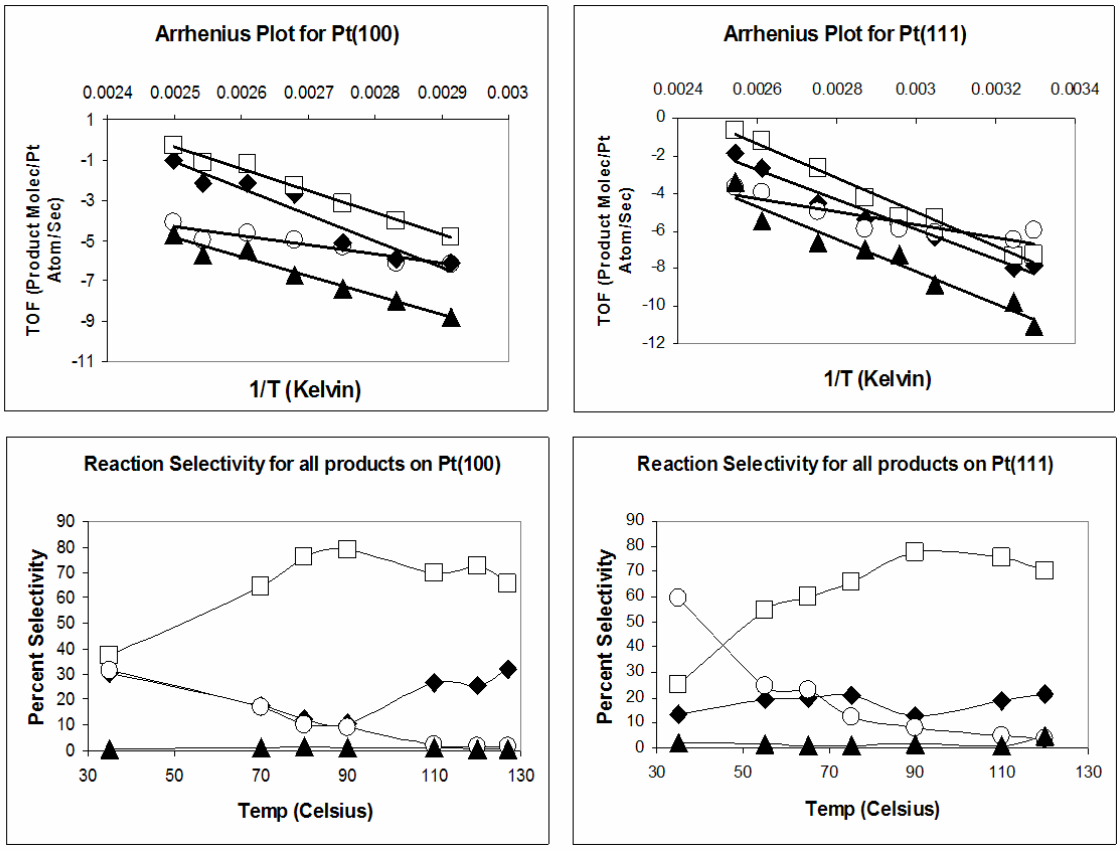

Figure 7.6. Arrhenius plots (top) and reaction selectivities (bottom) taken once a steady state was reached for the hydrogenation of crotonaldehyde over Pt(111) (right) and Pt(100) (left). The major reaction products are butyraldehyde (□), crotylalcohol (○), propylene (♦), and butanol (▲).

Figure 7.6 shows the Arrhenius plots and reaction selectivities over both metal surfaces, and Table 7.3 displays the apparent activation energies for all reaction pathways. The activation energy for the formation of crotyl alcohol is significantly less than that for the formation of butyraldehyde.

	Pt(111)	Pt(100)
Butyraldehyde	75	90
Crotylalcohol	35	38
Propylene	68	63
Butanol	59	79

Table 7.3. Activation energies in kJ/mol for the various products of crotonaldehyde hydrogenation carried out over Pt(111) and Pt(100) with 1 Torr crotonaldehyde and 100 Torr hydrogen.

This is evident also in the reaction selectivities of Figure 7.6 which show a significantly enhanced selectivity for the formation of the unsaturated alcohol at low temperatures (35° C). At such low catalytic temperatures however the turnover frequencies (TOF, product molecules/Pt site/sec) are very low for all products, on the order of 10^{-3}, while as the temperature is raised to 130° C the TOF for the formation of butyraldehyde approaches $\sim 10^{0}$ over both surfaces. It is interesting to note that the apparent activation energy for the production of crotyl alcohol is lower than that for the production of butyraldehyde, yet at most temperatures butyraldehyde is the dominant product. The reason for this is two-fold. First, the reported "apparent" activation energy for crotyl alcohol formation would be underestimated if for instance the cracking product resulted only from molecules which first formed crotyl alcohol. In fact, it has been shown that the sticking

coefficient for an unsaturated alcohol is significantly higher than its corresponding saturated aldehyde[11] which may lead to longer residence times and further reactions, such as decarbonylation. Secondly, the pre-exponential factors for the two reaction pathways could conceivably be different. Given that there may exist more than one adsorption mode of the crotonaldehyde molecule on the Pt(111) surface, it is reasonable that one adsorption mode may favor the formation of crotyl alcohol while another favors the formation of butyraldehyde, changing their associated reaction entropies.

Pt(111) shows a higher selectivity for the formation of the unsaturated alcohol, especially at low temperatures, while Pt(100) shows a higher selectivity for the formation of the decarbonylation "cracking" product propylene (Fig 7.6). The selectivity for the totally saturated product butanol remained low, less than 1%, on both surfaces at the temperatures studied.

Similar to the results reported by Lawrence and Schreifels[32] the selectivity for the formation of the desired unsaturated alcohol, crotyl alcohol, varied with time. Figure 7.7 shows the time dependence for the hydrogenation of 1 Torr crotonaldehyde with 100 Torr hydrogen for 2 hours at 90°C. Initially, the selectivity for the formation of crotyl alcohol is as high as 45%, but by the time the reaction reaches a steady state product distribution the crotyl alcohol selectivity has dropped to ~10%. This change in selectivity may be due to either the selective blocking of active sites by CO during the decarbonylation of crotonaldehyde or by carbonaceous deposits both of which have previously been reported to deactivate this reaction over model Pt nanoparticle catalysts.[33] This gives further reason why the reaction appears to shift to favor crotyl alcohol production at low temperatures. At lower temperatures the deactivation mechanism which causes the shift

in selectivity with time may be less active. STM experiments are currently underway to help elucidate this effect.

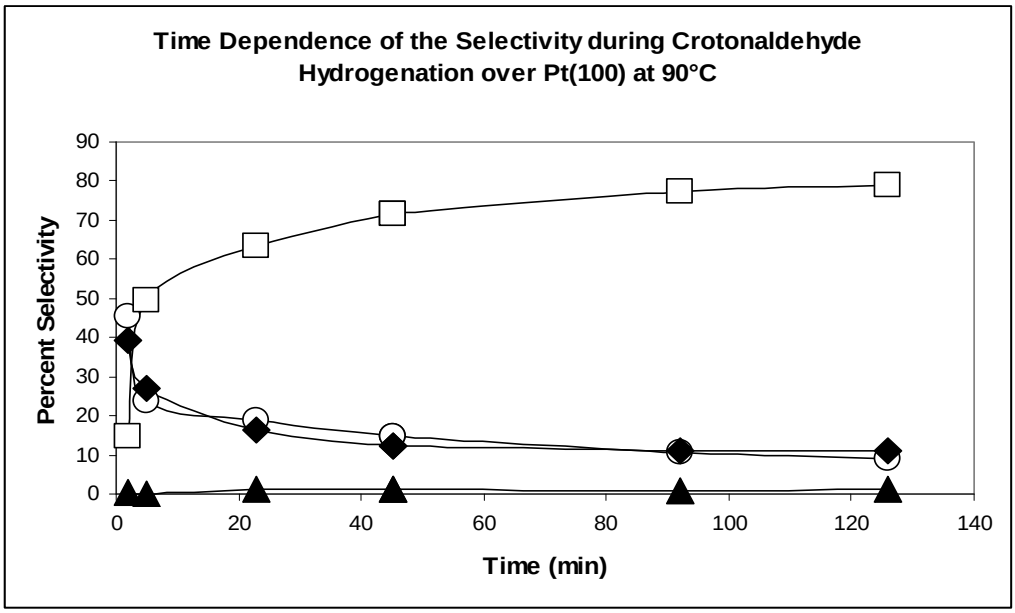

Figure 7.7. Product selectivities in the hydrogenation of crotonaldehyde (1 Torr crotonaldehyde/100 Torr hydrogen) at 90°C. The major reaction products are butyraldehyde (□), crotylalcohol (○), propylene (♦), and butanol (▲). A dramatic change in reaction selectivity is seen during the first 20 minutes and a steady state product distribution is reached at around 2 hours.

Figure 7.8 compares a spectrum taken over Pt(111) to one taken over Pt(100) under 1 Torr crotonaldehyde and 100 Torr hydrogen at 295K. The vibrational features between the two crystal faces were identical here and for all temperatures studied. This argues that the dominant surface reaction intermediates are the same for both crystal faces for the hydrogenation of crotonaldehyde. This is in contrast to theoretical work done by Delbecq et al[34] which demonstrated significantly different adsorption modes for crotonaldehyde between the Pt(111) and Pt(100) surfaces. However, it is consistent with the reaction selectivities and kinetics above which demonstrated very similar activities and selectivities for the two surfaces, the primary difference simply being in the barrier heights for the various reaction pathways evidenced by the differing activation energies calculated allowing for some kinetic control of the product distribution.

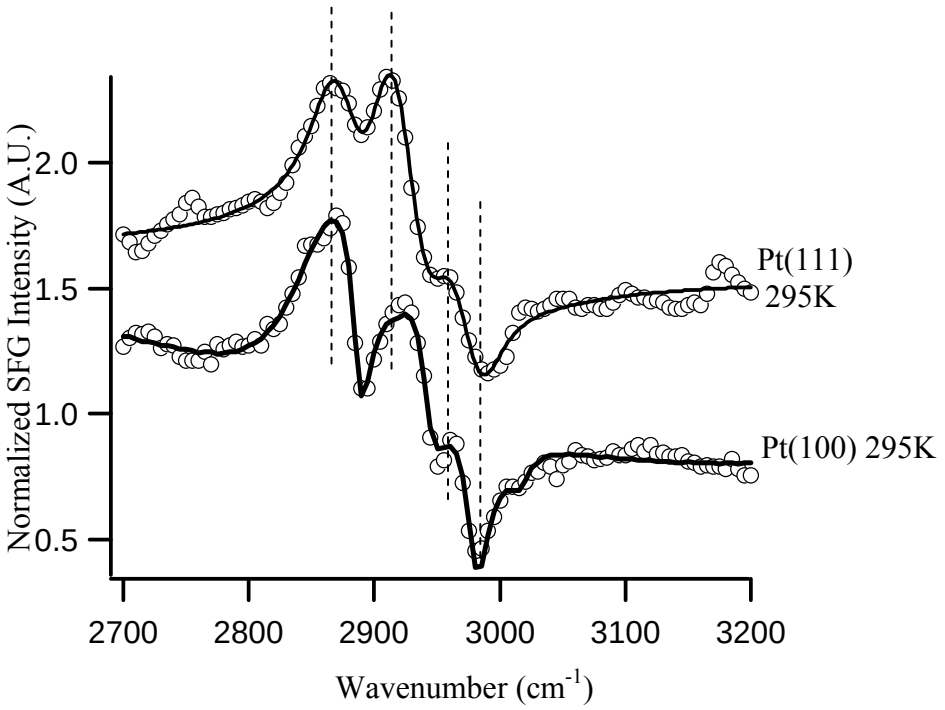

Figure 7.8. SFG-VS spectra of 1 Torr crotonaldehyde and 100 Torr hydrogen at 295K over Pt(100) (bottom) and Pt(111) (top). SFG-VS spectra over Pt(111) and Pt(100) showed identical features at all temperatures from 295-415K.

7.3.3. Hydrogenation of Prenal over Pt(111): Kinetic Results

For comparison to the results obtained for the hydrogenation of crotonaldehyde, the hydrogenation of prenal was carried out over Pt(111) over the temperature range 35°C – 130°C under 1 Torr prenal and 100 Torr hydrogen. The addition of the extra methyl group (Scheme 7.3) to the C=C bond adds steric hindrance to the adsorption of this moiety, and thus may increase the selectivity to the unsaturated alcohol product. Figure 7.9 displays the time dependence of the reaction selectivity for prenal hydrogenation over Pt(111) at 70°C for 2.5 hours. The initial reaction selectivity was 100% for the production of the desired unsaturated alcohol, but the reaction selectivity reached a steady state at about 1.5 hours and the production of unsaturated alcohol had fallen to 33% by this time.

As can be seen in Figure 7.10, the selectivity for the formation of unsaturated alcohol at 100°C was 37%. This is more than 5 times higher than the selectivity for the unsaturated alcohol during crotonaldehyde hydrogenation at this temperature. As the temperature is raised to 130°C however, the onset of cracking product formation appears to come at the cost of unsaturated alcohol production. The selectivity for 3-methyl-2-buten-1-ol drops to ~10% at this temperature as the selectivity for the cracking products concomitantly rises. To obtain the reaction selectivity at 35°C the reaction was allowed to proceed for 14 hours. The only major detectable product was the desired unsaturated alcohol; however, this effect may be somewhat exaggerated as the reaction may not have yet reached its final steady state product distribution.

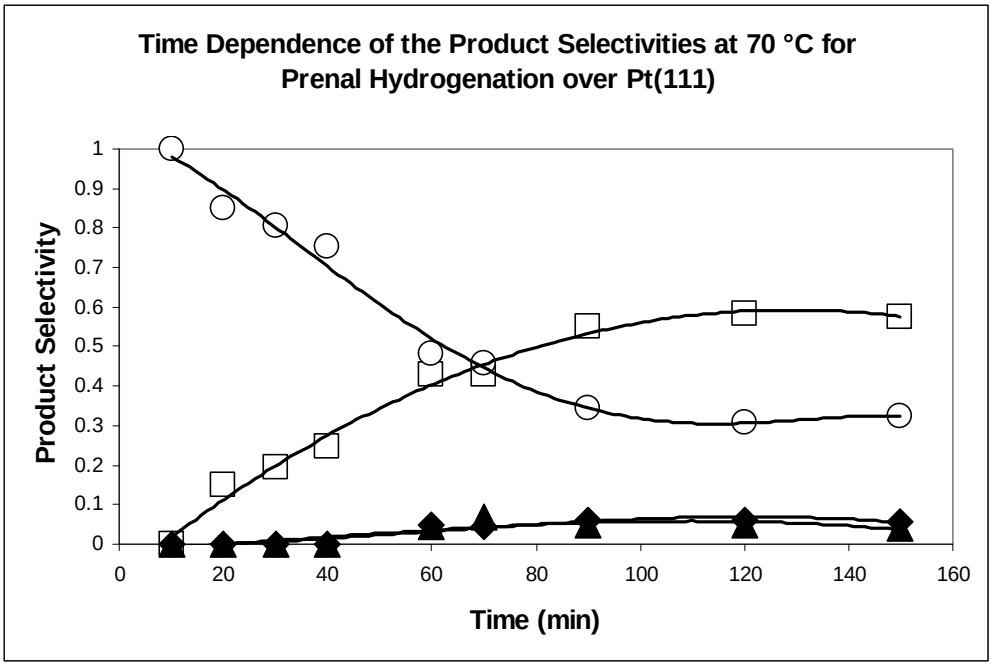

Figure 7.9. Product selectivities as a function of time for prenal hydrogenation over Pt(111) using 1 Torr prenal and 100 Torr hydrogen. Initial selectivity was 100% for the unsaturated alcohol, but as the reaction progressed to a steady state after about 2 hours the selectivity for the unsaturated alcohol fell to 33%. The major reaction products are 3-methylbutyraldehyde (□), 3-methyl-2-buten-1-ol (○), C_4 cracking products (♦), and 3-methylbutanol (▲).

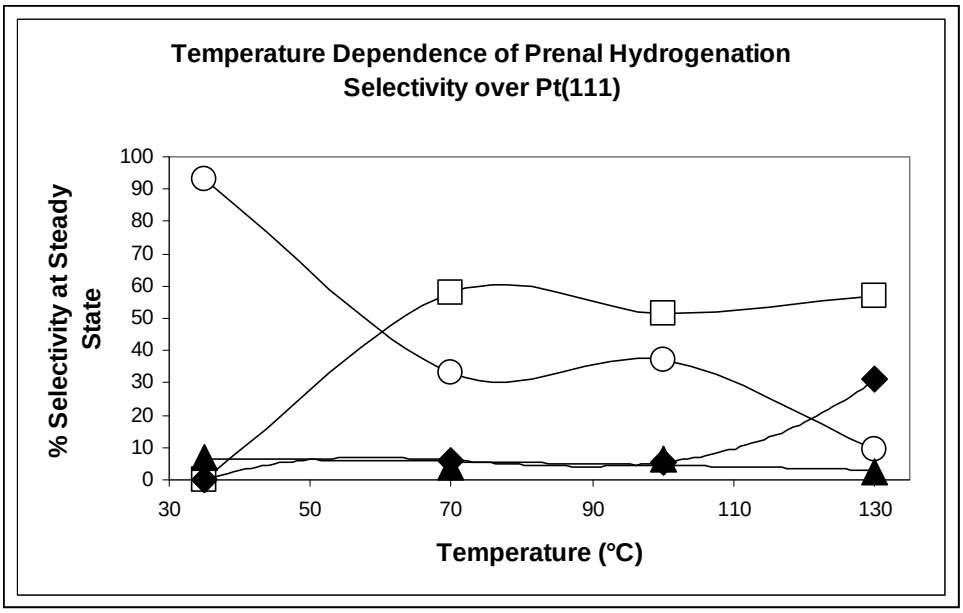

Figure 7.10. Product selectivities during the hydrogenation of prenal over Pt(111) as a function of temperature. All selectivities were taken once a steady state had been reached, typically about 2 hours into the reaction. At 35°C, the data points were taken at 14 hours. The major reaction products are 3-methylbutyraldehyde (□), 3-methyl-2-buten-1-ol (○), C_4 cracking products (♦), and 3-methylbutanol (▲).

7.4. Conclusions.

Using a combination of SFG vibrational spectroscopy and kinetic measurements, along with detailed comparison to published IR, HREELS, and DFT calculations, the surface species during the catalytic hydrogenation of acrolein, crotonaldehyde, and prenal have been clarified. The effect that catalyst structure has on the hydrogenation of crotonaldehyde has been elucidated by comparing both the reaction kinetics and SFG-VS spectra over Pt(111) and Pt(100) single crystals.

In the case of acrolein, a mixed adsorption state existed including η_2-cis and η_2-trans species as well as more highly coordinated η_3 or η_4 species. However, upon the addition of hydrogen the η_2-trans surface species vanished. Further, as the Pt(111) crystal was heated to 415K all of the surface intermediate peaks vanished except that of ethylidyne, forming from the decarbonylation of acrolein.

The reaction kinetics for crotonaldehyde hydrogenation showed a lower activation energy for the formation of the industrially desired crotylalcohol than for the formation of the thermodynamically favored butyraldehyde. Thus, at lower temperatures the selectivity for the desired product was enhanced.

For the adsorption of crotonaldehyde to Pt(111) at 150K, both cis and trans species were found with SFG-VS. However, in the presence of hydrogen at 295K and hotter the only surface species observed was η_2-cis. This may be an indication that the η_2-trans species is not stable at the higher temperature, or is simply the fastest one to react and desorb, not allowing a significant surface concentration to build up. The SFG-VS data, then, agree nicely with the reaction kinetics, given that the η_2 adsorption modes do not

have the carbonyl interacting with the surface and the selectivity for the hydrogenation of the C=O was low in the case of crotonaldehyde hydrogenation.

Pt(111) and Pt(100) showed little structure sensitivity for this reaction. The Pt(111) had a somewhat higher selectivity for the formation of crotylalcohol, while Pt(100) had a higher selectivity for the decarbonylation "cracking" reaction. Further, the SFG-VS spectra of crotonaldehyde hydrogenation over both surfaces were identical.

For the hydrogenation of prenal over Pt(111), the SFG-VS results indicated the presence of an –OH group even without the presence of excess hydrogen. This is consistent with the flipped selectivity for the hydrogenation of prenal in which the dominant product is the unsaturated alcohol. SFG-VS spectra demonstrated the presence of the η_2 surface species definitively. Further, upon heating the Pt(111) crystal to 415K a highly coordinated η_3 or η_4 species grows in on the surface. This clear difference from crotonaldehyde also agrees with the difference in reaction selectivities. The C=O of prenal interacts with the surface at higher temperatures, unlike the case for crotonaldehyde, and the C=O is hydrogenated significantly more during prenal hydrogenation than crotonaldehyde hydrogenation.

(1) Gallezot, P.; Richard, D. *Catalysis Reviews-Science and Engineering* **1998**, *40*, 81-126.

(2) Maki-Arvela, P.; Hajek, J.; Salmi, T.; Murzin, D. Y. *Applied Catalysis a-General* **2005**, *292*, 1-49.

(3) Ponec, V. *Applied Catalysis a-General* **1997**, *149*, 27-48.

(4) Claus, P. *Topics in Catalysis* **1998**, *5*, 51-62.

(5) Englisch, M.; Ranade, V. S.; Lercher, J. A. *Journal of Molecular Catalysis a-Chemical* **1997**, *121*, 69-80.

(6) Beccat, P.; Bertolini, J. C.; Gauthier, Y.; Massardier, J.; Ruiz, P. *Journal of Catalysis* **1990**, *126*, 451-456.

(7) Birchem, T.; Pradier, C. M.; Berthier, Y.; Cordier, G. *Journal of Catalysis* **1996**, *161*, 68-77.

(8) Marinelli, T.; Ponec, V. *Journal of Catalysis* **1995**, *156*, 51-59.

(9) Englisch, M.; Jentys, A.; Lercher, J. A. *Journal of Catalysis* **1997**, *166*, 25-35.

(10) Hoang-Van, C.; Zegaoui, O. *Applied Catalysis a-General* **1997**, *164*, 91-103.

(11) Birchem, T.; Pradier, C. M.; Berthier, Y.; Cordier, G. *Journal of Catalysis* **1994**, *146*, 503-510.

(12) Bratlie, K. M.; Flores, L. D.; Somorjai, G. A. *Surface Science* **2005**, *599*, 93-106.

(13) Kung, K. Y.; Chen, P.; Wei, F.; Rupprechter, G.; Shen, Y. R.; Somorjai, G. A. *Review of Scientific Instruments* **2001**, *72*, 1806-1809.

(14) Shen, Y. R. *Annual Review of Physical Chemistry* **1989**, *40*, 327-350.

(15) Shen, Y. R. *Nature* **1989**, *337*, 519-525.

(16) Yang, M. C.; Tang, D. C.; Somorjai, G. A. *Review of Scientific Instruments* **2003**, *74*, 4554-4557.

(17) Loffreda, D.; Jugnet, Y.; Delbecq, F.; Bertolini, J. C.; Sautet, P. *Journal of Physical Chemistry B* **2004**, *108*, 9085-9093.

(18) Hamada, Y.; Nishimura, Y.; Tsuboi, M. *Chemical Physics* **1985**, *100*, 365-375.

(19) Murillo, L. E.; Chen, J. G. *Surface Science* **2008**, *602*, 919-931.

(20) Chen, P.; Westerberg, S.; Kung, K. Y.; Zhu, J.; Grunes, J.; Somorjai, G. A. *Applied Catalysis A: General* **2002**, *229*, 147-154.

(21) de Jesus, J. C.; Zaera, F. *Surface Science* **1999**, *430*, 99-115.

(22) Loffreda, D.; Delbecq, F.; Sautet, P. *Chemical Physics Letters* **2005**, *405*, 434-439.

(23) Loffreda, D.; Delbecq, F.; Vigne, F.; Sautet, P. *Angewandte Chemie-International Edition* **2005**, *44*, 5279-5282.

(24) Dignam, M. J.; Moskovit.M; Stobie, R. W. *Transactions of the Faraday Society* **1971**, *67*, 3306-&.

(25) Pearce, H. A.; Sheppard, N. *Surface Science* **1976**, *59*, 205-217.

(26) Haubrich, J., Universitat Bonn, 2006.

(27) Oelichmann, H. J.; Bougeard, D.; Schrader, B. *Journal of Molecular Structure* **1981**, *77*, 179-194.

(28) Haubrich, J.; Loffreda, D.; Delbecq, F.; Jugnet, Y.; Sautet, P.; Krupski, A.; Becker, C.; Wandelt, K. *Chemical Physics Letters* **2006**, *433*, 188-192.

(29) Loffreda, D.; Delbecq, F.; Vigne, F.; Sautet, P. *Journal of the American Chemical Society* **2006**, *128*, 1316-1323.

(30) Haubrich, J.; Loffreda, D.; Delbecq, F.; Sautet, P.; Jugnet, Y.; Krupski, A.; Becker, C.; Wandelt, K. *Journal of Physical Chemistry C* **2008**, *112*, 3701-3718.

(31) Hirschl, R.; Delbecq, F.; Sautet, P.; Hafner, J. *Journal of Catalysis* **2003**, *217*, 354-366.

(32) Lawrence, S. S.; Schreifels, J. A. *Journal of Catalysis* **1989**, *119*, 272-275.

(33) Grass, M.; Rioux, R.; Somorjai, G. *Catalysis Letters* **2009**, *128*, 1-8.

(34) Delbecq, F.; Sautet, P. *Journal of Catalysis* **1995**, *152*, 217-236.